12-2006

Laboratory Evaluation of Unbound RAP as a Pavement Base Material

Wenbin He
University of Tennessee - Knoxville

To the Graduate Council:

I am submitting herewith a thesis written by Wenbin He entitled "Laboratory Evaluation of Unbound RAP as a Pavement Base Material." I have examined the final electronic copy of this thesis for form and content and recommend that it be accepted in partial fulfillment of the requirements for the degree of Master of Science, with a major in Civil Engineering.

Baoshan Huang, Major Professor

We have read this thesis and recommend its acceptance:

Eric C. Drumm, Zhongguo Ma

Accepted for the Council:
Carolyn R. Hodges

Vice Provost and Dean of the Graduate School

(Original signatures are on file with official student records.)

To the Graduate Council:

I am submitting herewith a thesis written by Wenbin He entitled “Laboratory Evaluation of Unbound RAP as a Pavement Base Material” I have examined the final electronic copy of this thesis for form and content and recommend that it be accepted in partial fulfillment of the requirements for the degree of Master of Science, with a major in Civil Engineering.

Baoshan Huang
Major Professor

We have read this thesis
and recommend its acceptance:

Eric C. Drumm

Zhongguo Ma

Accepted for the Council:

Linda Painter
Interim Dean of Graduate Studies

(Original signatures are on file with official student records)

Laboratory Evaluation of Unbound RAP as a Pavement Base Material

A Thesis Presented for
the Master of Science
Degree
The University of Tennessee, Knoxville

Wenbin He
December 2006

ACKNOWLEDGEMENTS

I would like to take this opportunity to extend my acknowledgements to all those who made this thesis possible.

The greatest appreciation is for my thesis advisor Dr. Baoshan Huang for his constant guidance and encouragement to leading me in the completion of this thesis. I would also like to thank my committee members Dr. Eric C. Drumm and Dr. Zhongguo Ma for their many suggestions/corrections to this thesis.

In addition, I would like to thank my classmates and colleagues, Dr. Gang Zuo, Dr. Xin Chen, for their friendship and help during my stay at University of Tennessee.

Special thanks are for Harry Moore, who served as geology specialist in Tennessee Department of Transportation, for his enthusiastic suggestion and help in the research.

Finally, I would like to thank my dearest wife Wei Li, without her love and support I wouldn't have made it this far.

.

ABSTRACT

More than 50 million tons of asphalt pavements are milled every year in the United States (Taha 1999). The economical benefit attracts the recycling practice of utilizing RAP as paving materials.

In unbound RAP material, aged asphalt wraps aggregates. It is believed that unbound RAP performs differently from usual unbound material due to the existence of asphalt wrap. In the present study, triaxial tests were conducted for the unbound RAP under different temperatures. In addition, limestone and gravel were tested in order to compare with RAP. The resilient modulus, triaxial static creep behavior and hysteresis loops were obtained to compare the differences between the unbound RAP, limestone and gravel. The specimens were prepared at optimum moisture content and equivalent compaction work. The laboratory results indicated the RAP characteristics change with different temperature. It was found that RAP requires more compaction work than limestone and gravel. According to AASHTO 307-99, higher resilient moduli were obtained in RAP than limestone and gravel. However, larger permanent deformation was observed in RAP. Specific design consideration should be added for utilizing RAP as base material.

As part of my graduate research, finite element analysis was conducted for pile foundation over cavernous bedrock and for an Accelerated Loading Facility (ALF) in Louisiana Transportation Research Center (LTRC). The FE simulations were attached in Appendices.

TABLE OF CONTENTS

LIST OF TABLES

Table Page

LIST OF FIGURES

Figure Page

Chapter 1 Introduction

1.1 Literature Review

In United States, more than 50 million tons of asphalt pavement are milled annually (Taha 1999). The predominant recycling practice is mixing the reclaimed asphalt pavement (RAP) into new hot-mix asphalt mixture. However reclaimed asphalt pavement is not totally utilized for recycling in Hot Mix Asphalt (HMS). At the same time, the increasing need for rehabilitation of old pavement contributes to the shortage of virgin aggregate. Further more, engineers need an alternative economical way to deal with increasing landfill cost of disposing demolished pavement materials due to the availability of landfill space. Recent research on the potential use of RAP as a base material indicates that RAP is a viable substitute for conventional aggregate base.

The application of RAP as base materials dates back to early 80s'. RAP was utilized as a bituminous stabilized base in Michigan (Defoe 1982). Cold in-place recycling of existing asphalt pavement was tested to be structurally equivalent to a roadway with new separate base course (Defoe 1982). The replacement of separate base course with RAP was evaluated in Ontario, Canada. The performance showed that RAP is slightly better than aggregates (Hank 1984).

The significant cost reduction due to RAP application in base is attractive too. Some counties in US charge high fee for generating construction debris to encourage recycling and to save space due to the rapidly diminishing landfills, for example San Diego (Munzenmaier 1994). In 1990, reclaimed asphalt pavement was used as base in EI Cajon, California (Munzenmaier 1994). The unit bid price for the reclaimed asphalt decreased significantly as a sign of the contactor's confidence (Munzenmaier 1994).The use of reclaimed asphalt pavement as base avoided all disposal charges and save the valuable resources.

In certain regions where engineers experience virgin aggregate shortage, RAP could be economically reused as base or subbase aggregate (Taha 1999)

1.1.1 The Positive and Negative Effects of Using RAP as a Base Material (as Compared to Virgin Aggregate)

Although there are obvious advantages of utilizing RAP as base materials, the application is still limited due to the lack of systematic laboratory evaluation study. Since the mid 1990's, series of standard tests and traffic-type tests have been conducted to study the design criteria of RAP base. Those tests indicated RAP has good behavior in early stage of pavement life. Most test results reported the resilient modulus of RAP is slightly larger than that of aggragate's (Maher 1997, Bennert 2000). No Asphalt Concrete transverse cracking or Asphalt Concrete fatigue cracking was found in a project in Illinois after two years of traffic (Garg 1996). The Falling Weight Deflectometer data indicated sufficient structural support and subgrade protection are provided by RAP base in the Lincoln Avenue Project in Illinois (Garg 1996). However, the accumulated permanent deformation tends to large with the load cycle increase in the later age (Bennert 2000). Garg (1996) reported average California Bearing Ration (CBR) value of RAP base is less than CBR of aggregates (CA-6). Rapid shear testing was also employed to investigate RAP's Mohr-Coulomb failure envelope (Garg 1996). The test results indicated similar friction angle of RAP and aggregate. RAP exhibits lower cohesion value than aggregate (Garg 1996).

Maher (1977) reported higher resilient modulus values in RAP than crushed concrete and crushed granite. He also found slight degradation occurred between 38 and 13mm size of RAP during compaction (Maher 1977). This phenomenon contributed at least partially to the large permanent deformation. Several methods were employed to improve the quality of RAP base (Bennert 2000).

Bennert (2000) used standard tests to characterize RAP, recycled concrete aggregate (RCA) and dense-graded aggregate base aggregate (DGABC). Traffic-type loading tests were also conducted to analyze RAP, RCA and DGABC blends. The 100% RAP and 100% RCA obtained higher resilient value than 100% DGABC's which is currently used in pavement design in New Jersey. Conversely, the 100% RAP accumulated largest permanent strain. The result appears to be a discrepancy. Bennert (2000) stated the possible reason is the breakdown of the asphalt binder under the larger loading during of the permanent deformation test. Additionally, the controversy between resilient modulus and permanent strain of RAP may be due to the fact that resilient test procedures can not account for the initial permanent stain before the final cycles. RAP shows the trend to accumulate large permanent deformation. The blends with 25% RAP and 75% DGABC have resilient modulus and permanent deformation similar to 100% DGABC. The use of RAP in base and subbase is recommended by Bennert (2000) as a viable and cost-effective material for pavement design.

In May 1996, a 350 m long and 7 m wide test section of New Jersey Highway 1 in North Brunswick was constructed with 3 types of base material, 100% dense graded aggregate (DGA), 100% RAP, and blends of 75%DGA and 25%RAP (Maher et al. 1997). Field evaluation was conducted by a Seismic Pavement Analyzer (SPA). The Results shows comparable magnitudes of Young's moduli in variation of sections. 100% RAP and 25% RAP sections exhibited a higher degree of damping than section with 100% DGA (Maher 1997).

1.1.2 Application of Recycling Asphalt Pavement as Base Materials

Although some disadvantages were recognized, the reduced cost, environmental benefit and other advantages lead to increased interests in utilizing RAP as base materials for highway construction. Generally, three main methods have been reported to improve the quality of RAP base.

1) Mixing virgin aggregate with RAP (Maher 1997, Taha 1999)

2) Recycling existing AC by pulverizing and mixing with underlying poor quality base material to yield new base material (Coetzee 1995)

3) Cement stabilized RAP base (Li 2004)

In this study, our focus was on the unbound RAP base material.

1.1.3 Laboratory Characterization of RAP and Aggregate Blend

Taha (1999) employed modified proctor testing procedure (AASHTO T180), California Bearing Ratio (AASHTO T193) and resilient modulus test to explore the blend of RAP and virgin aggregate. Blends were mixed at 100/0, 80/20, 60/40, 20/80 and 0/100 percent RAP to virgin aggregates. The more aggregate was mixed in a blend, the smaller maximum dry density was observed (Taha 1999). Due to the open-graded nature of RAP aggregate and particle break-down trends during the compaction, the more virgin aggregate is added in the blend, the easier it is the blend to be compacted (Taha 1999). With the percent of virgin aggregate increasing, the CBR value increased accordingly (Taha 1999). The potential reason of this phenomenon is that virgin aggregate contributes to better interlocking which lead to the increases in the shear strength of the blend (Taha 1999)

Both RCA and RAP were mixed at various percentages with the DGABC to evaluate whether an optimum mix blend could be formulated (Bennert 2000). The permanent deformation results indicated that the RCA mixed samples exhibit the lowest amount of permanent deformation when the material was cyclically loaded to 100,000 cycles. In contrast, the permanent deformation testing on RAP mixed samples result in the highest amount of permanent deformation at the same number of cycles (Bennert 2000). Laboratory test results indicated that log N (N is the number of load cycles) model could be used for predicting permanent deformation in unbound RAP with less deviation (Bennert 2000).

After decades of asphalt pavement construction, the amount of demolished asphalt pavement increases. RAP has been to be recycled as base material since early 80's. RAP is economically attractive but it is limited in use due to the lack of systematic experimented study, relevant specifications and field experience.

According to current research, RAP has larger resilient modulus than dense gradated aggregate. But the low CBR value and potential large permanent deformation need to be eliminated through certain treatment. Mixing virgin aggregate with RAP is one of the effective methods as listed in the literature. Generally, blend of 25% RAP and 75% aggregate is suggested and applied by some researcher (Maher 1996 and Bennert 2000)

In Summary, RAP is a viable alternative to conventional base. The permanent deformation tends to be higher in RAP. Thus, sophisticated treatment needs to be added for sophisticated RAP application. However, among the research results, the viscous essence of asphalt in RAP has been ignored. In this study, the different behavior of RAP due to viscosity was investigated.

1.2 Objective and Scope

The main objective of present study was to evaluate the different behavior of RAP, gravel and limestone as base material. Through laboratory comparison, the potential usage of RAP as pavement base material was discussed. Because of the existence of asphalt in RAP, temperature dependency was investigated through triaxial tests at different temperatures.

Resilient modulus, triaxial static creep behavior and Hysteresis loop were selected for the comparison of material characteristics in RAP, limestone and gravel.

Resilient modulus tests were conducted to evaluate the response of base materials under pulse deviator stress. According to AASHTO designation (T 307-99 2003), resilient moduli of RAP, gravel and limestone were obtained. In addition, the temperature-dependent material characteristics of RAP were evaluated by measuring resilient moduli at different temperatures.

Triaxial static creep tests were employed to verify viscous behavior in RAP. Constant deviator stress was applied on specimens. LVDTs were installed to record the vertical deformation while and the recovered deformation after unloading. In order to investigate whether the temperature dependency exists in viscous behavior in RAP, triaxial static creep tests were conducted at different temperature.

Cyclic axial loading and unloading tests under constant confining pressure (CCP) were conducted to obtain hysteresis loops of limestone, gravel and RAP. The stress-strain relationships were obtained for all cycles.

Chapter 2 Test Methodology

2.1 Material Preparation

Incompletely milled reclaimed asphalt pavement (RAP) samples came from Renfro Construction., Forks of the River Plant, no. 1# RAP storage pile

Firstly, the incompletely milled RAP from east Tennessee quarries was separated using sieve analysis. Remains on each sieve were collected. According to Table 1, remains of RAP on each sieve were blended with corresponding weight on the basis of Table 1. The new blends had same gradation as listed in Table 1. Because the purpose of this laboratory investigation was in early phase of materials characteristics for Accelerate Loading Facility simulation (Appendix B), sieve analysis data in Table 1 was obtained from sieve analysis of base material of Accelerated Loading Facility in Louisiana Transportation Research Center. Therefore, new blends had same gradation as the unbound RAP material used in base course of Accelerate Loading Facility test lane.

Table 1 RAP Base Gradation

	LTRC Gradation Data	
Sieve Size (mm)	Passing %	Remain %
19	100%	0.00%
12.5	90.68%	9.32%
9.5	80.13%	10.55%
4.75	58.14%	22.00%
2.36	40.97%	17.17%
1.18	38.16%	2.81%
0.6	21.66%	16.50%
0.43	15.60%	6.06%
0.3	11.00%	4.60%
0.15	3.48%	7.52%
0.075	0.51%	2.97%
0	0.00%	0.51%

The gradation curve of base material in Accelerated Loading Facility is presented in Figure 1. In this study, we assumed that unbound RAP materials with equal gradation perform similarly. The laboratory investigation conducted for blends on basis of Table 1 is similar to the investigation conducted directly on RAP base in Accelerated Loading Facility in LTRC.

Because 4-in diameter cylinder specimens were used in triaxial tests, the maximum particle size was selected as 19mm in order to assure the test accuracy (AASHTO T-307). Rotary extraction of the milled RAP indicated an average bitumen content of 5% by weight of the mix.

Using the same preparation procedures, limestone and gravel were separated by sieve analysis. The remains on each sieve were collected and weighted. The sieve size is smaller than 19mm. Batches in each category are obtained to blend. According to gradation data (Table 1), the weight equals to corresponding components of the RAP material in ALF base.

Because either in situ moisture content or the in-place density data are not available, the maximum dry density and corresponding optimum water content were determined by the modified proctor test (AASHTO T-99). The maximum dry density of RAP is 1910 kg/m^3. The optimum moisture content of milled RAP with above-mentioned gradation (as in Figure 1) is 7.95%. The maximum dry density of limestone, which contains same gradation with RAP by weight, is 2179 kg/m^3. The optimum moisture content of limestone is 6.25%. The maximum dry density of gravel with same gradation as RAP is determined as 2160 kg/m^3. The optimum moisture content of gravel is 7.10%.

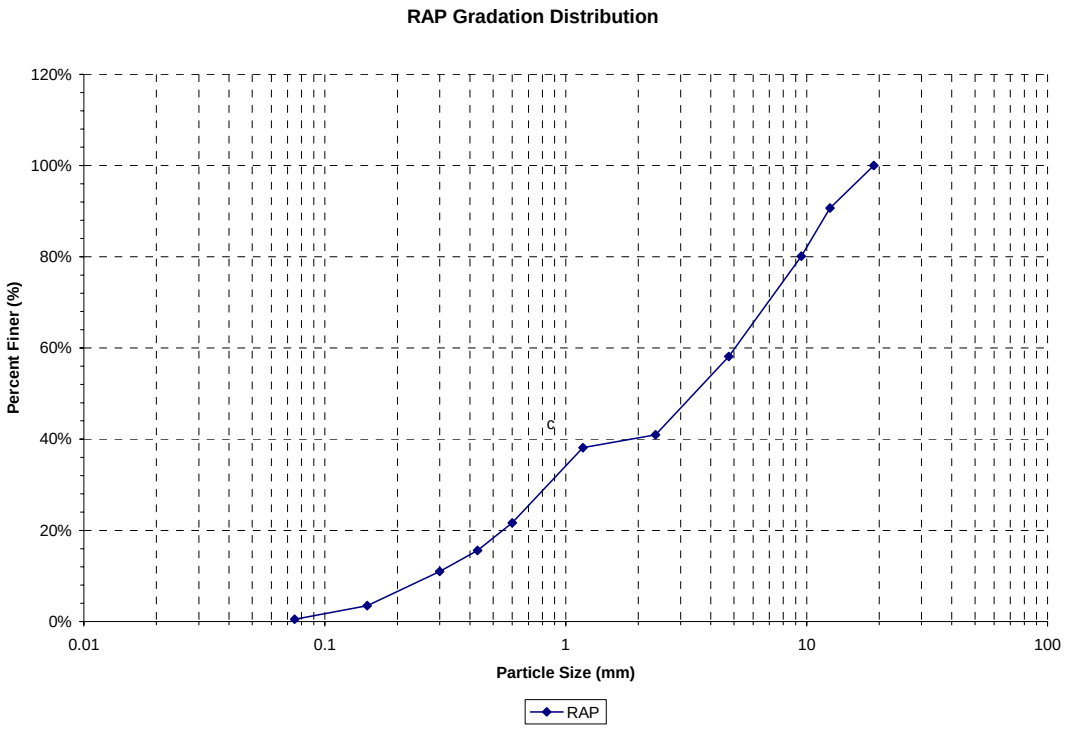

Figure 1 Gradation of Unbound RAP in ALF Base

2.2 Specimen Preparation

The unbound RAP, limestone and gravel were prepared with the procedures described in material preparation. About 250 g material were obtained from each material, respectively. According to AASHTO T 307-99, the mass of water required to change current water content to optimum moisture content was determined with 250g sample. The materials were placed into mixing pans. Determined mass of water was added to obtain desired water content. The samples were mixed thoroughly after each small amounts addition. Then, seal and cure the samples for 24 hours.

As conventional triaxial cell, the samples were prepared in a cylindrical steel mold composed of two half-cylinders bolted together. The mould is internally covered with

a latex membrane which is for facilitating confining pressure during triaxial testing. The inside diameter of mold is 4 inch. The height of mold is 9.31 inch.

One end of latex membrane was set to connect with pedestal. Cylindrical steel mold was put on the pedestal. Another end of latex membrane was turned over to cover the top of cylindrical steel mold. Five layers of equal mass of material should be put into the mould in sequence. 25 blows using the heavy Proctor rammer (5 lb, 2 in diameter) and a height drop of 12-in (305mm) were applied on each layer. The compact procedures are similar to modified proctor tests (AASHTO T-99), which is employed to determine the maximum dry density and optimum moisture content.

The specimens compacted with optimum moisture content and equal compaction work with modified proctor tests were considered to obtain maximum dry density. After compaction, the densities of RAP, limestone and gravel were obtained as 1925kg/m^3, 2191kg/m^3 and 2117kg/m^3. The properties of specimens were listed in Table 2.

Table 2 Properties of Specimens

Type	Optimum Moisture Content	Density (kg/m^3)	Specimen Dry Density (kg/m^3)	Maximum Dry Density (kg/m^3)
Gravel	7.10%	2116.38	1976.08	2160
RAP	7.95%	1925.30	1783.51	1910
Limestone	6.25%	2191.27	2062.37	2179

2.3 Apparatus

Material Test System (MTS) 810 is the main apparatus to measure resilient moduli, creep curve and Hysteresis loop. Its servohydraulic testing system provides axial repeated load with haversine-shaped form. The versatile computer-based interface allows the repeated axial load to be adjusted as sinusoidal load according to AASHOTO T 307-99. Wired LVDTs bolted in opposite positions along diameter direction accurately monitor the axial displacement. While testing, the load and displacement data could be recorded simultaneously. Computer-based software, TESTSTAR, was employed to edit and send the commands.

In order to investigate the performance of unbound RAP base related to temperature factors, the compacted and molded cylindrical specimens were mounted onto MTS 810 into an environmental chamber. The environmental chamber allows the test samples within a range of temperatures from -129 to 540 ºC. A customer specified temperature controller is mounted in the electrical box. At the same time, the temperature could be adjusted by the test template software. Cooling is processed by the use of gases introduced to the chamber. An electric fan and baffle diffuse were used to heat for uniform temperature. Figure 2 shows the triaxial test setup and environmental chamber. A thermometer was installed inside the confining pressure cylinder to monitor the accurate sample temperature.

Within environmental chamber, the temperature could be adjusted simultaneously by template. The loading process is computer-based controlled by servohydraulic system. In this study, model 651.34 of series 651 environment chambers was employed. However, the confining pressure could only be controlled manually through air compressor out of confining chamber. During the triaxial test, the confining pressure was kept constant.

Figure 2 MTS with Chamber

2.4 Resilient Modulus Tests

The appropriately prepared and conditioned cylindrical test specimen was subjected to repeated axial deviator stress of fixed magnitude, duration and frequency. According to AASHTO T307-99, the required load pulse form is haversine-shaped load form which is $(1-\cos\theta)/2$. In one pulse load cycle, haversine load pulse lasts 0.1s, the rest period will be 0.9s. During the dynamic deviator stress applications, specimens are subjected to a static all-around stress provided by means of a triaxial pressure chamber. The resilient axial strain response of the specimen is measured. The resilient modulus (Mr) is defined as the ratio of deviator stress to the magnitude of recoverable strain for a given loading sequence. (AASHTO 1993)

5000 lb load cell of MTS 810 was selected for this study. Following the sample preparation procedures, the specimen was compacted layer by layer with optimum moisture content. Then, the specimen was carefully installed on the load cell. The latex membrane was sealed by rubber bands to hydraulic rod which rested on the top

of specimen. A vacuum was connected with both head and bottom of the specimen. After specimen installation and sealing the membrane, the specimen was vacuumed and initial confining pressure was established. After a while, the bolted steel hollow cylindrical mould was released. A transparent toughened glass chamber was installed around the specimen to introduce confining pressure. Seal cream was applied in the connection portion between confining chamber and load cell. A tube which connected with an air compressor introduced pressure through the confining chamber. A manometer with connection of chamber is employed to assure the chamber has target pressure. As soon as the confining pressure is implemented, the vacuum should be stopped.

2.5 Triaxial Static Creep Test

The objective of triaxial static creep test was to investigate the viscosity of unbound RAP base material. The specimen preparation follows the same procedures with resilient modulus test. The specimens were considered to achieve maximum dry density. During the whole test procedure, constant confining pressure was applied. In loading step, 500 lb axial load was applied with increment rate 50 lb/sec. Then, ultimate load is 500 lb (40 psi). Consequently, constant axial load was applied and hold for 2 hours. In unloading step, the load was released with decreasing rate of 50 lb/sec as well. Then, the zero load condition (contact load is 10 lb) was hold for 2 hours as well. The confining pressure was applied during the whole test process. The confining pressure is 20 psi which is the same as the confining pressure of the last sequence of resilient modulus test in AASHOTO T-307-99. The recorded axial load and displacement were obtained to investigate the creep behavior of unbound material.

2.6 Cyclic Triaxial Load Tests for Hysteresis Loop

Because of the existence aged asphalt in RAP, the stress-strain relationship is believed to be significantly different from aggregates due to viscous nature of asphalt.

Cyclic triaxial loading and unloading test was designed to obtain the Hysteresis Loop. The specimen preparation followed the same procedures in AASHTO T-307-99. The constant confining pressure was applied during the whole testing process. The confining pressure was 20 psi which equals the confining pressure in last sequence of resilient modulus test in AASHTO T-307-99.

The specimens were axially loaded and unloaded continuously. The triaxial loading is firstly increased from zero to 500 lb at 5 lb/sec. Right after the load peak, unload process was implemented at rate of 5 lb/sec. The end of unload process is the beginning of sequent load cycle. There are 20 load cycles totally for each specimen. The axial load and displacement were measured simultaneously. RAP, limestone and gravel were tested under equivalent situation.

Chapter 3 Results and Discussion

3.1 Resilient Modulus Tests

Resilient modulus is one of important properties of unbound material. Similar to elastic material defined by the Young's modulus and Poisson's ratio, resilient modulus is employed to replace Young's modulus. The resilient modulus indicated the nonlinearity of unbound materials, such as dependency on stress level).

The measured modulus versus mean stress and octahedral shear stress are listed in Figure 3 and Figure 4. The dependency of stress level and temperature were observed. The resilient moduli at low temperature are higher than high temperature at the same mean stress. In addition, the resilient modulus of RAP at the same mean stress is higher than limestone and gravel. Nonlinear relationship between octahedral stress and temperature is indicated in Figure 4. Although no systematic relationship can be observed from Figure 4, but the change in resilient modulus at equal octahedral stress is obvious. This phenomenon leaded to the conclusion that the temperature dependency exists in RAP resilient recovery behavior.

3.1.1 Multiple Regression Analysis on Resilient Modulus Test Data

In order to investigate the dependency of temperature and stress level, Uzan-Witczak model (1988) was employed. Uzan-Witczak model is represented by mean stress and octahedral shear stress. The resilient modulus has power law relationship with mean stress and octahedral shear stress.

$M_r = K\theta^n \tau_{oct}^m$

where $\tau_{oct} = \frac{1}{3}\sqrt{(\sigma_1-\sigma_2)^2+(\sigma_2-\sigma_3)^2+(\sigma_3-\sigma_1)^2}$ -octahedral shear stress

$\theta=(\sigma_1+2\sigma_2)/3$-mean stress

K, n and m are material constants.

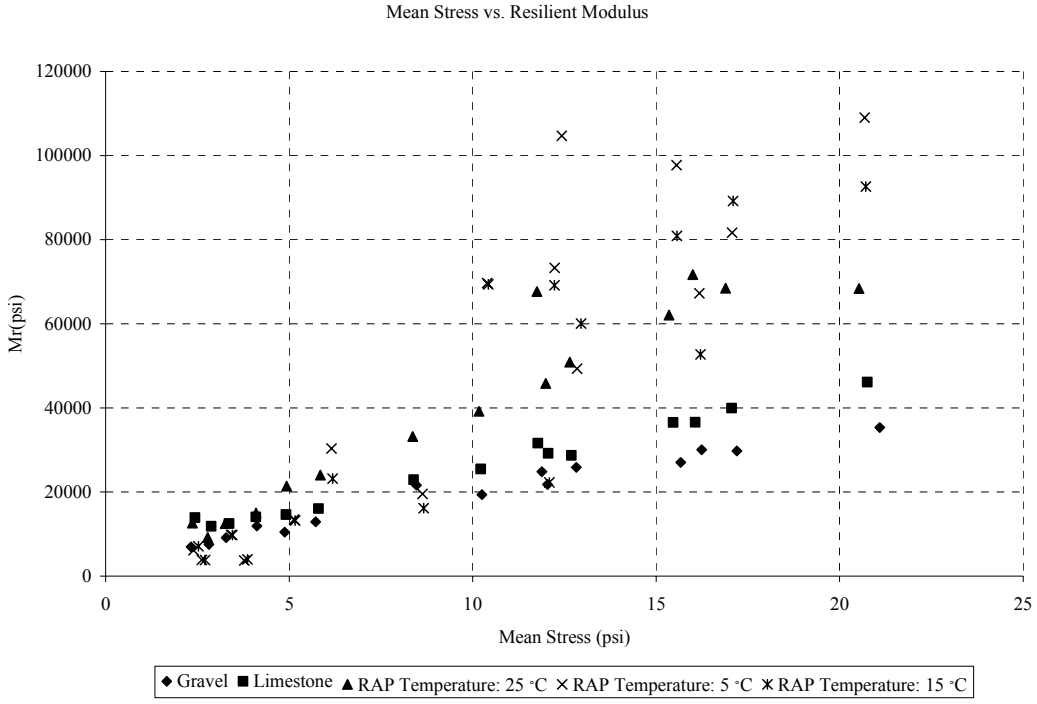

Figure 3 Resilient Modulus of RAP, Limestone and Gravel vs. Mean Stress

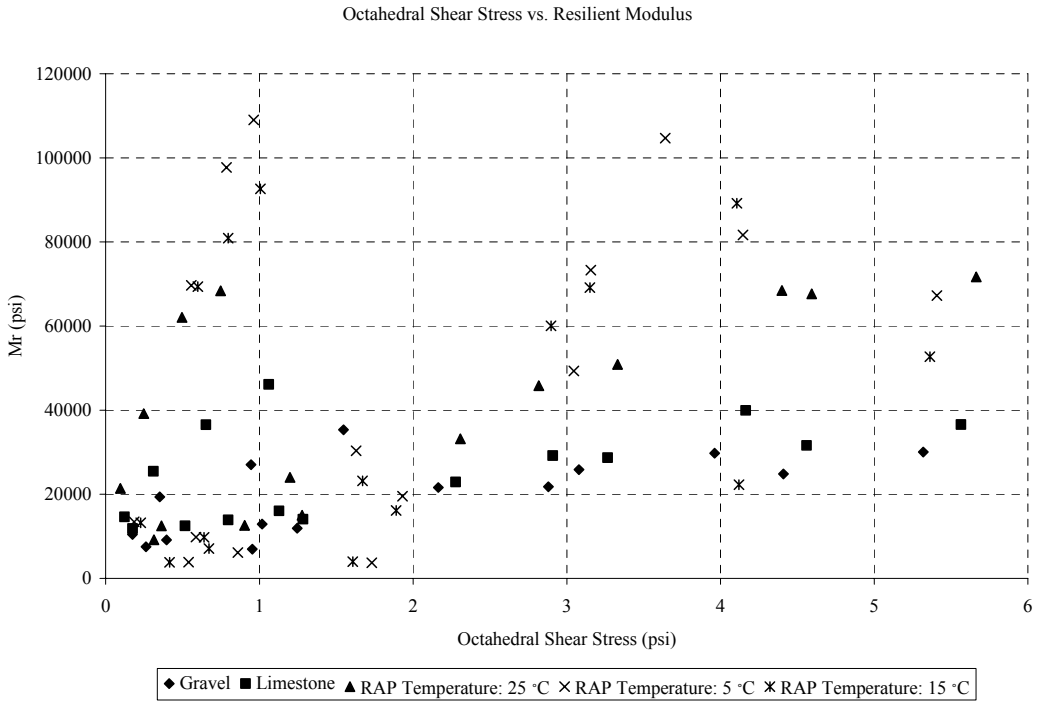

Figure 4 Resilient Modulus of RAP, Limestone and Gravel vs. Octahedral Stress

Uzan-Witczak model was assumed to predict the resilient modulus of RAP, limestone and gravel. Multiple linear regression method was the statistical methodology used to fit Uzan-Witczak models.

In order to transform the power law relationship between the resilient modulus and mean stress and octahedral shear stress, logarithm is applied on both sides of Uzan-Witczak model.

$$\log M_r = \log K + n \log \theta + m \log \tau_{oct}$$

$\log \theta$ and $\log \tau_{oct}$ were considered as predictor variables. $\log M_r$ was taken as response variable. Least Square Method was employed in multiple regression models. Multiple linear regression was implemented on triaxial resilient modulus test data in logarithmic form. Commercial statistics software JMP 10.0 was employed to perform the multiple linear regression.

Multiple Regression Analysis on RAP Resilient Modulus

First, scatter lot matrix was produced to check out-of-region points. (Figure 5)

From Figure 5, no out-of-region data was detected. Logarithm of meaning stress has higher correlation with logarithm of resilient modulus than logarithm of octahedral shear stress. Due to essential relationship between mean stress and shear stress, correlation between logarithm of meaning stress and octahedral shear stress was observed.

Multivariate

Correlations

	Lg(Mr)	lg(¦È)	lg(¦Óoct)
Lg(Mr)	1.0000	0.9784	0.5504
lg(¦È)	0.9784	1.0000	0.4901
lg(¦Óoct)	0.5504	0.4901	1.0000

Scatterplot Matrix

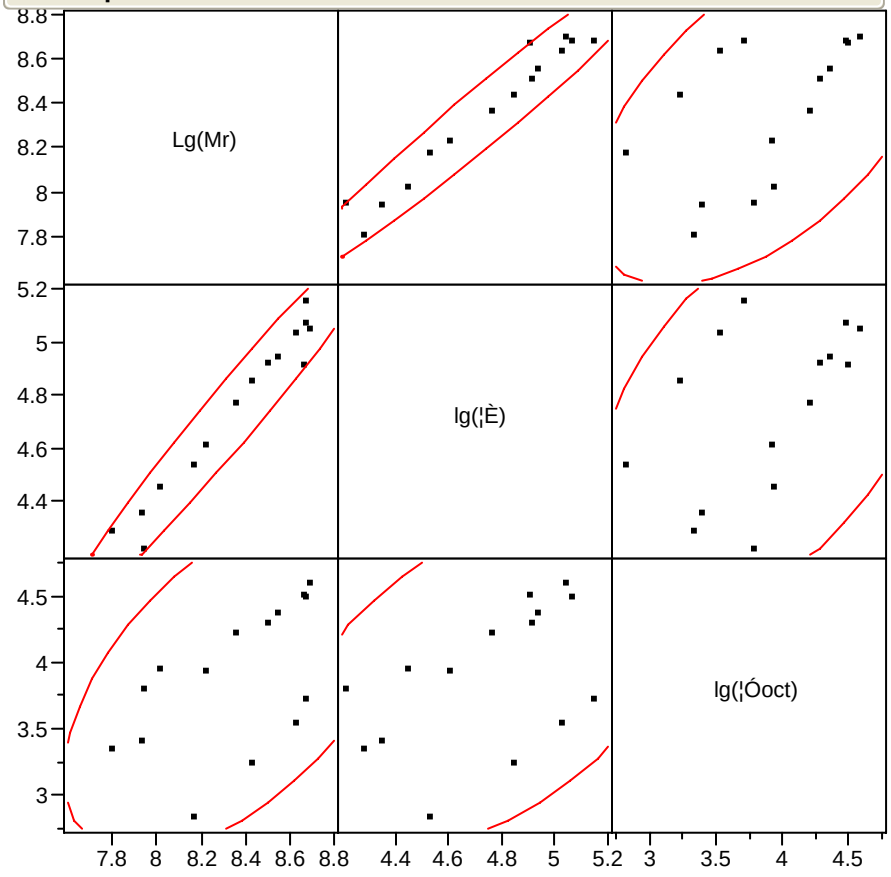

Figure 5 Correlations and Scatter plot Matrix of RAP Resilient Modulus

The intercept of multiple linear regression was recognized as coefficient K in logarithmic form. The partial regression coefficients reflect n and m, which are the power coefficients of mean stress and octahedral shear stress. The regression results for RAP were listed in Figure 6. Uzan-Witczak model for RAP is $4564\theta^{0.945}\tau_{oct}^{0.055}$ based on multiple regression.

Multiple Regression Analysis on Limestone Resilient Modulus

Pairwise correlations were conducted firstly. One out-of-region value was found. Higher correlation between logarithm of mean stress and logarithm of resilient modulus was detected. The correlation between two predictors, mean stress and octahedral shear stress was indicated.

Delete the out-of-region data, the correlation between logarithm of resilient modulus and logarithm of mean stress increased from 0.9761 (Figure 7) to 0.9921 (Figure 8). The correlation between logarithm of resilient modulus and logarithm of octahedral shear stress keeps almost constant (Figure 7 and 8). However, the correlation between two predictors increased from 0.5779 (Figure 7) to 0.6128 (Figure 8).

The regression results for limestone were listed in Figure 9. Uzan-Witczak model for Limestone is $5158\theta^{0.705}\tau_{oct}^{0.005}$ based on the multiple regression.

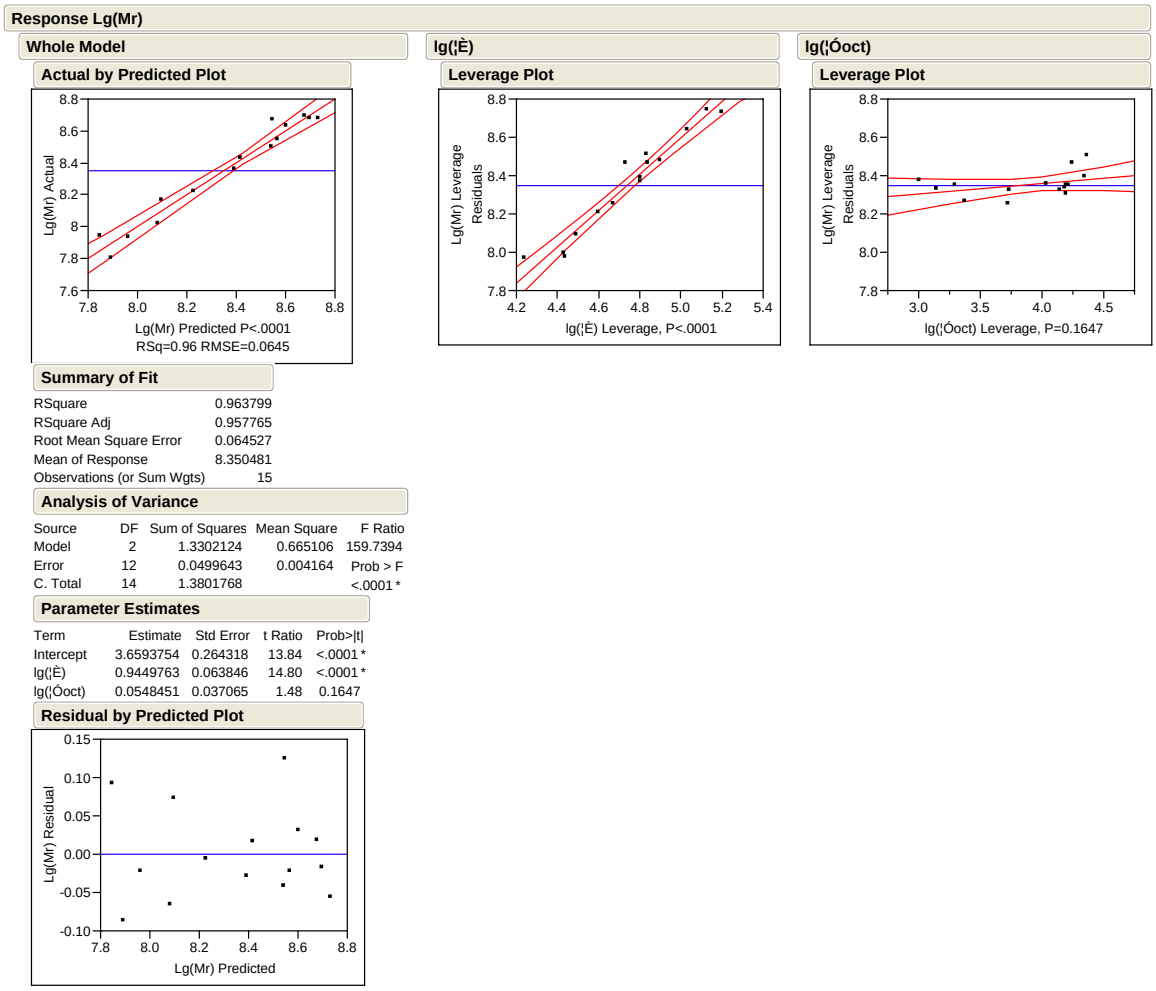

Figure 6 Multiple Linear Regression on RAP Resilient Modulus

Multivariate

Correlations

	Lg(Mr)	lg(¦È)	lg(¦Óoct)
Lg(Mr)	1.0000	0.9761	0.6102
lg(¦È)	0.9761	1.0000	0.5779
lg(¦Óoct)	0.6102	0.5779	1.0000

Scatterplot Matrix

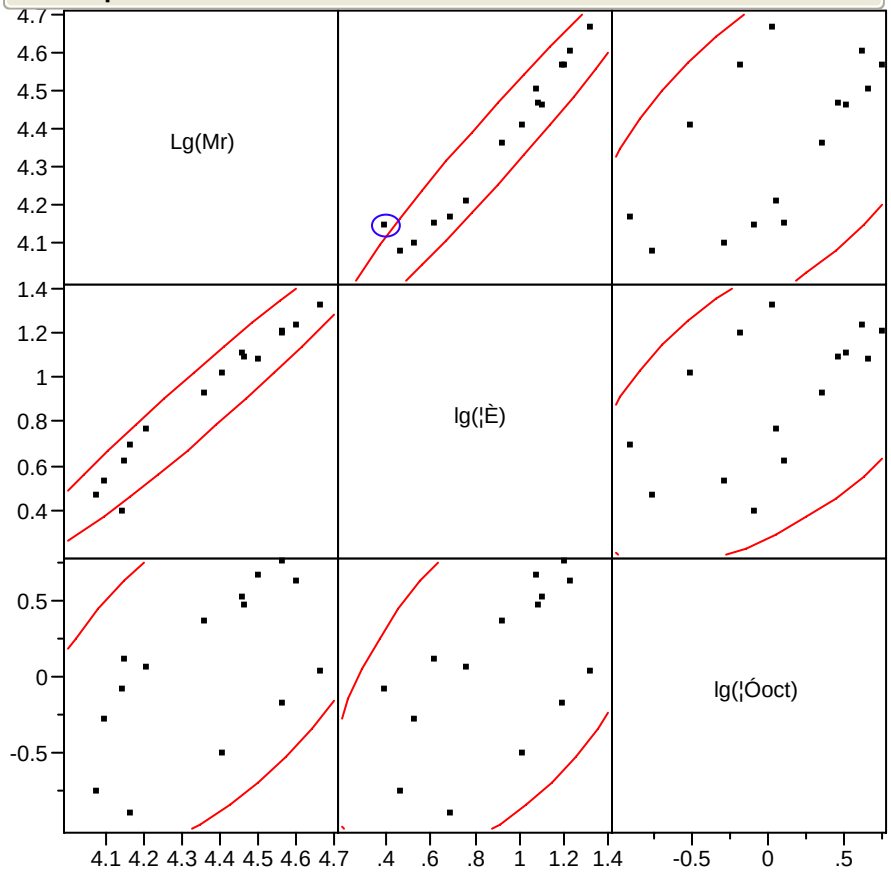

Figure 7 Correlations and Scatterplot Matrix of Limestone Resilient Modulus

Multivariate

Correlations

	Lg(Mr)	lg(¦È)	lg(¦Óoct)
Lg(Mr)	1.0000	0.9921	0.6157
lg(¦È)	0.9921	1.0000	0.6128
lg(¦Óoct)	0.6157	0.6128	1.0000

Scatterplot Matrix

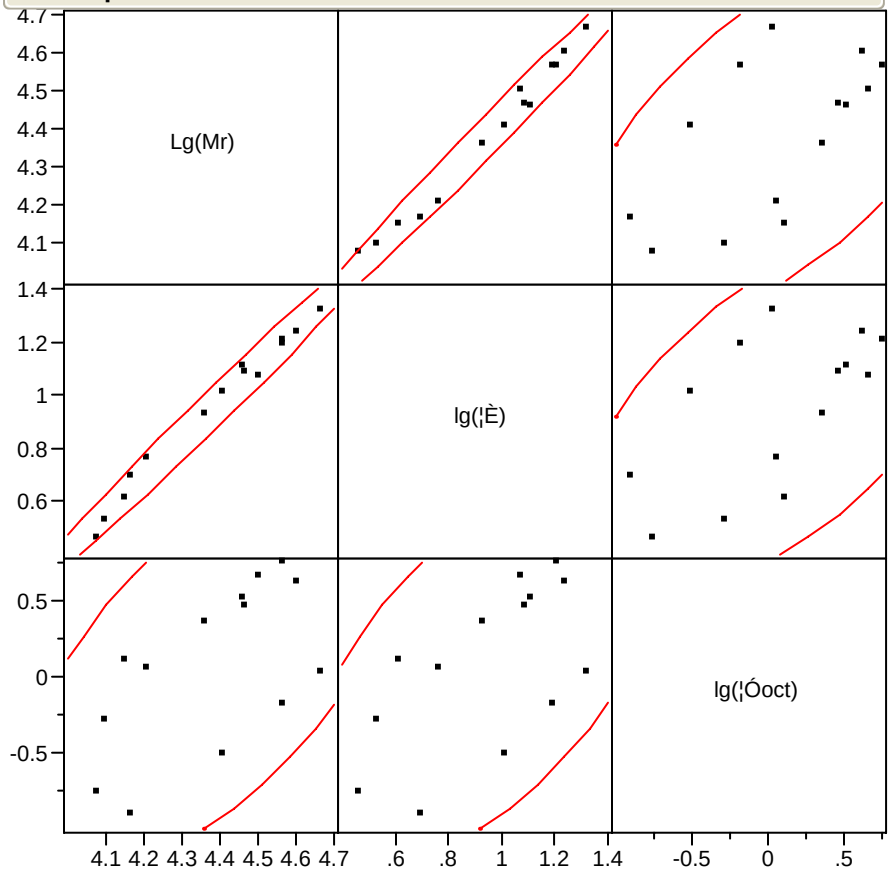

Figure 8 Correlations and Scatterplot Matrix of Limestone Resilient Modulus without Out of Region Data

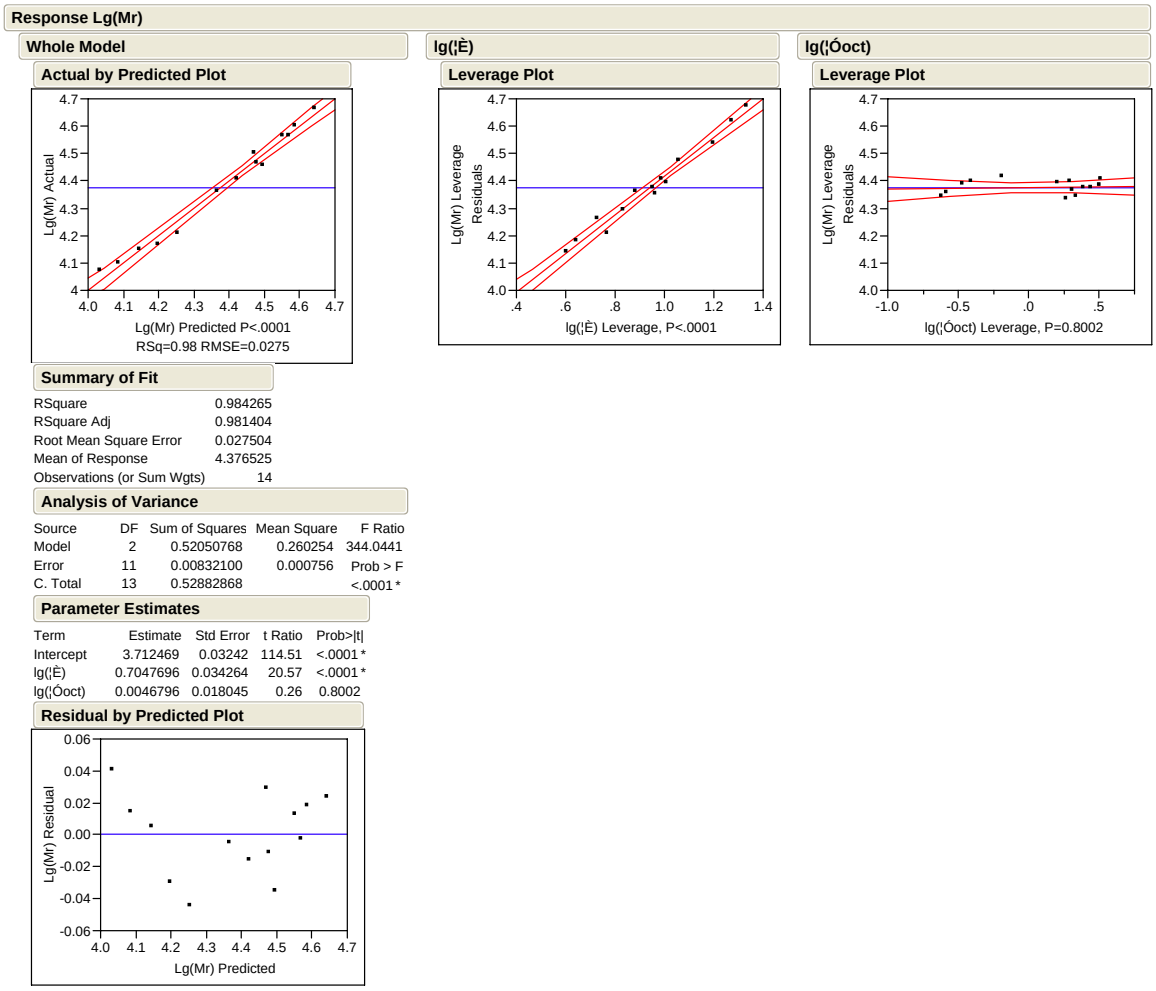

Figure 9 Multiple Linear Regression on Limestone Resilient Modulus

Multiple Regression Analysis on Gravel Resilient Modulus

Pairwise correlations were conducted firstly. No out-of-region data were indicated in Figure 10. High correlation between logarithm of mean stress and octahedral shear stress was observed. It is indicated that octahedral shear stress is less important than mean stress in resilient stress prediction. In addition, high correlation between two predict values was observed.

The regression results for gravel were listed in Figure 11. Uzan-Witczak model for Gravel is $4137\theta^{0.683}\tau_{oct}^{0.063}$ on the basis of multiple regression.

Summary of Multiple Linear Regression on Resilient Modulus

The R squares of RAP, limestone and gravel modulus are above 95%. The R squares closer to 1 represent better fits. The linear relationship between logarithm of resilient modulus and logarithm of mean stress and octahedral shear stress was accepted. The Uzan-Witczak models for RAP, limestone and gravel could be represented as $4564\theta^{0.945}\tau_{oct}^{0.055}$, $5158\theta^{0.705}\tau_{oct}^{0.005}$ and $4137\theta^{0.683}\tau_{oct}^{0.063}$ respectively.

In order to compare the stress dependency of resilient moduli of RAP, limestone and gravel, the Uzan-Witczak models are plotted into 3D surfaces. The x coordinate represents mean stress. The y coordinate represents octahedral shear stress. The z coordinate represents resilient modulus. In Figure 12, RAP, limestone and gravel are presented in blue, grey and red respectively. In triaxial test stress range, RAP tends to achieve higher resilient modulus than limestone and gavel at room temperature.

Multivariate

Correlations

	Lg(Mr)	lg(¦È)	lg(¦Óoct)
Lg(Mr)	1.0000	0.9886	0.7041
lg(¦È)	0.9886	1.0000	0.6365
lg(¦Óoct)	0.7041	0.6365	1.0000

Scatterplot Matrix

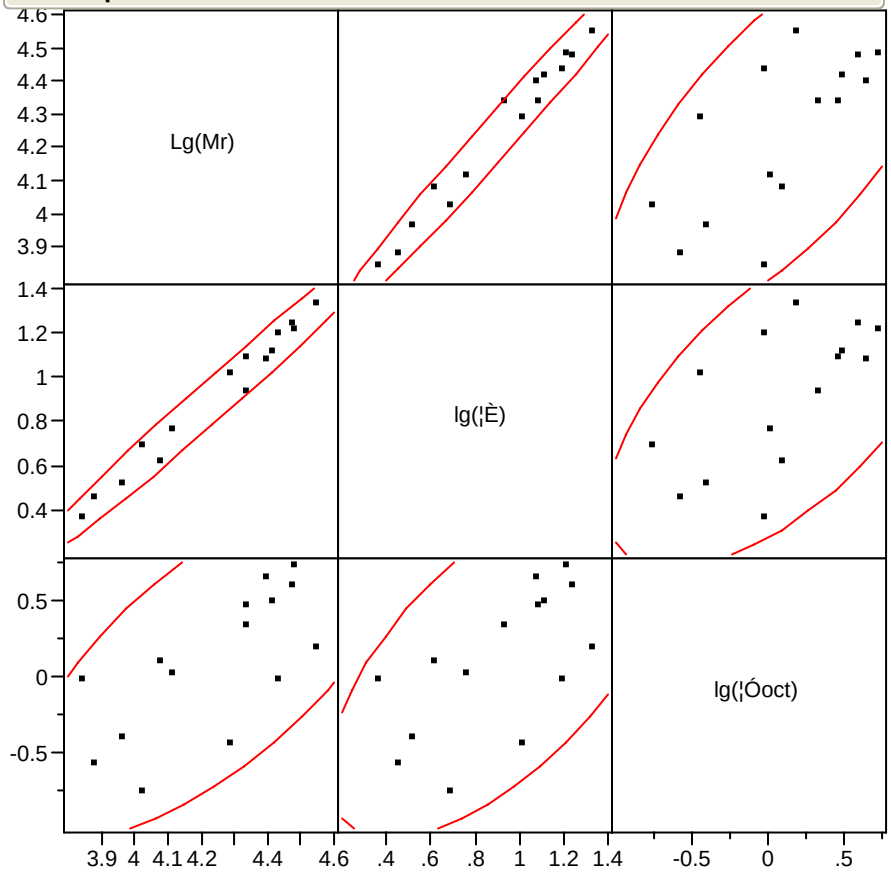

Figure 10 Correlations and Scatterplot Matrix of Gravel Resilient Modulus

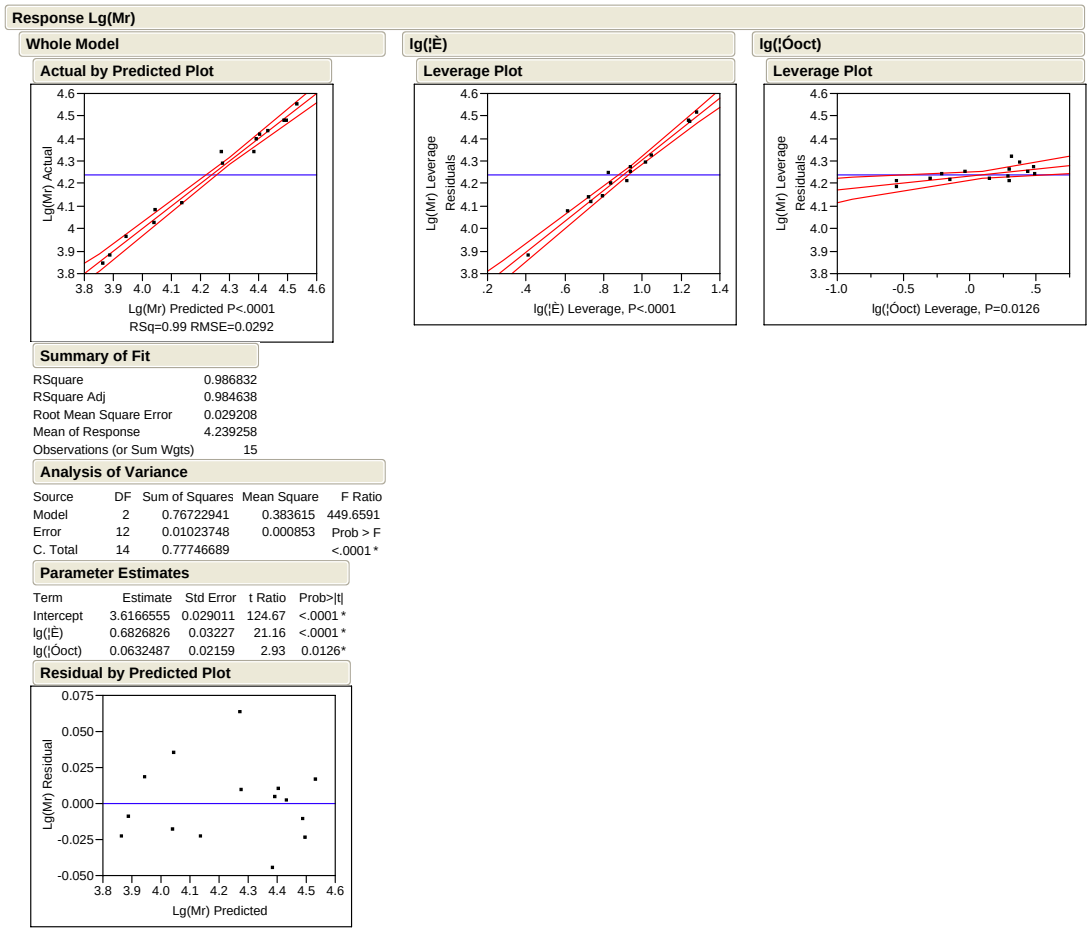

Figure 11 Multiple Linear Regression on Gravel Resilient Modulus

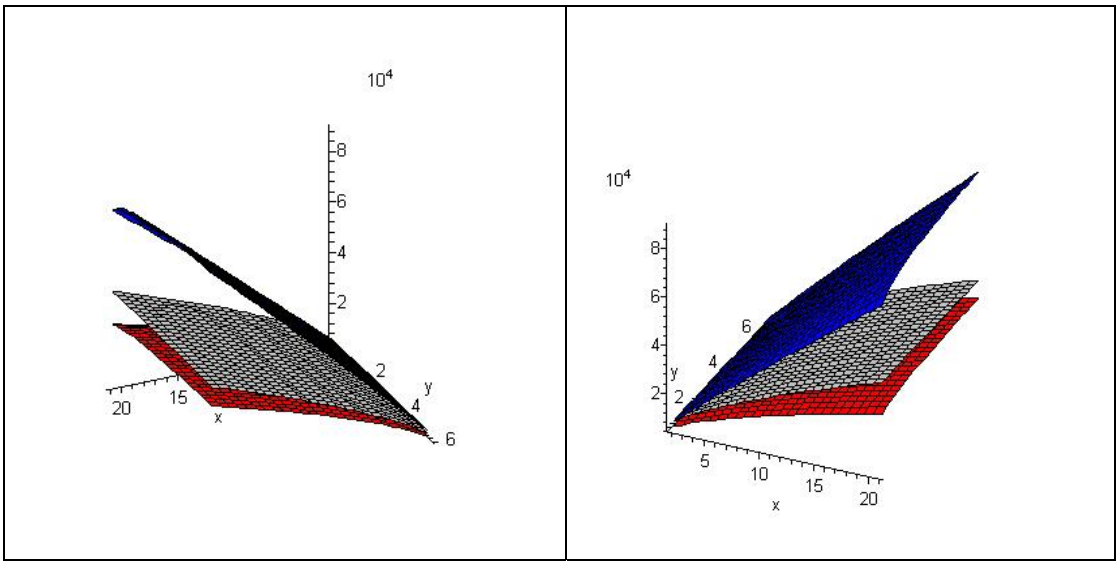

Figure 12 3D Resilient Surfaces

3.2 Triaxial Creep Tests

Triaxial static creep tests of RAP were conducted at three temperatures: 5 °C, 15°C and 25°C. From Figure 13, the viscosity in unbound RAP is observed. At 25°C, RAP specimen exhibited typical viscous material property. From Figure 14, the viscosity in unbound RAP at low temperature could be neglected. Permanent axial deformations were significantly larger than those at 15°C and 25°C. There are two possible reasons to account for this phenomenon. One is that there is difficulty to compact RAP in room temperature. RAP has open graded nature. The aged asphalt is coated around the aggregate. Thus, water is difficult to be contained during compaction. Leakage was observed during compaction of RAP. The actual moisture content of RAP may be lower than optimum moisture content. In addition, the asphalt binder coated aggregates experience reduced the interlock in RAP. More compaction work may be required for RAP. Another reason is that the viscosity exists in RAP. The creep behavior of RAP nature leads to larger permanent deformation than specimens at

lower temperature. Further discussion about the trends of RAP to higher permanent deformation would be discussed in cyclic load and unload tests.

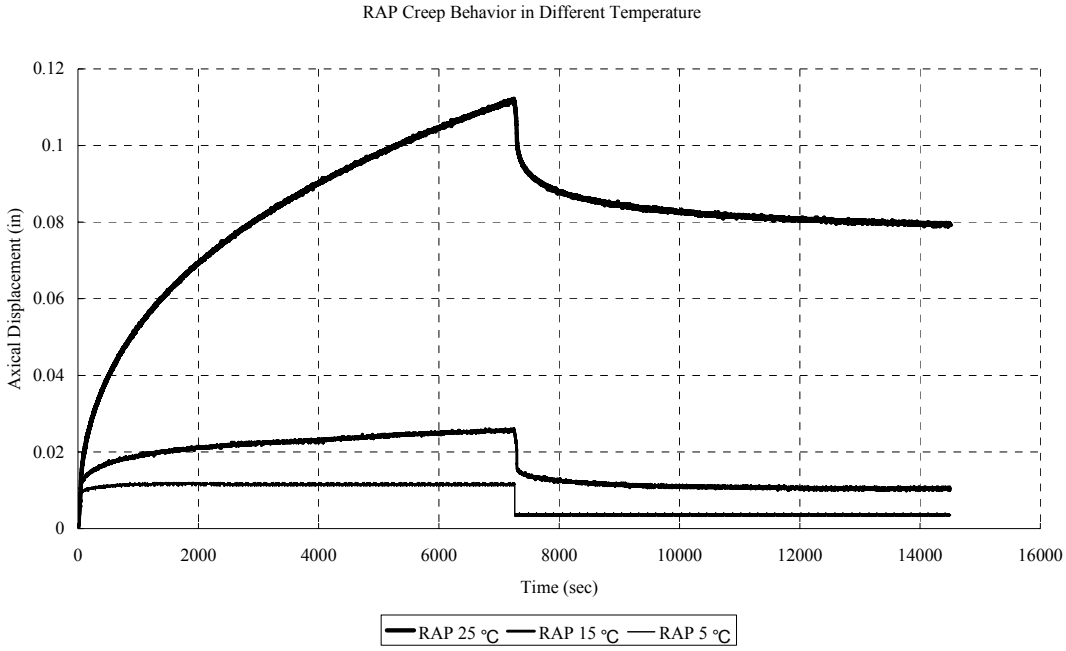

Figure 13 RAP Creep Behavior in Different Temperature

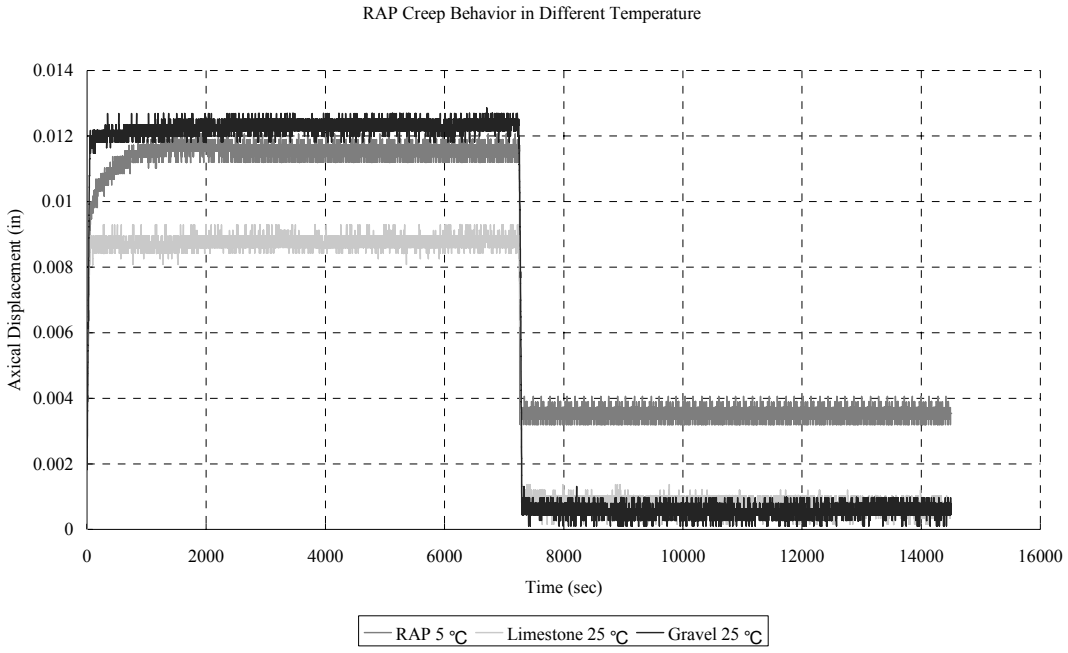

Figure 14 Creep Behavior of Limestone, Gravel and RAP

Although we can not conclude all of the permanent deformation is due to viscosity, it is observed the viscosity is not constant. The temperature dependency of viscosity can be proposed. Viscosity varies in terms of temperature. The viscosity of RAP tends to reduce when temperature drops. At 15°C, the creep behavior became insignificant. The permanent deformation was smaller than that in 25°C. At 5°C, viscosity in RAP could be neglected. The permanent deformation decreases to a low value compared with that at 25°C and 15°C.

3.3 Cyclic Triaxial Load Tests for Hysteresis Loop

The cyclic triaxial load test was conducted for RAP, limestone and gravel. Hysteresis loops were obtained through these tests.

From Figure 13 and 14, it was observed that RAP exhibited in different behavior compared with limestone and gravel at normal room temperature 25°C. In the first cycle, in Figure 15, RAP had approximate equal initial modulus with gravel. The initial modulus of limestone was larger than RAP and gravel. The modulus of RAP decreased with the increasing of load amplitude. In unloading process, the significant retarded strain recovery was observed due to the viscosity of RAP. Therefore, biggest loop area was produced in RAP specimen during its first load cycle. In addition, RAP also produced biggest permanent strain. Gravel played the second largest permanent strain. Limestone had the smallest permanent strain. This phenomenon indicated that after compaction equivalent of work, RAP was the most difficult specimen to be compacted among the three types of specimens. Limestone had been compacted most easily. Additionally, the loops in first load cycle indicated that part of permanent deformation in Figure 15 is due to the difficulty of compaction in RAP.

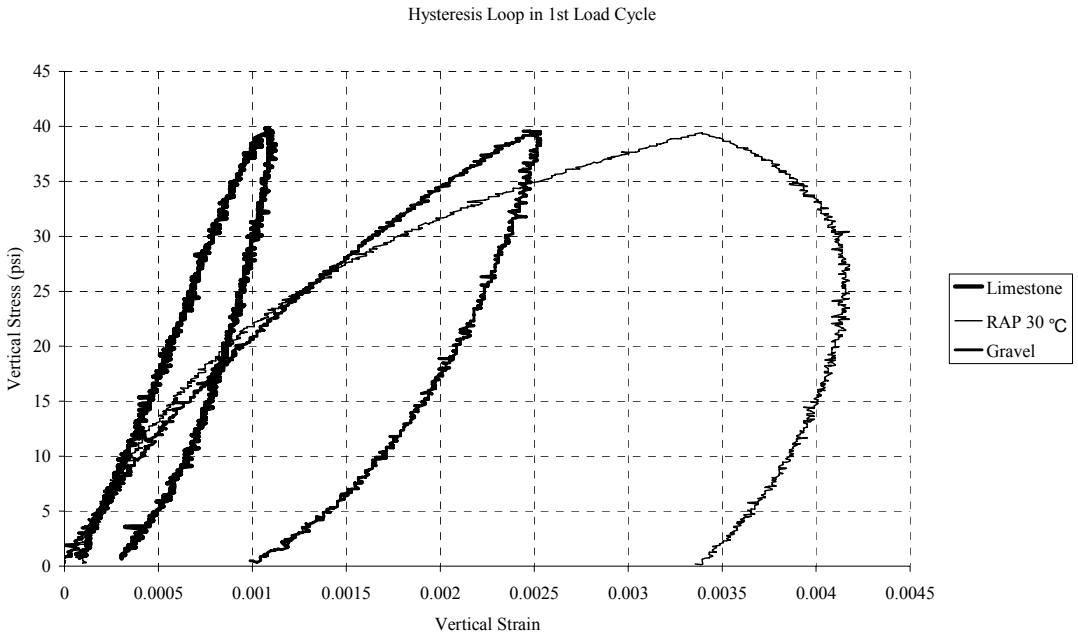

Figure 15 Stress-Strain Relationships in First Load Cycle

In Figure 16, three types of materials produced different ultimate permanent axial deformations after equivalent load cycles. The three types of specimens were

compacted with equivalent work. Theoretically, the specimens contained optimum and achieved maximum dry density. After same load cycles, the ultimate Hysteresis loops indicated that RAP specimen was not fully compacted. In other words, no additional permanent strain was produced in the last load cycle for limestone and gravel. For RAP, the additional permanent deformation was observed in the last load cycle. This indicated RAP base may more likely cause severer rutting than limestone and gravel material. Further more, in Figure 16, the total permanent strain in RAP was larger than those in limestone and gravel.

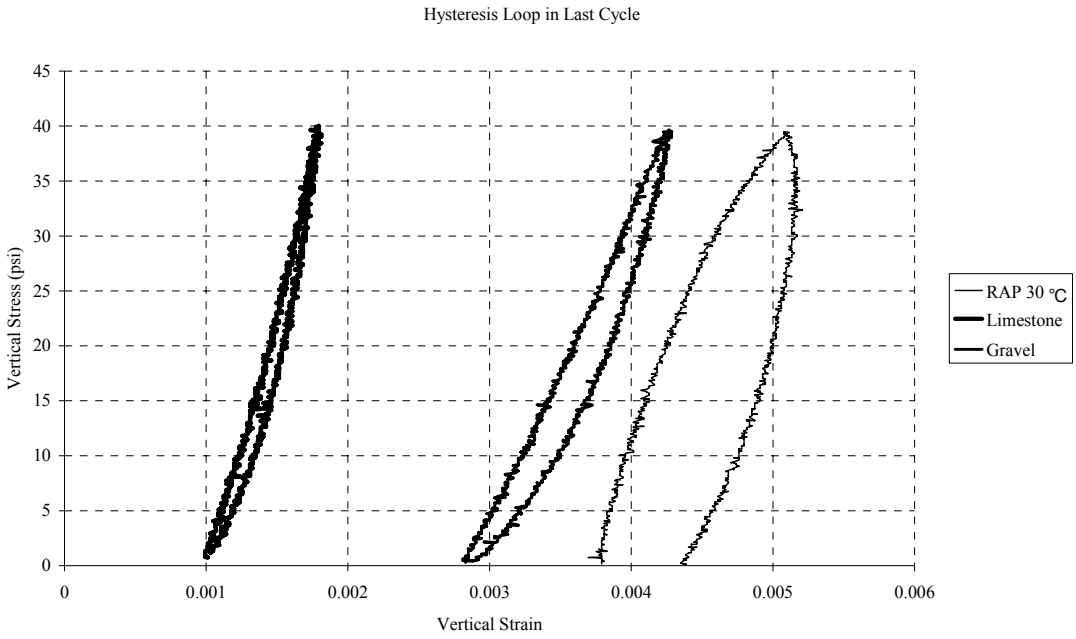

Figure 16 Stress-Strain Relationships in Last Load Cycle

3.4 Conclusion and discussion

In this study, RAP, limestone and gravel were prepared with same gradation and compaction equivalent of work. Under this condition, the following conclusion can be drawn based on the experiment tests.

- ✓ Significant viscous behavior of unbound RAP was observed. The viscosity in RAP could be neglected at low temperatures.
- ✓ At room temperature 25°C, higher resilient modulus of RAP was obtained under equal mean stress than that of limestone and gravel.
- ✓ The resilient moduli of RAP decreased while the temperature drops under room temperature.
- ✓ RAP will accumulate more permanent deformation than limestone and gravel.
- ✓ RAP requires more compaction work to eliminate permanent strain during load cycles. Longer process of compaction for RAP is estimated than limestone and gravel due to its viscous behavior.
- ✓ Limestone exhibited better resistance to permanent deformation than RAP and gravel. However it was not observed that limestone had larger resilient modulus than gravel. No significant temperature sensitivity of limestone and gravel was observed but RAP material.

In future research and practice implementation, no pure RAP base is recommended through this laboratory study. Although AASHTO T-307 resilient modulus test indicated resilient modulus of RAP with gradation in Table 1 is higher than limestone and gravel, less resistance to rutting is founded in RAP than that of limestone and gravel. Additionally, extra compaction work is required for RAP material. Alternative method of recycling RAP could be innovated on the basis of characteristics of RAP. For example, blend of RAP with limestone may reduce the viscosity and climate sensitivity in RAP and increase the resistance to rutting. The application of RAP base should avoid high temperature regions.

In some areas, the asphalt pavement layer is thinner than full pavement layer. The base temperature varies with the climate changes due to weak temperature protection from asphalt layer. Because of that, use of RAP as base material is not recommended under thin asphalt pavement and in areas with high temperature in summer.

LIST OF REFERENCES

LIST OF REFERENCES

ABAQUS CAE User's Manual, Version 6.4(2004).

Acum, W., and Fox, L., "Computation of Load Stresses in a Three-Layer Elastic System," Geotechnique, Vol. 2, 1951.

Adu-Oser, A., Little, D., and Lytton, R. (2000). "Structural characterization of unbound aggregate bases to meet AASHTO 2002 design requirements." Res. Rep. No. ICAR-502-1, Aggregate Foundation for Technology, Research, and Education.

Ahlborn, G., "ELSYM5, Computer Program for Determining Stresses and Deformatins in Five Layer Elastic System," University of California, Berkeley, 1972.

Ayers, S. "California Town Rolls Out Pavement Recycling", City Engineer, Brawley, California, 1992

Bahuguna, S., "Permanent Deformation and Rate Effects in Asphalt Concrete: Constitutive Modeling and Numerical Implementation," Ph.D. Dissertation, Case Western Reserve University, 2003.

Bennert, T., W. J. Papp, Jr. A. Maher, and N. Gucunski, "Utilization of Construction and Demolition Debris Under Traffic-Type Loading in Base and Subbase Applications", Transportation Research Record, n 1714, Nov, 2000, p 33-39

Burmister, D., "The Theory of Stresses and Displacements in Layered Systems and Application to the Design of Airport Runways," Proceedings, Highway Research Board, 1943.

Chan, F., Barksdale, R.D., and Brown, S.F., "Aggregate Base Reinforcement of Surfaced Pavements," Geotextiles and Geomembranes, Vol. 8, 1990, pp. 165-189.

Christoffersen, J., Mehrabadi, M., and Nemat-Nasser, S. (1981). " A micromechanical description of granular material behavior." J. Appl. Eng., 48, 339-344

Coetzee, N. F., B. L. Urban, and S. K. Takahashi, "Oxnard Airport and Base Course Recycling", Proceedings of the Transportation Congress, v 1, 1995, p 489-499

Cowin, S. C. (1985). "The relationship between the elasticity tensor and the fabric tensor" Mech. Mater., 4, 137-147.

Defoe, J. H. "Use of Recycled Asphalt Materials in the Construction of a Bituminous Stabilized Base." Final Report. Michigan Department of Transportation, 1982

Dehlen, GL., Monismith, CL., "Effect of Nonlinear Material Response on the Behavior of Pavements Under Traffic" Highwy Research Record 310, HRB, Washington, DC, 1970, pp 1-16

Duncan, J.M., Monismith, C.L., and Wilson, E.L., "Finite Element Analysis of Pavements," Highwy Research Record 228, HRB, Washington, DC, 1968, pp18-33

Du, J., Dusseault, M. (1994). "A generalized D matrix for anisotropic elastic granular media." Int. J. Numer. Analyt. Meth. Geomech., 18, 107-120

Freeme, C.R., and Marais, C.P., "The Structural Behaviour of Bituminous Surfacings in an Experimental Asphalt Pavement," Proceedings, Third International Conference on Structural Design of Asphalt Pavements, University of Michigan, 1972.

Freeme, C.R., "Comparison between Field Measurements and Elastic and Non-Linear Finite Element Solutions of the Flexibility Sections of the S12/2 Experimental Asphalt Pavement," Research Report, National Institute of Road Research, South Africa, 1971, pp 34

Figueroa, JL; Thompson, MR, "Simplified Structural Analyses of Flexible Pavements for Secondary Roads Based On Illi-Pave". *Transportation Research Record, Issue 766,* 1980, pp 5-10.

Garg, N., Thompson, M. R. "Lincoln avenue reclaimed asphalt pavement base project" Transportation Research Record, n 1547, Nov, 1996, p 89-95

Garza, S. G., "Integration of Pavement Nondestructive Evaluation, Finite Element Simulation, and Air Quality Modeling for Enhanced Transportation Corridor Assessment and Design," The University of Mississippi, 2003

Giroud, J. P., and Noiray, L. (1981). "Geotextile reinforced unpaved road design". J. Geotech. Eng. Div., Am. Soc. Civ. Eng., 107(9), pp 1233-1254

Gomez, M. and Thompson, M.R., "Mechanistic Design Concepts for Full-Depth Asphalt Concrete Pavements," *FHWA-IL-UI-207; UILU-ENG-84-2006,* 1984, pp 229.

Hank, A. J., and E. R., Magni. "The Use of Recovered Bituminous and Concrete Material in Granular and Earth." Final Report. Ministry of Transportation. Ontario, Canada, 1984—(need to find out)

Hoffman, MS; Thompson, MR., "Backcalculating Nonlinear Resilient Moduli From Deflection Data," *Transportation Research Record,* Issue, 852, 1982, pp 42-51

Holtz, R. D., and Sivakugan, K. (1987). " Design charts for roads with geotextiles." Geotext. Geomembr., 5(3), 191-200

Hjelmstad, K. D. and Taciroglu, E. (2000), "Analysis and Implementation of Resilient Modulus Models for Granular Solids" Journal of Engineering Mechanics, Vol. 126, No. 8, pp. 18211

Hua, J. "Finite element modeling and analysis of accelerated pavement testing devices and rutting phenomenon," Ph.D. Dissertation, Purdue University, West Lafayette, Ind., 2000

Huang, B. (2000),"Fundamental Characterization and Numerical Simulation of Large Stone Asphalt Mixtures" PhD thesis, Louisiana State University, Baton Rouge.

Huang, S. (2004), Mei, S. and Gong, W., "Testing study on bearing behavior of piles for Nanpan river great bridge in karst area" Yanshilixue Yu Gongcheng Xuebao/Chinese Journal of Rock Mechanics and Engineering, v 23, n 5, Mar 1, 2004, p 809-813

Huang, Y. H., "Pavement Analysis and Design," Prentice Hall, Englewood Cliffs, 1993

Irwin, L.N. "Determination of Pavement Layer Moduli from Surface Deflection Data for Pavement Performance Evaluation". Proceedings of Fourth International Conference on Structural Design of Asphalt Pavements, No.1, University of Michigan, Aug. 1977.

Jong, D.L., eutz, M.G.F., and Korswagen, A.R., "Computer Program BISAR: Layered Systems under Normal and Tangential Loads," External Report AMSR.0006.73, Koninklijke Shell-Laboratorium, Amsterdam, 1973.

Kanatani, K. (1984). “Stereological determination of structural anisotropy.” Int. J. Eng. Sci., 22(5), 531-546.

Kenis, WJ., “Predictive Design Procedures, Vesys Users Manual--An Interim Design Method For Flexible Pavements Using the Vesys Structural Subsystem”. *FHWA-RD-77-154 Final Rpt.; FCP 25C0-000,* 1978, pp 133.

Kent, JS; Buddin, AL., “An Evaluation of the Bird/Aircraft Strike Hazard Dyess Air Force Base, Texas,” *Report No: AFETO-TM-8-78*, 1978, pp 54.

Konrad, J. M., and O. Juneau. “Limit-State Curve of Base-Course Material and its Relevance for Resilient Modulus Testing. Journal of Geotechnical and Geoenvironmental Engineering, Vol. 132, No. 2, February 1, 2006.

Li, Q., S. L. Ma, P. F. Wang, and Z. Li, “Experiment Study on the Performance of Cement Stabilized Recycled Asphalt Mixture” Journal of Highway and Transportation Research and Development, Vol. 21, No. 5, 2004

Long, F. M., “Permanent Deformation of Asphalt Concrete Pavements: A Nonlinear Viscoelastic Approach to Mix Analyses and Design,” University of California, Berkeley, 2001

Love, J. P., Burd, H. J., Milligna, G. W. E., and Houlsby, G. T. (1987). “Analytical and model studies of reinforcement of a layer of granular fill on a soft clay subgrade.” Can. Geotech. J., 24, pp 611-622

Maher, M. H., Gucunski, N., and Papp Jr., W. J., “Recycled Asphalt Pavement as a Base and Sub-base Material”, Testing Soil Mixed with Waste or Recycled Materials, ASTM STP 1275, American Society for Testing and Materials, 1997

Majidzadech, K., Kaufmann, E., and Saraf, C.L., "Analysis of Fatigue of Paving Mixtures from the Fracture Mechanics Viewpoint," ASTM Special Technical Publications (STP), 1972, pp 67-84.

McCullough, B. F., and A. Taute. "Use of Deflection Measurements for Determing Pavement Material Properties". Transportation Research Record 852, TRB, National Research Council, Washington, D. C., 1982, pp. 8-14

Mun, S., "Nonlinear Finite Element Analysis of Pavements and its Application to Performance Evaluation," Ph.D. Dissertation, North Carolina State University, 2003

Munzenmaier, A. Marvin "City saves by using recycled asphalt as base", Public Works, v 125, n 7, Jun, 1994, p 62-63

Nemesdy, E; Keleti, I; Boromisza, T; Gaspar, L, Jr., "Trends in the Development of Flexible Pavement Design in Hungary," Proceedings of 4th International Conference on Structural Design of Asphalt Pavements, Vol. I, 1977, pp 417-423.

NRC(1994), SUPERPAVE mix design system manual of specifications, test methods, and practices, ET Harrgan, RB Leahy, and JS Youtcheff (eds), SHRP-A-379, Strategic Highway Research Program, National Research Council, Washington DC.

Oda, M., and Nakayama, N. (1989). "Yield function for soil with anisotropic fabric." J. Eng. Mech., 115(1), 89-104

SEIBI, A. C., "Development of Constitutive Relations for Asphalt Concrete under High Rates of Loading (Loading Durations, Viscoplastic Response)", The Pennsylvania State University, 1993

SHRP. “SHRP’s Layer Moduli Backcalculation Procedure: Software Selection”. Contract No. SHRP-90-P-001B, Prepared by PCS/Law Engineering for SHRP, 1991.

Sherwood, JA; Kenis, WJ., “Sulphlex Pavement Performance Evaluations From Laboratory Tests”. *Transportation Research Record, Issue 85,* 1982, pp 60-68.

Smith, R.B., and Yandell, W.O., “Use of Mechano-Lattice Analysis in Prediction of Pavement Performance,” Australia Road Research Vol. 16, No. 1, 1986, pp. 10 – 17.
Waterhouse, A., “Stresses in Layered Systems under Static and Dynamic Loading,” Proceedings, Second International Conference on the Structural Design of Asphalt Pavements, University of Michigan, 1967.

Stubstad, R.N., and B. Connor. “Use of the FWD to Predict Damage Potential to Alascan Highways during Spring Thaw”. Transportation Research Record 930, TRB, National Research Council, Washington, D. C., 1983, pp. 46-51.

Taha, R., Ali, G., Basma, A., Al-Turk, “Evaluation of reclaimed asphalt pavement aggregate in road bases and subbases” Transportation Research Record, v 1, n 1652, 1999, p 264-269

Tobita, Y. (1989). “Fabric tensors in constitutive equations for granular materials.” Soils Found., 29(4), 99-104.

Truesdell, C., and Noll, W. (1965). “ The nonlinear field theories of mechanics.” Handbuch del Physik III/3, S. Flugge, ed.

Tutumluer, E., and Seyhan, U. (1999). “Laboratory determination of anisotropic aggregate resilient moduli using an innovative test device.” Transportation Research Record. 1687, Transportation Research Board, Washington, D. C., 13-21.

Uzan, J; Livneh, M; Shklarsky, E, "Cracking Mechanism of Flexible Pavements," *ASCE Journal of Transportation Engineering*, Vol. 98, Issue: te1, 1972, pp 17-36

Uzan, J; Livneh, M; Eshed, Y., "Investigation of Adhesion Properties between Asphaltic-Concrete Layers," *Association of Asphalt Paving Technologists Proc,* Vol. 47, 1978, pp 495-521

Uzan, J; Sides, A; Perl, M., "Viscoelastoplastic Model For Predicting Performance Of Asphaltic Mixtures," *Transportation Research Record,* Issue 1043, 1985, pp 78-89

Waterhouse, A., "Stresses In Layered Systems under Static and Dynamic Loading," *Intl Conf Struct Design Asphalt Pvmts* Preprint Supplement, 1967, pp 26-39

William, G.W., "Backcalculation of Pavement Layers Moduli Using 3D Nonlinear Explicit Finite Element Analysis" M.S. Thesis, West Virginia University, 1999

Witczak, M. W. and Uzan, J. (1988). "The universal airport pavement design system." Rep. I of V: Granular Material Characterization, Dept. of Civ. Engrg., University of Maryland, College Park, Md.

Yandell, W.O., "Prediction of the Behavior of Elastoplastic Roads during repeated rolling Using Mechano-Lattice Analogy," Highway Research Record 374, 1971, Washington, D.C., pp. 29 – 41.

Yandell, W.O., "How the Plastic Behavior of Asphalt Mixtures Influences Pavement Life," Asphalt Rheology: Relationship to Mixture, 1987, pp 76-98.

Yoo, P. J.,I. L. Al-qadi, M. A. Elserfi and I. Janajreh. (2006) "Effect of Moving Wheel Load Amplitude and Interface Condition on Flexible Pavement Responses"

Zaghloul, SM; White, TD; Kuczek, T., "Use Of Three-Dimensional, Dynamic, Nonlinear Analysis To Develop Load Equivalency Factors For Composite Pavements," Transportation Research Record, Issue 1449, 1994, pp. 199-208.

Zysset, P. K., and Curnier, A. (1995). "An alternative model for anisotropic elasticity based on fabric tensors." Mech. Mater., 21, 243-250

Zuo, G. (2003). "Impacts of Environmental Factors on Flexible Pavements" PhD thesis, University of Tennessee, Knoxville.

APPENDIX

A: FE Simulation of Pile Socketed into rock with Cavity

Chapter 1 Introduction

As Karst causes serious problems for highway engineering, certain measures need to be taken before construction. Predicting the influence of karst to various forms of highway foundations will help to design appropriate treatment thus to minimize the adverse effect of Karst.

There are two critical considerations for the construction and design of drilled shaft socketed in rocks. One is the selection and implementation of construction, the other is the utilization of load transfer in skin friction and end-bearing for design. Reese and O'Neill(1988) presented comprehensive studies of drilled shaft. The compressive strength of rock and the settlement between the drilled shaft and rock influences the magnitude and distribution of side resistance transferred downward significantly. Base simple engineering judgment, the cavernous bed rock will cause larger settlement comparing to sound bed rock. Thus, different side resistance load transfer mechanism is produced. Simultaneously, the end bearing capacity changed.

After many load tests are conducted in order to study load-transfer mechanisms. It is widely accepted that the ultimate shaft resistance for large bored piles is mobilized after small displacements of the shaft with respect to the surrounding weathered rock (De Beer 1986; Reese and O'Neill 1988; Ghionna et al. 1993). However, before the ultimate capacity is achieved, the settlement was accumulated enough to cause the collapse of supported structure.

Although much works has been done for rock-shaft interaction (Webb 1977; Hassan 1977), less is known about the behavior of drilled shafts over cavernous bedrock.

This part focuses on the numerical simulation of influence of karst cavity to the stability of highway bridge foundation. The commercial finite element software, ABAQUS 6.4, was utilized for the numerical simulation. 2-D and 3-D finite element

analyses (FEA) were employed to analyze the stress and strain distributions due to karst cavities. Comprehensive sensitivity analyses were conducted for a better understanding of the influence of karst cavities. The FE model was validated through the comparison of numerical simulation to an actual pile load test. Finally, 3-D FEA was conducted for a simulated bridge foundation with group of piles, in which the influence of karst to the structure-subgrade interaction was numerically simulated.

The bearing capacity of drilled shaft consists of two portions: one is end bearing capacity; the other is side frictional resistance. The load-deformation relationship for drilled shaft is often employed to predict the load capacity. There are several predicting techniques for f-w curves in soils (Kraft et al. 1981; Castelli et al. 1992; Vijayvergiya 1977) and rocks (Baquelin et al. 1982; O'Neill and Hassan 1997). Both finite-difference techniques and finite-element methods are used to predict load-deformation curve. Usually, finite difference techniques are based on the assumption that the load transfer of a certain pile section and pile tip resistance are independent of pile displacement in other place. These techniques are generally based on load tests on full-scale, instrumented shafts. Additionally, parametric finite-element analyses are often employed for p-w curve prediction (Hassan 1997).

Johnston et al. (1989) have conducted significant experimental and analytical researches to view that the shaft-rock interface consists of triangular asperities. More recently, for the situation like geomaterial is massive or horizontally bedded, shaft was drilled with an auger, and water is introduced into the borehole, the writers in claystone formations in Texas have revealed that the interface profile is approximately sinusoidal. Hassan and O'neill(1997) assumed sinusoidal undulations along shaft-geomaterial interface in their elastic-plastic axisymmetric finite element analyses of drilled shafts socketed into cohesive intermediate geomaterials.

Dr. Jori O. Osterberg, Professor Emeritus of Civil Engineering at Northwestern University, invented and developed a deep foundation load testing device to meet the

construction industry's need for an innovative effective method for testing high capacity drilled shafts and piles. Osterberg-Cell method is developed to provide a more economical means for conducting load tests for drilled shaft (Osterberg and Pepper 1984). It has been used for the field load testing of drilled shafts (Schmertmann 1993). A load test made with the Osterberg Load Cell is different from a conventional load test, since there is a separation of the end bearing and skin friction components for resisting applied loads. Consequently, this test method allows geotechnical engineers to more accurately estimate pier capacity and to design and construct more cost-effective foundations. The expense of unnecessary conservative designs can be reduced and the risk of underdesigned foundations can be minimized. The Osterberg Load Cell is a specialized pressure cell that is placed at the bottom of the excavation for a drilled test pier or pile. It has a hydraulic line extending from the cell to the top of the excavation. After placement, the pier excavation is filled with concrete. The cell is designed to expand both upward and downward when it is pressurized by way of the hydraulic line. The downward force from the bottom of the cell is resisted by the bearing stratum while the upward force from the top of the cell is resisted by the weight of the pier and by the skin friction along the sides of the pier. The test pier is instrumented with telltales to measure the upward and downward displacement of the cell. Very large loads can be applied with the Osterberg Load Cell. Test piers can be constructed vertically, slanted, in a building, in water, or in otherwise inaccessible locations

For nowadays rapid development in computer technology, much more accurate algorithms could be precedent over earlier concerns to computing speed and capacity. That made it possible for detailed modeling on O-cell tests with consideration of roughness of shaft-rock interface. Fellenius (1999) used the Advanced Geotechnical Analysis Code (AGAC) FE program developed by Altaee(1991) to simulate O-cell tests applied on barrettes to support interior columns with rectangular shaped, 2.4m2 cross section. The program assumed the soil as an elastic-plastic material. The bounding surface plasticity model (Bardet 1986; Altaee 1991) was employed to

model the stress—strain-strength response of the soil. More recently, Zuo and Drumm (2004) performed an axisymmetric model to simulate the O-cell tests applied on shafts socketed into mica schist. The sinusoidal interface profile of Hassan and O'Neill (1997) was adopted in the models.

Since there are few of efforts has been done to find the load-deformation relationship of drilled shaft under cavernous bed rock, the O-cell test results are used to validate axisymmetric models and 3 dimensional models which are constructed to analysis load capacity sensitivity under the assumption of roughness side resistance sinusoidal interface.

Chapter 2 Methodology

For the economical purpose of computing time, axisymmetric model was first employed to back calculate the rock and concrete properties and rock-shaft frictional interface. An O-cell field test was simulated with the axisymmetric model. The field test date was fitted by the finite element model's load-deformation curves. Related to axisymmetric model, 3-dimensional models were constructed. Comparing the two groups of computation results is adopted to validate 3-D models. Subsequently 3-dimentional models were used to analysis the sensitivity under variety of cavities' location and different rock types. Both end-bearing capacity and side resistance were analyzed. In order to provide practical guide, 3-D elastic-plastic model of pile groups with six shafts are employed to estimate the influence for safety factor under static load.

2-D Finite Element Modeling

An axisymmetric model was adopted in the analysis using ABAQUS (2004), with the mesh extending 32.5 m laterally from the axis of symmetry and 100 m vertically from the bottom of the shaft. As shown in Figure 17, this width is about 12 times the socket diameter and the depth is 2 times the length of the rock socket. The weight of the rock and the shaft were applied as gravity to the model with equilibrium to initial geostatic stress. The model consists of the upper portion of the pile, the lower portion of the pile, and the rock surrounding the shaft.

8-node biquadratic axisymmetric quadrilateral elements were assigned to both the rock portion and shaft portion with reduced integration., The left and right boundaries of model were restricted in the horizontal or U1 direction, and the entire bottom boundary was assumed to have zero vertical displacement (in the U2 direction).

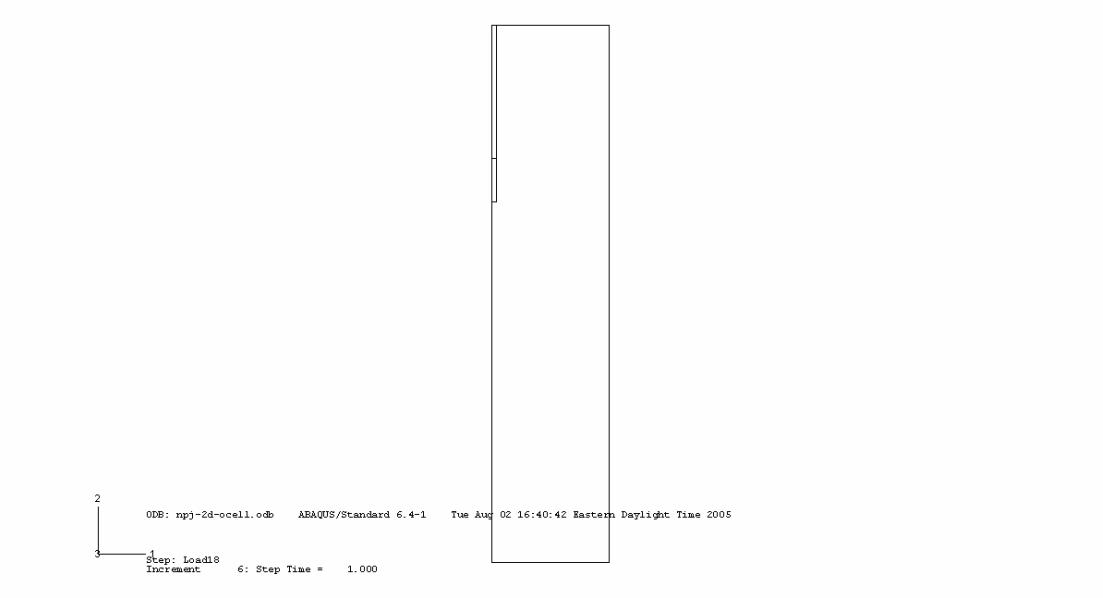

Figure 17 Axisymmetric Model for the Cast-in-place Pile

The general analysis consists of two stages: firstly, the initial geostatic stresses is applied due to the dead-load of rock and shaft. Then, structural axial upward and downward are applied where the load cell locates. According to the field test report from China Southeast University, the O-cell was installed 12 m from the bottom of shaft.

Two dimensional axisymmetric FE model was considered for single pile FE analysis without any cavities. The adoption of 2-D FE analysis significantly reduced the time amount in computation and greatly increase the efficiency for certain analyses. 2-D FEA was mainly used to calibrate material properties in this study.

Concrete and Rock Material Properties

The material property of concrete shaft was assumed to be linear elastic. Both the slightly weathered and highly weathered dolomites were assumed to be elastic-perfectly plastic and were represented by the Drucker-Prager model (ABAQUS,

2004). The highly weathered dolomite surrounding the lower 12 m of the shaft below the position of the O-cell (which included the repaired cavity) was assigned different material properties than the slightly weathered dolomite elsewhere in the mesh, as indicated in Table 3. The bulk rock properties were based on information from the geotechnical exploration. Although there are limitations to the types of response that can be represented by the Drucker-Prager model, it is a relatively simple constitutive model, requires relatively fewer parameters which are usually available in practice, and thus was used for the rock response. A non-associative flow rule was used with the dilation angle ψ assumed to be half the angle of friction to avoid unrealistically high dilation.

Concrete – Rock Interface Modeling

Hassan and O'Neill (1997) proposed a sinusoidal profile to simulate the rough interface between a shaft and rock socket. In their models, the rough interface was idealized by sequential curvilinear segments that formed a sinusoidal profile with a long wavelength. They considered a sinusoidal curve with a wavelength of about 0.3 m as the longest wavelength normally observed, and chose double amplitude of the sinusoidal wave 25.4 mm.

Table 3 Rock Properties List

Rock property	Rock #1	Rock #2	Rock #3	Rock #4
Compressive strength (MPa)	150	110	70	30
Cohesion (MPa)	16	7.8	3.5	1.1
Friction angle	42	36	30	24
Young's Modulus (GPa)	75	32	11	3
Poisson's Ratio	0.2	0.23	0.26	0.3

In cases where the observed side resistance at the interface is greater than the resistance due solely to friction, the sinusoidal interface can be used to provide an apparent cohesive strength. Zuo et al. (2004) used the sinusoidal rock socket approach to model the friction developed in a drilled shaft in weathered schist. Using the observed response from O-cell testing, the properties of the rock and concrete-rock interface were back-calculated and then used to model the top down loading. It was shown that the interface properties could be calibrated based on the O-cell data based on the following steps:

- ✓ Assume that the rock concrete could be represented as linear elastic with known Young's modulus and Poisson's ratio. Assume an interface with an asperity wavelength of 0.3 m (after Hassan and O'Neill (1997) recommendation and an initial estimate of the asperity magnitude
- ✓ Back-calculate Young's modulus for the rock by matching the initial (nearly linear) portion of the O-cell loading curve.
- ✓ Based on the nonlinear portion of the lowered O-cell loading plate, tune the Drucker –Prager parameters to obtain the approximate measured response.
- ✓ By varying the interface friction angle and double amplitude of asperities, tune the model to approximate the measured response of the O-cell test.

A similar approach was utilized here, except that because of the limited resistance offered by the highly weathered rock surrounding the bottom of the shaft, the friction parameters of the upper shaft in the slightly weathered dolomite were calibrated first. Due to the long length of the shaft in the slightly weathered dolomite (about 37 m), a wavelength of 2 m was used to reduce the number of interface elements. The double amplitude of the asperities was then varied to achieve the best match between measured and computed displacements in the upper shaft above the O-cell.

The profile of the interface between the shaft and the rock socket is a series of concave and convex segments. Before the shaft is loaded, there is no relative movement and the shaft is in close contact with the rock with no gap in between.

When the shaft is loaded, the front of a convex part on the shaft is pushed towards the relevant concave part in the rock, and it leaves a gap behind. Therefore, it would be anticipated that the stress distribution along the sinusoidal interface is not as gradual as along a straight interface. Part of the deformed mesh of the shaft-rock contact is shown in Figure 18. It should be noted that the deformation has been exaggerated. In reality, the interface is always rough to some extent, although the wavelength and the amplitude are neither constant nor usually known. A sinusoidal interface with constant wavelength and amplitude is an artificial mechanism to impart a cohesive strength term to the interface and in this case would appear as a very smooth contact surface when viewed with respect to the size of the shaft. By varying the interface properties to generally follow the upward load–deflection response as recorded on the top surface of the O-cell, the interface parameters were determined. These calibrated interface parameters are shown in Table 3, and were used for the contact both above and below the O-cell. The modulus of the highly weathered rock in the lower socket was chosen based on the reported rock properties and to provide reasonably good prediction of the observed downward response of the O-cell.

3-D Finite Element Modeling

With the introduction of cavities, it was necessary to use 3-D FEA to simulate the pile-subgrade interaction when cavities locate underneath the shaft with variety of eccentric location. Similar to axisymmetric model, the model is made up of three portions: up shaft, down shaft and rock surrounding the shaft. The shaft is assumed to depart into up portion and down portion where Osterberg load cell was set. As Figure 19 and Figure 20 shows, 3-D model was constructed exactly with the same geometry size of the axisymmetric model. The single pile is assumed as in a continuous elastoplastic medium. A plane passing the axis and paralleling the axis is imagined to cut the rock and shaft along the vertical axis of shaft. The area extending 32.5m laterally and vertically 100m nearly 2 times of shaft's length are modeled. 10-node modified quadratic tetrahedron elements (C3D10M) and 20-node quadratic brick with reduced integration elements (C3D20R) are assigned on shaft and rock portion.

Table 4 Model Parameters Calibrated from Numerical Analysis

Slightly Weathered Dolomite		
Elastic:	Young's modulus (Pa)	3.00E+10
	Poisson's Ratio	0.3
	Mass Density (kg/m^3)	2400
Plastic: (Drucker Prager)	Angle of Friction (degrees)	24
	Flow Stress Ratio	0.8
	Dilation Angle (degrees)	12
	Yield Stress (Pa)	1.10E+06
	Abs plastic strain	0
Highly Weathered Dolomite		
Elastic:	Young's modulus (Pa)	1.60E+08
	Poisson's Ratio	0.3
	Mass Density (kg/m^3)	2400
Plastic: (Drucker Prager)	Angle of Friction (degrees)	24
	Flow Stress Ratio	0.8
	Dilation Angle (degrees)	12
	Yield Stress	1.1E+06 Pa
	Abs plastic strain	0
Drilled Shaft Concrete		
Elastic:	Young's modulus (Pa)	3.00E+10
	Poisson's Ratio	0.2
	Mass Density (kg/m^3)	2400
Sinusoidal concrete/rock Interface		
Elastic:	Friction Coefficient	0.115
	Specific maximum displacement (m)	0.01
	Amplitude (m)	0.005
	Wavelength (m)	2

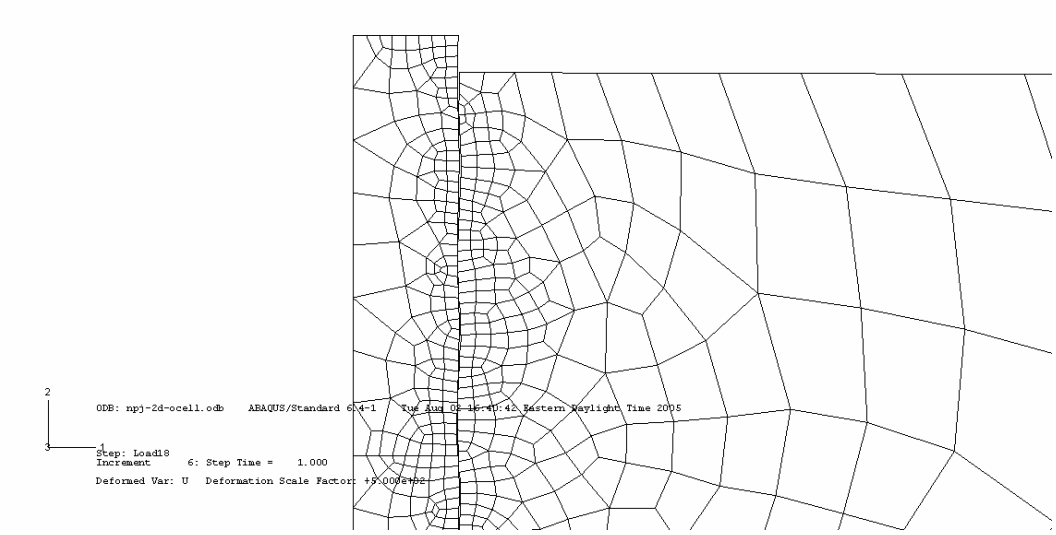

Figure 18 Deformed Mesh of Rock-Concrete Sinusoidal Contact Interface

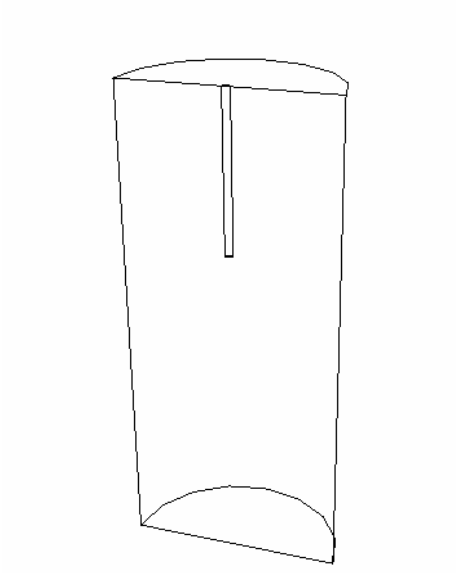

Figure 19 3-D model for the Osterberge Test Simulation

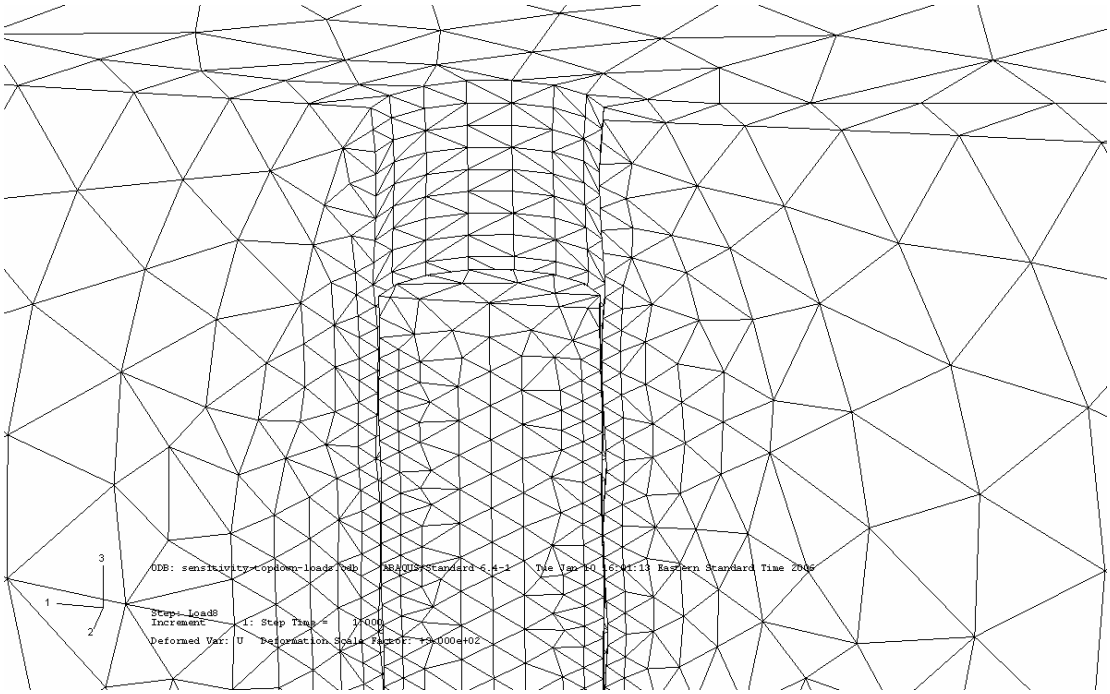

Figure 20 3D Deformed Shaft-rock Interface

Chapter 3 Model Validation

Back-calculation of Weathered Rock Properties

The integrity of rock is commonly destroyed in Karst terrain. It causes reduced strength and instability which lead to the difficulties in design and construction practice.

The self-balanced load tests (similar to O-cell tests) data (Huang et al. 2004) in Nanpanjiang Bridge was employed to back-calculated the surrounding rock properties. The back-calculated properties were assigned to 3 dimensional pile-rock models for sensitivity analysis purpose.

Napanjiang Bridge is a prestressed rigid frame bridge (Huang et al. 2004). No.1 and No. 2 piers are supported on pile foundations. Limestone cavities were found in

south-west and southwest of No. 1 Pier. Loose residual from underground river was investigated heaping on the bottom of cavities. The underground water in neighbor region is active and periodically changes from turbid to clear. The limestone cavities distributed on dissolvent gypsum areas. Thus, those cavities at the south-east side of pile were believed to be unstable. Grouted riprap was poured into the cavities and gaps as the foundation reinforcement treatment. Self-balanced load tests similar to Osterberg-cell tests were conducted by Southeast University (China) to evaluate the single pile bearing capacity, axial stress, layered rock friction stress, ultimate end bearing capacity, elastic and plastic deformation.

The load-displacement curves of the O-cell test were used to calibrate the model and the following information was to be obtained from the calibration: (a) Young's modulus of the rock; (b) Drucker-Prager parameters (related to cohesion c and friction angle φ); (c) Double amplitude of the shaft-rock interface profile and (d) Coulomb friction coefficient of the interface.

The rock modulus was first obtained by matching the linear part of the load-displacement curve of the O-cell bottom plate. The nonlinear part of the same curve was used to determine Drucker-Prager parameters. Finally, a close match between calculated and measured load-displacement curve of the O-cell top plate was obtained by varying the double amplitude of the interface profile and the Coulomb friction coefficient. Loading steps were set up on the basis of field Ocell test and listed in Table 5.

Due to the mechanism of the shaft load testing, it is hard to separate the downward displacement contribution of the elastic shortening of the concrete shaft and the deformation of the rock under shaft tip. If the properties of one material are known, the properties of the other material can be determined from parametric study of the numerical analyses. If the properties of both materials are unknown, the calibrated model is not one and only. Different combinations of material properties of the rock

and concrete can yield the same load-displacement relationship that closely matches the one from load testing.

Figure 21 compares the response as measured at the top and bottom of the O-cell load cell. The overall upward and downward deformations are similar to those measured, except that the degree of inelastic or permanent deformation after the unloading was under predicted. This is primarily due to the elastic nature of the interface model, which leads to recovery of the interface slip upon unloading. The permanent deformation that is shown is the result of yielding at the rock-concrete interface. It should be noted that because these are relatively high capacity shafts (2.5 m diameter and 37 m long rock socket), the ultimate load was not reached and the measured deformations were relatively small (<10mm).

Comparing 3-D Model with Axisymmetric Model

To verify the same parameters in 3-D model works as well as those in axisymmetric model, we compared the load-displacement curves. Additionally, we need to convince that 3-D model could totally represent load-deformation behavior of axisymmetric model. Otherwise, the 3-D sensitivity analysis could not be accurate.
The displacements on four points were selected to validate the 3-D model through the comparison with 2-D model. The loading process was simulated under variety of Young's moduli. Number 1-5 represented the Young's moduli from 100MPa to 500Mpa. Figure 22-25 shows the comparison of load-settlement curve under instantaneous upward and downward load which is similar with O-Cell test condition with variety of rock Young's moduli.

Table 5 Loading Steps and Field O-Cell Test Data

Structure Load Steps	Load(T)	Load Period(min)		Up Displacement(mm)		Down Displacement(mm)		Displacement on Top of Shaft(mm)		Load(Pa)	
		Current	Accumulated	Current	Accumulated	Current	Accumulated	Current	Accumulated	Current	Accumulated
1	265	60	60	0.68	0.68	-0.17	-0.17	0.03	0.03		529057
2	398	90	150	0.46	1.14	-0.24	-0.41	0	0.03	265526	794583
3	531	60	210	0.58	1.72	-0.4	-0.81	0.08	0.1	265526	1060109
4	663	60	270	0.72	2.44	-0.35	-1.16	0.1	0.21	263530	1323639
5	796	60	330	0.62	3.06	-0.39	-1.55	0.1	0.31	265526	1589166
6	929	60	390	0.49	3.55	-0.42	-1.97	0.15	0.45	265526	1854692
7	1061	60	450	0.46	4.01	-0.58	-2.55	0.21	0.67	263530	2118222
8	1194	60	510	0.68	4.68	-0.52	-3.07	0.02	0.69	265526	2383749
9	1327	60	570	0.62	5.3	-1.04	-4.11	0.26	0.95	265526	2649275
10	1459	60	630	0.39	5.69	-0.82	-4.93	0.31	1.26	263530	2912805
11	1592	60	690	0.4	6.09	-0.92	-5.85	0.26	1.52	265526	3178332
12	1725	60	750	0.44	6.53	-0.85	-6.7	0.34	1.85	265526	3443858
13	1857	60	810	0.47	7	-0.82	-7.52	0.22	2.07	263530	3707388
14	1990	60	870	0.48	7.48	-1.32	-8.84	0.4	2.47	265526	3972915
15	1592	60	930	-0.73	6.75	0.48	-8.36	-0.25	2.23	-794583	3178332
16	1194	60	990	-0.71	6.04	0.89	-7.47	-0.2	2.02	-794583	2383749
17	796	60	1050	-0.9	5.14	0.85	-6.62	-0.48	1.54	-794583	1589166
18	398	60	1110	-0.54	4.6	1.25	-5.37	-0.4	1.14	-794583	794583
19	0	60	1170	-0.4	4.2	0.75	-4.62	-0.15	0.99	-794583	0

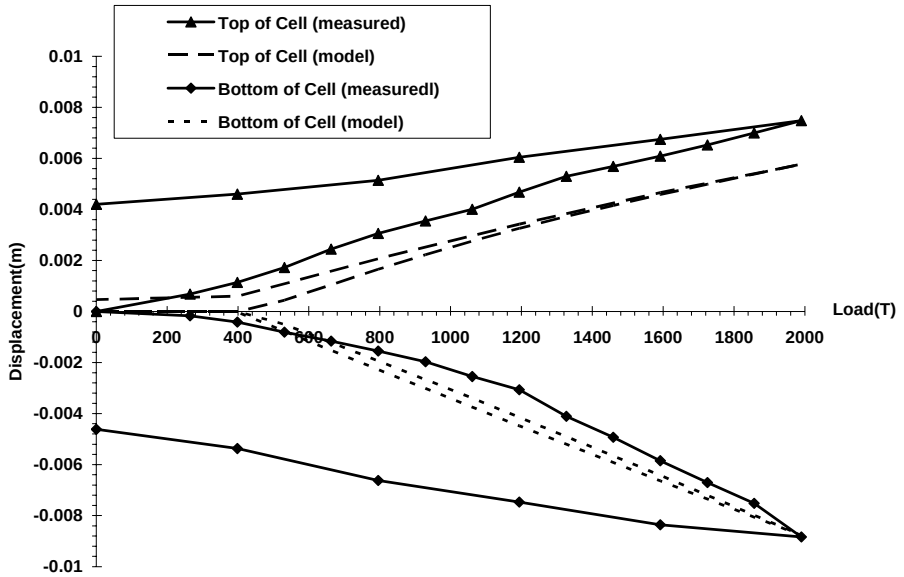

Figure 21 Comparison of Measured and Calculated O-Cell Displacement

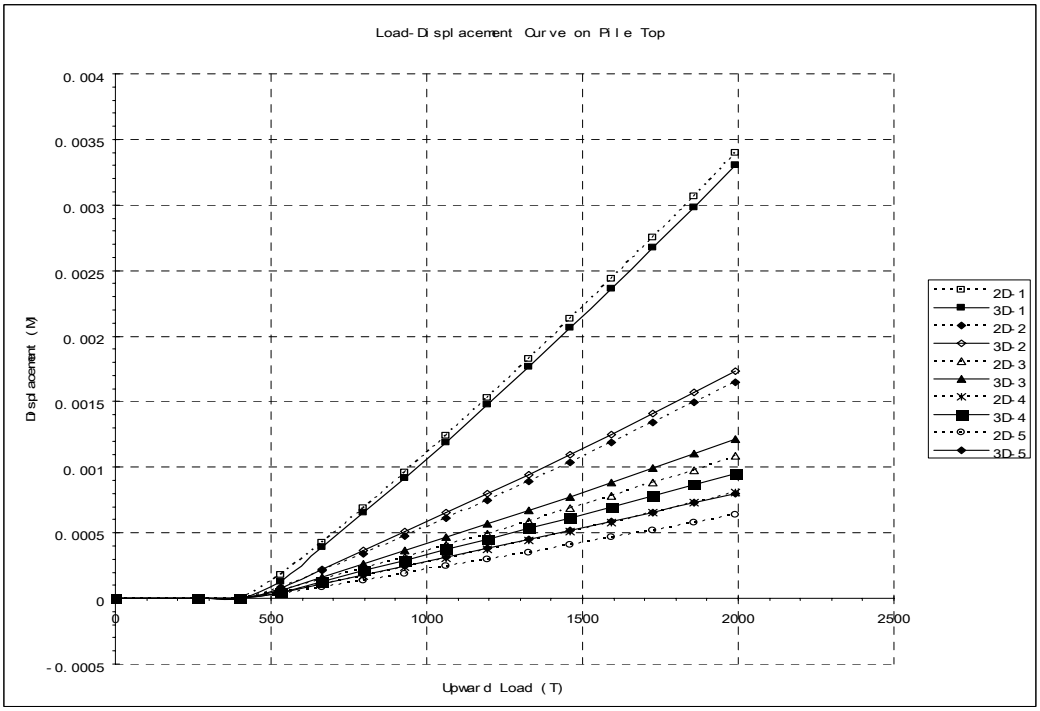

Figure 22 2-D and 3-D Comparison of Load-Displacement Curve on Shaft Top

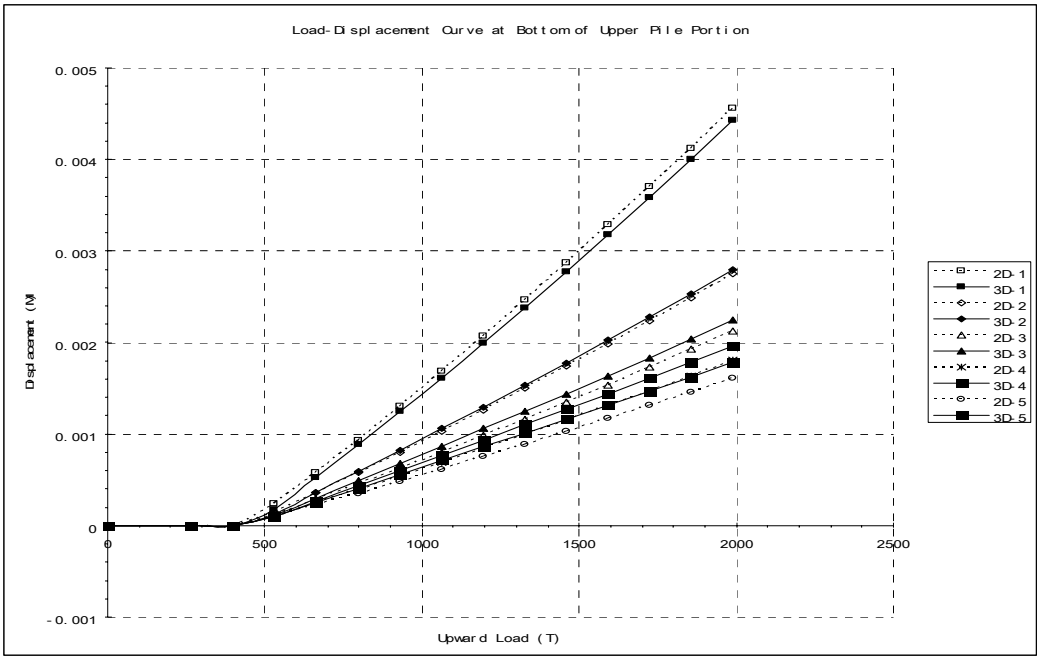

Figure 23 2-D and 3-D Comparison of Load-Displacement Curve on Bottom of Up Shaft Portion

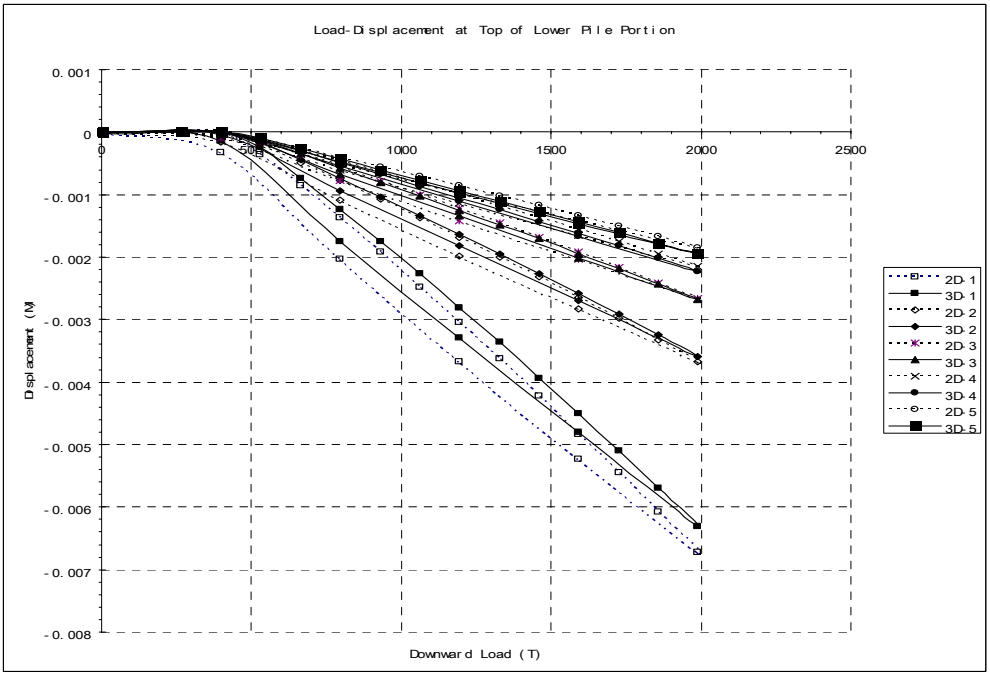

Figure 24 2-D and 3-D Comparison of Load-Displacement Curve on Top of Lower Shaft Portion

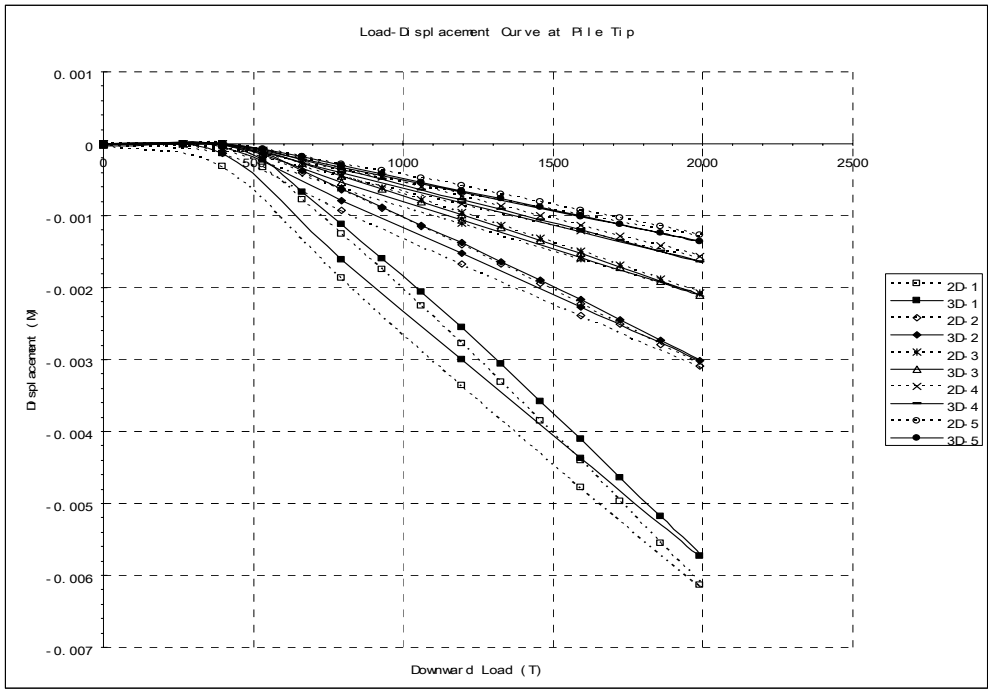

Figure 25 2-D and 3-D Comparison of Load-Displacement Curve on Bottom of Lower Shaft Portion

Chapter 4 Sensitivity Analysis

After the 3-D model was validated, series cavities were extruded in 3-D model. On the basis of factors infecting shaft bearing capacity, the distance from shaft butt to cavity top, the diameter of cavity, the elevation and eccentricity were considered. Geometry Data for 3-D Sensitivity Analysis was shown in Table 6. Four models for each factor. There are 16 models totally. The models are exhibited in Figure 26 - 29.

Description of the Variety of 3D Models

From Figure 26~29, the models were divided into 4 cases on the basis of the locations and sizes of the cavities. The sizes and locations were scaled by times of pile's diameter. The locations were measured by vertical distance from cavity top to pile tip and the horizontal distance from the cavity center to the axial line of pile. Detailed multiples are listed in Table 6.

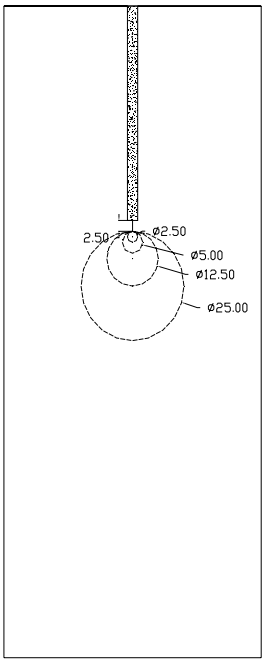

Figure 26 3D Pile Model with Cavity-Case 1

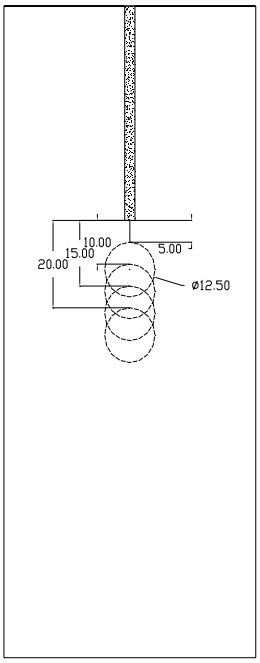

Figure 27 3D Pile Model with Cavity-Case 2

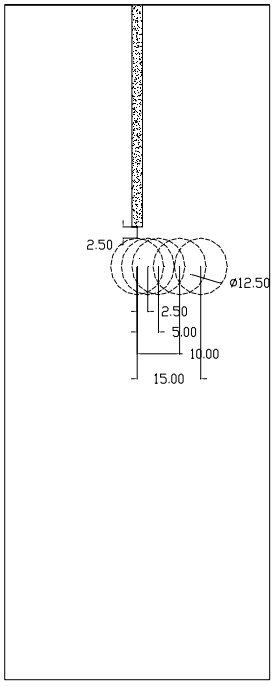

Figure 28 3D Pile Model with Cavity-Case 3

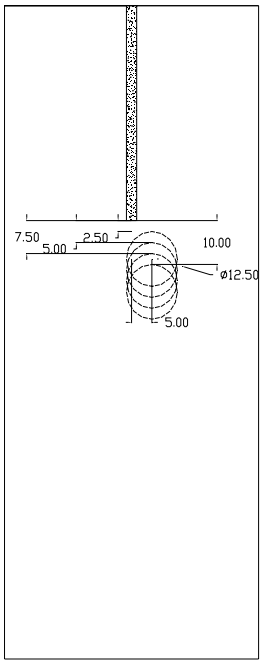

Figure 29 3D Pile Model with Cavity-Case 4

Table 6 Geometry Data for 3-D Sensitivity Analysis

Shaft Diameter	Thickness between shaft and cavity	Multiples of cavity diameter	Top Coordinate 3	Center Coordinate 3	Down Coordinate 3
2.5	2.5	1	2.5	3.75	5
2.5	2.5	2	2.5	5	7.5
2.5	2.5	5	2.5	8.75	15
2.5	2.5	10	2.5	15	27.5

Shaft Diameter	Distance from Shaft tip to cavity top	Multiples of Distance from shaft tip to cavity top	Top Coordinate 3	Center Coordinate 3	Down Coordinate 3	Multiples of cavity diameter
2.5	5	2	5	11.25	17.5	5
2.5	10	4	10	16.25	22.5	5
2.5	15	6	15	21.25	27.5	5
2.5	20	8	20	26.25	32.5	5

Shaft Diameter	Distance from Shaft tip to cavity top	Multiples of Eccentricity	Top Coordinate 3	Center Coordinate 3	Down Coordinate 3	Coordinate 1	Multiples of cavity diameter	Multiples of Distance from shaft tip to cavity top
2.5	2.5	1	2.5	8.75	15	2.5	5	1
2.5	2.5	2	2.5	8.75	15	5	5	1
2.5	2.5	4	2.5	8.75	15	10	5	1
2.5	2.5	6	2.5	8.75	15	15	5	1

Shaft Diameter	Distance from Shaft tip to cavity top	Multiples of Eccentricity	Top Coordinate 3	Center Coordinate 3	Down Coordinate 3	Coordinate 1	Multiples of cavity diameter	Multiples of Distance from shaft tip to cavity top
2.5	2.5	3	2.5	8.75	15	7.5	5	1
2.5	5	3	5	11.25	17.5	7.5	5	1
2.5	7.5	3	7.5	13.75	20	7.5	5	1
2.5	10	3	10	16.25	22.5	7.5	5	1

Results and Analyses

Case 1

From Figure 30 and 31, the influence on load-settlement relationship is demonstrated. While the cavity diameter increases from 1 times of pile diameter to 5 times of pile diameter, slight differences are observed on top of pile. However, relatively significant influence caused by cavities is indicated. Generally, the larger cavity diameter will lead to increasing of settlement under equal static load. The settlement increment is related with load amplitude too. In light static load condition, the increasing rate of settlement is not significant. But in case load is heavy, the influence on the settlement shows an approximate linear relationship with times of cavity diameter over pile diameter (Figure 32 and 33).

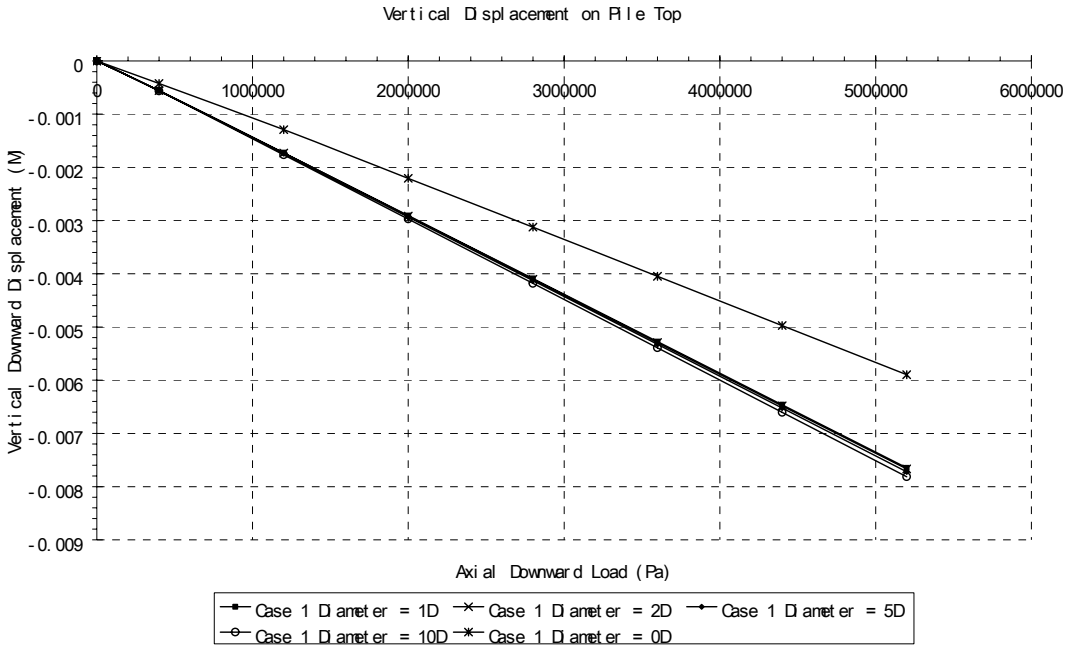

Figure 30 P-s curve on Pile Top - Case 1

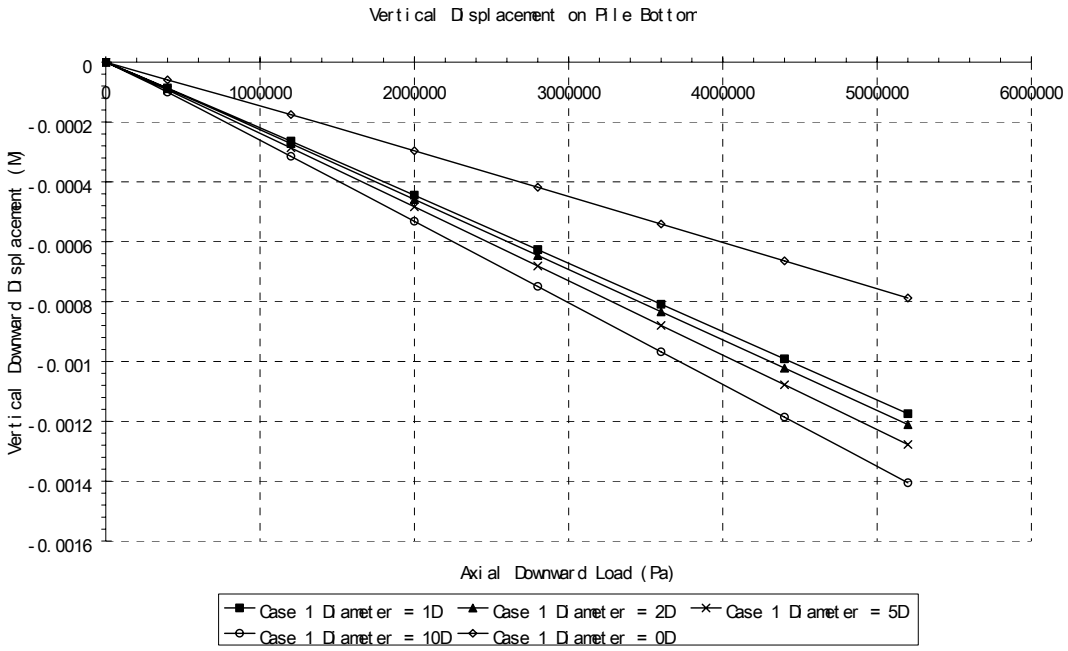

Figure 31 P-s curve on Pile Bottom - Case 1

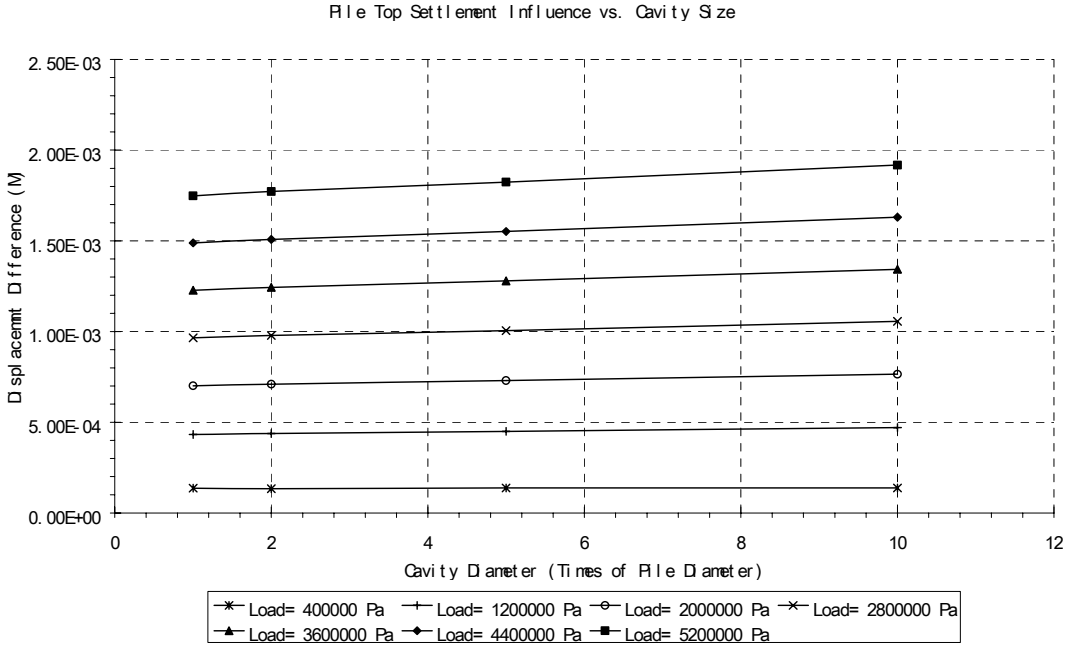

Figure 32 Influence in Vertical Displacement on Pile Top vs. Cavity Diameter – Case 1

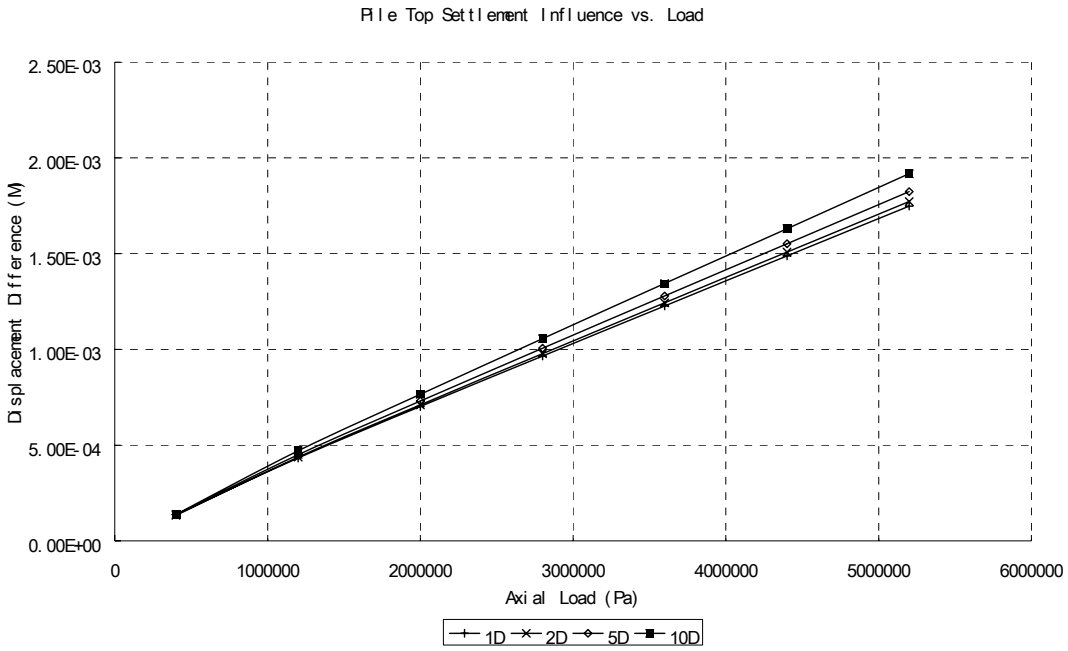

Figure 33 Influence in Vertical Displacement on Pile Top vs. Load – Case 1

Case 2

Figure 34 indicated that the settlement on pile top is not affected if the cavity is far away downward from the pile bottom. However, if we look into Figure 35 and 36, it is found that the settlement difference between different models is reduced along with the increasing of distance from pile bottom to cavity top. Especially, when the distance from pile bottom to cavity top is further than 4.5 times of pile diameter, the affect is reduced to a low and stable level (Figure 36). From Figure 37, it is observed that the larger load amplitude will cause the influence increasing.

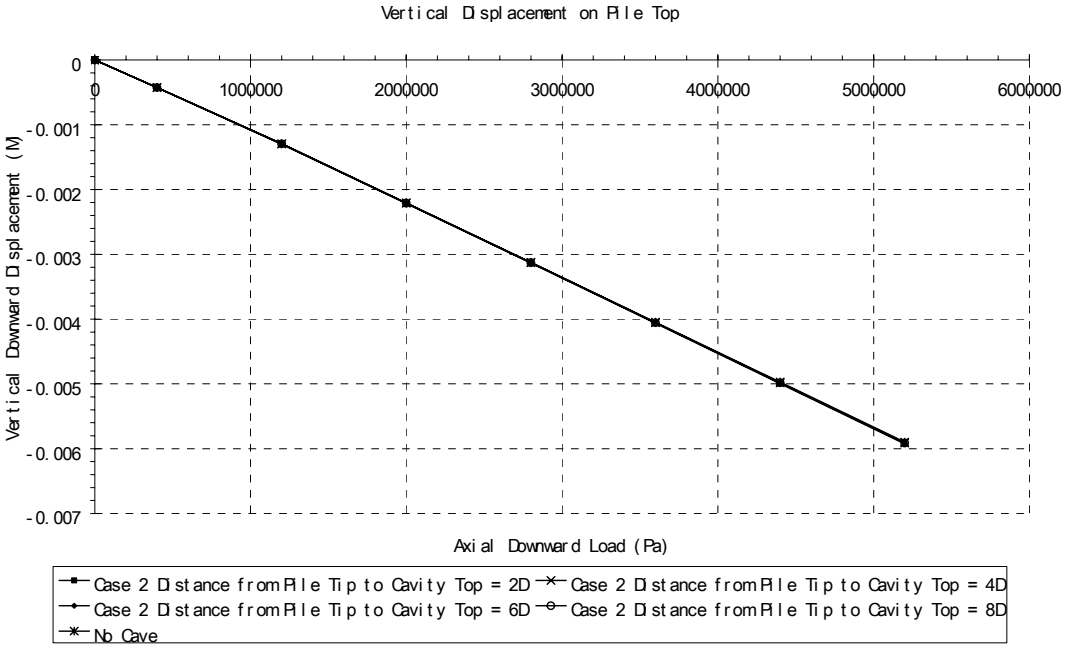

Figure 34 P-s curve on Pile Top - Case 2

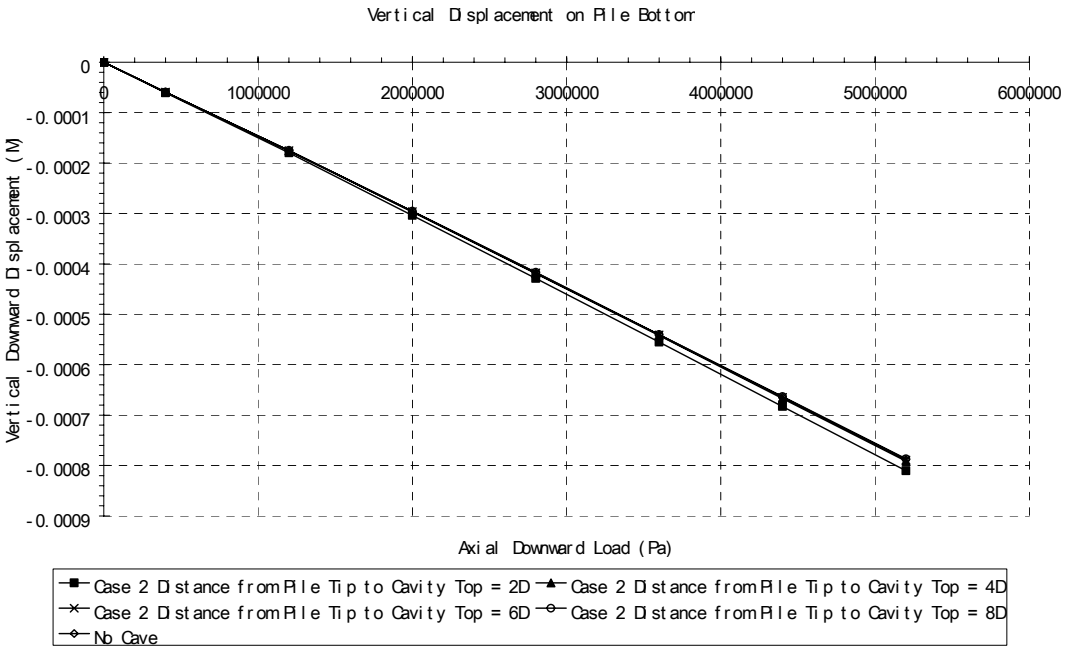

Figure 35 P-s curve on Pile Bottom - Case 2

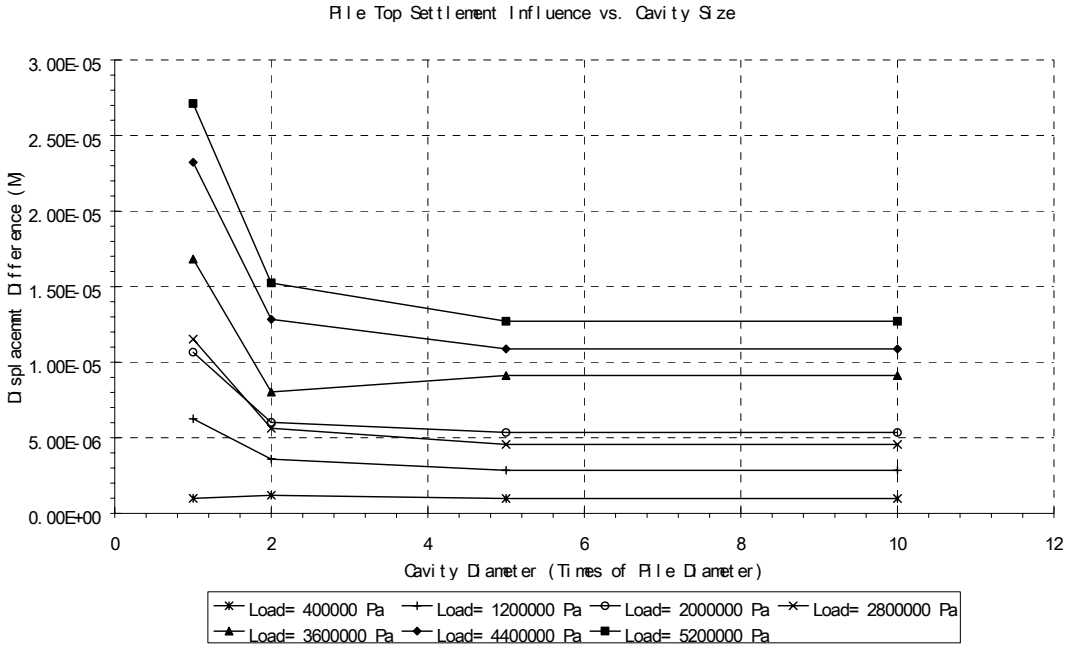

Figure 36 Influence in Vertical Displacement on Pile Top vs. Cavity Diameter – Case 2

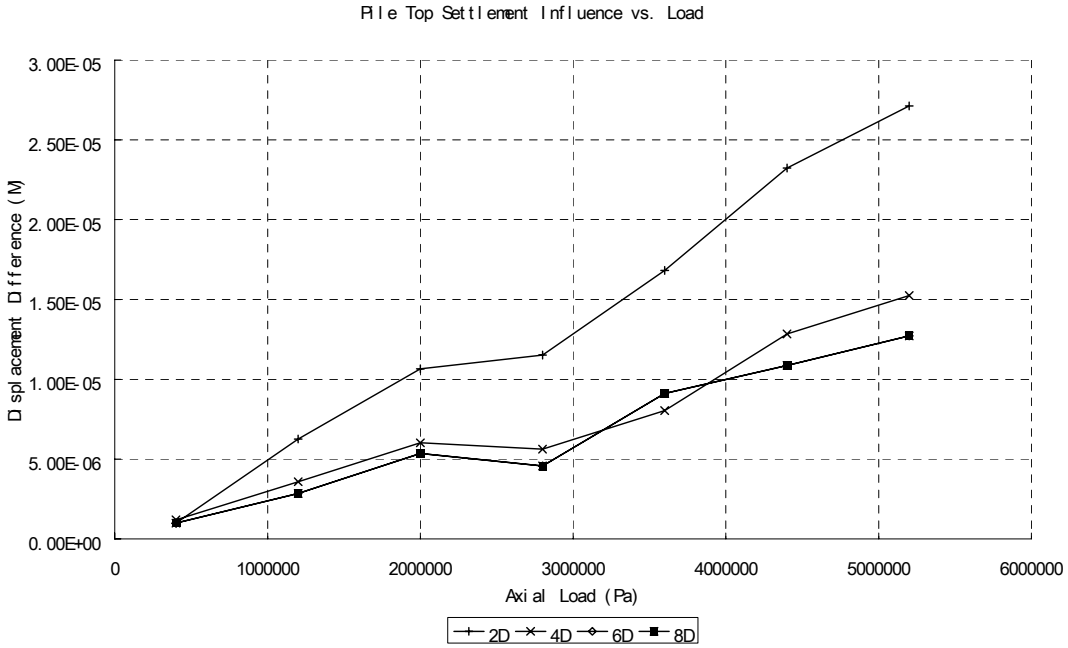

Figure 37 Influence in Vertical Displacement on Pile Top vs. Load – Case 2

Case 3

In this case, cavity does affect the load and displacement relationship. But this influence keeps approximately constant when the eccentricity changed (Figure 38). From Figure 39, the eccentricity will not be the factor to reduce the affect to pile bottom settlement. If the eccentricity is equal and less than 6 times of pile, the influence caused by the cavity will not change significantly due to change of eccentricity.

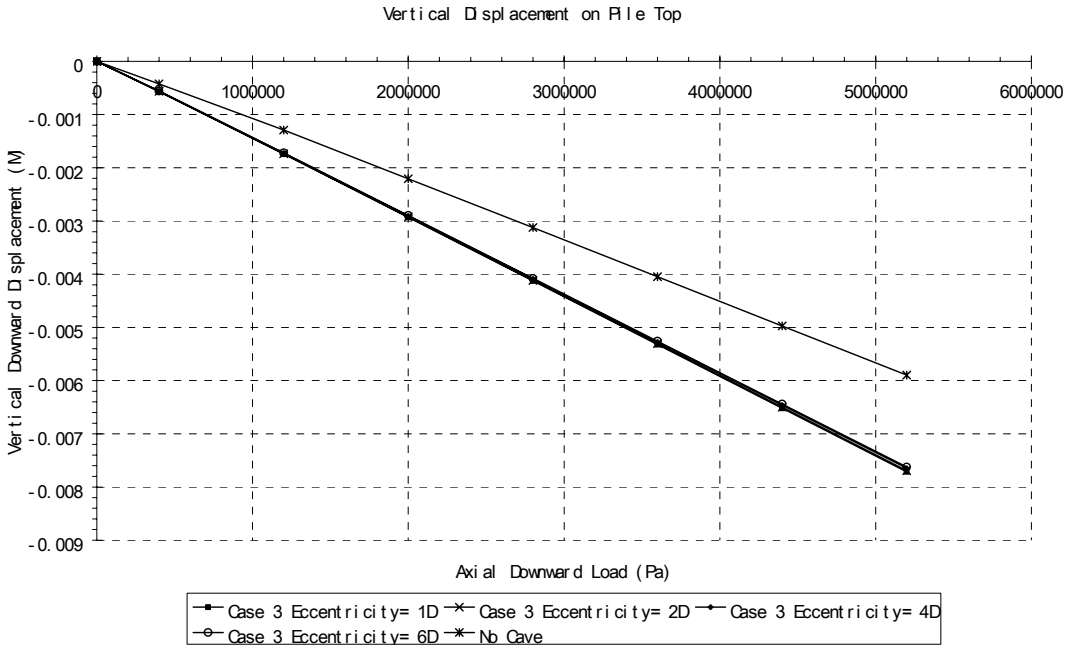

Figure 38 P-s curve on Pile Top - Case 3

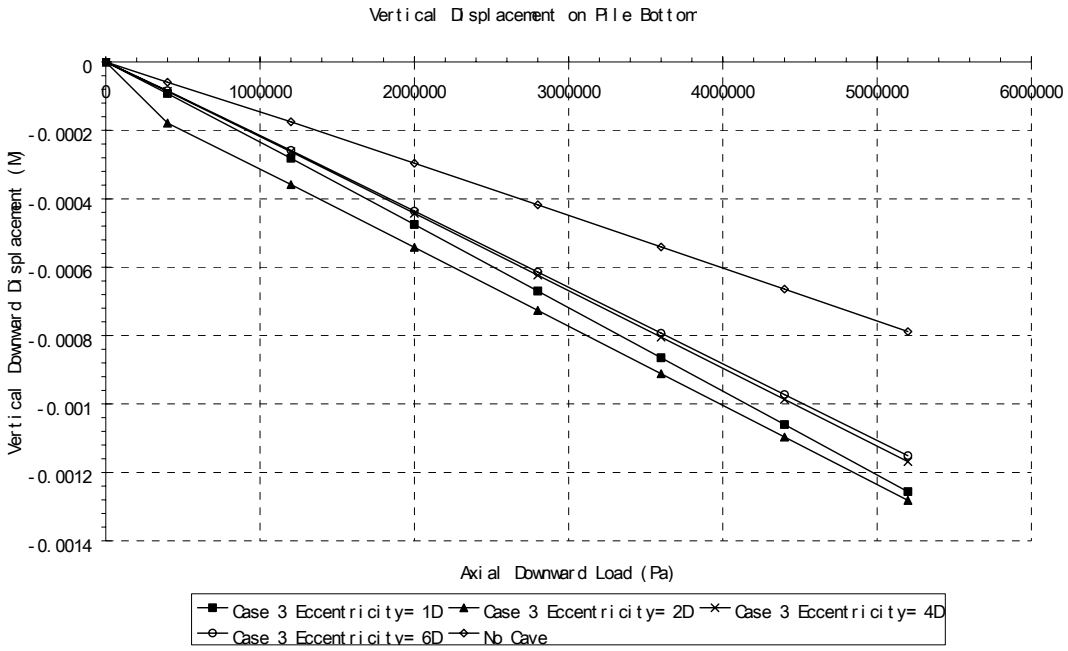

Figure 39 P-s curve on Pile Bottom - Case 3

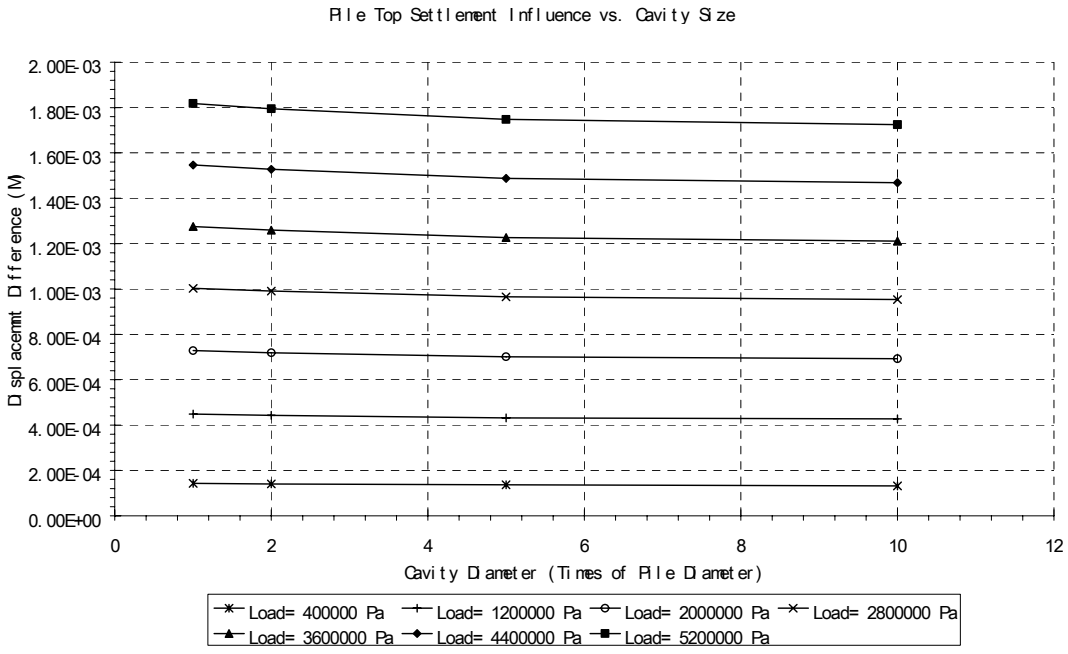

Figure 40 Influence in Vertical Displacement on Pile Top vs. Cavity Diameter – Case 3

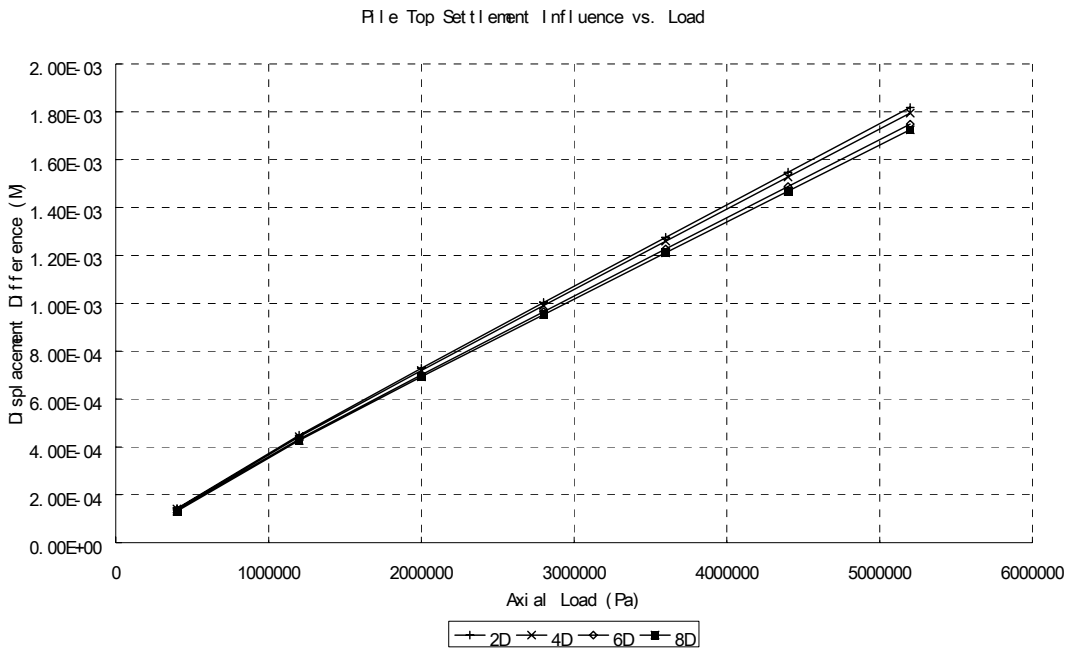

Figure 41 Influence in Vertical Displacement on Pile Top vs. Load – Case 3

Case 4

From Figure 42 and 43, we can observe that the cavity with certain eccentricity (2 times to pile diameter) and constant size (5 times to pile diameter) brings approximate equal influence on p-s curve in different depth.

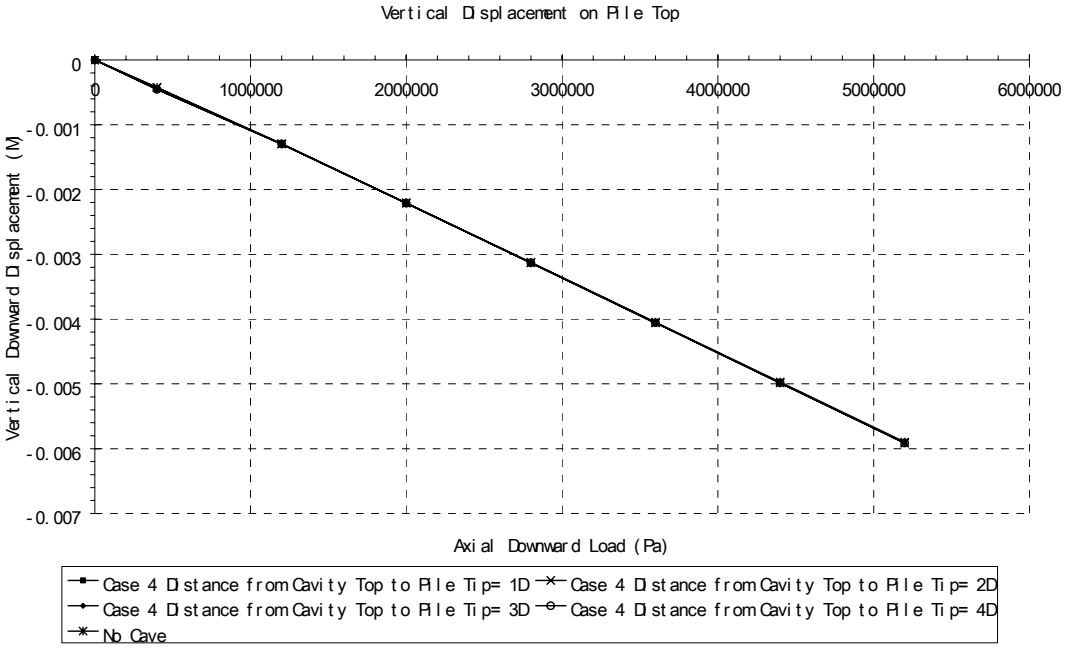

Figure 42 P-s curve on Pile Top - Case 4

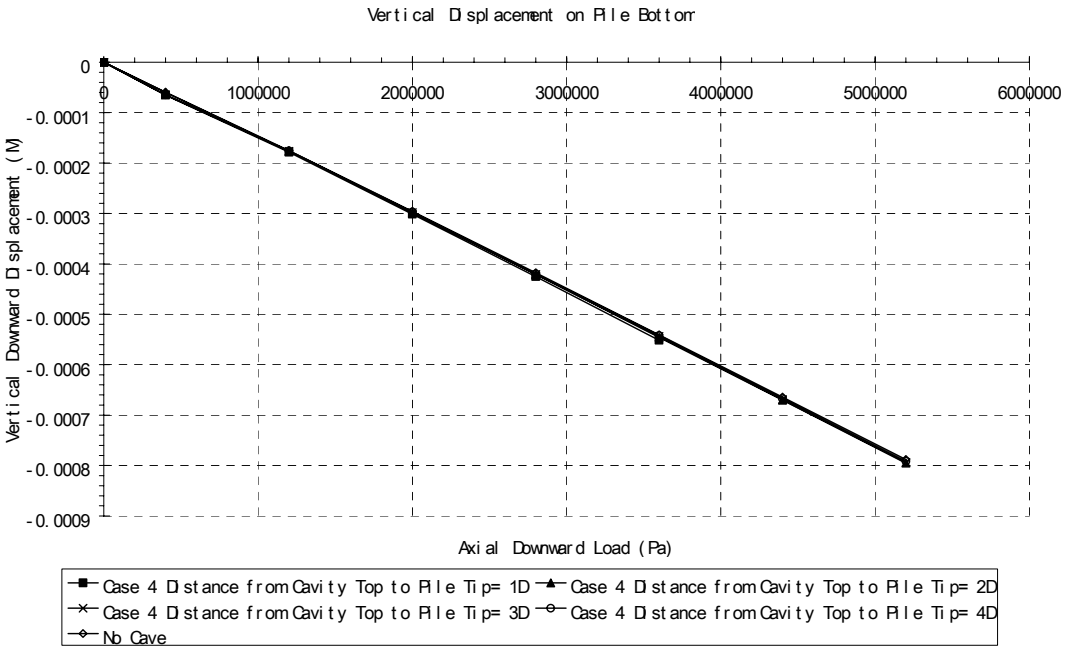

Figure 43 P-s curve on Pile Bottom - Case 4

Conclusion

In summary, from 3-D finite element models, there are four factors to cause the influence on pile top settlement when equivalent load is applied:

- ✓ Cavity diameter
- ✓ The distance from pile tip to cavity top
- ✓ The eccentricity of cavity
- ✓ Load amplitude

According to the 3D simulations, if the load amplitude is certain, the conclusion can be drawn as the following:

1. With constant distance from pile tip to cavity top, larger cavity diameter will lead to larger settlement;
2. With constant distance from pile tip to cavity top, smaller eccentricity of cavity will lead to larger settlement;
3. With constant cavity diameter, the deeper cavity will lead to less settlement than shallower cavity;

The difference between piles on bedrock with various cavities is increasing along with the load amplitude increases.

B: Numerical Simulation on Asphalt Pavement

Chapter 1 A Review of Numerical Simulation on Flexible Pavement

Flexible pavement is covered with asphalt concrete pavement. Comparing to another popular road pavement construction material- cement concrete, asphalt pavement is flexible due to the nature of the bituminous. Typically, asphalt concrete consists of aggregates graded continuously or non-continuously from a maximum 25mm to minimum 0.075mm. Appropriate asphalt is mixed with the aggregate and compacted to achieve certain material properties. The multi-phase material consists of mineral aggregate, filler, bitumen and air.

In addition to the complexity as a composite, the properties of asphalt mixture progressively change during the life of asphalt pavement. The microstructure activities within asphalt concrete are highly related to interactions at the constituent interface and within the constituents themselves. One intricate internal behavior of asphalt concrete is reflected as its complex time-dependent material properties as composite..

Initially, trial and error methods were introduced in asphalt pavement structural design. The design criteria were significantly dependent on the experience of material engineers. Within the last decades, mechanical-empirical methods have been widely adopted. The mechanical-empirical methods are developed gradually during SUPERPAVE research program. (NRC 1994; Von et al. 1991; Huang 1993). Instead of well-known constitutive models in continuum mechanics, the distress prediction models are proposed in flexible pavement design. In these models, the critical distress parameters are assumed to be related to distresses. The critical properties of asphalt pavement were measured to determine whether the mixture is accepted or rejected.

For the design purpose, establishment of appropriate models require to solute complicated material governing equations. Frequently, varieties of geometry boundary and material properties have to be considered. The numerical methods play

an important role in the development of asphalt pavement design. Closed form stress-strain or load-deformation analysis of many problems in these areas is invariably complex. For many of these analyses, solutions are difficult and tedious if possible to obtain at all. Alternatively, engineers resort to numerical methods for solution of such problems.

The most commonly applied numerical methods in flexible pavement are divided into two brunches. One is continuum methods: the finite difference method (FDM), the finite element method (FEM). The other is discrete methods: the discrete element method (DEM). Generally, the simulation of asphalt mixture macro-scale behavior often chooses continuum methods because of its continuum-based problem factors. For the micro-scale mechanism of asphalt mixture, DEM has more ability to represent the mixture ad hoc micro-scale behavior. No absolutely advantages of one method are over another. But suitable modeling assumption is essentially for the simulation accuracies.

In this literature review, the emphasis will be the Finite Element Method due to it's widely implementation. We concentrated the outstanding solved intricacies and the utility of FEM for flexible pavement engineering purposes.

Finite Difference Methods (FDM) for Flexible Pavement

The concept of finite difference methods (FDM) is the discretization of solution domain into a grid (quadrilaterals for 2D or cubes for 3D). Taylor's theorem can then be utilized to provide the difference. The governing partial differential equations are replaced by partial derivatives. With proper techniques, there is no global matrix of equations need to be solved. The direct straightforward simulation provided convenience and efficiencies for computation speed and memory storage handling of computer.

Although FDM is intuitive simulation protocol, it has significant shortcomings. No interpolation functions were employed between neighboring grid points. Additionally, the conventional FDM with regular grid systems is hard to cater fractures, complex boundary conditions and material heterogeneity.

Finite Element Methods for Flexible Pavement

In the late 1960's, when conventional FDM with regular grid encountered problems to fulfill the requirement in engineering application, finite element methods appeared as a effective protocol with adequate flexibility for the handling of material heterogeneity, non-linear behavior, complex boundary conditions and so on. Due to these advantages, it became the most widely used numerical simulation method through engineering world.

The finite element method can be used to solve engineering problems with complicated geometries, loading conditions and material properties, and for which it is extremely difficult or impossible to obtain an analytical solution.

The finite element formulation of the problem results in a system of simultaneous algebraic equations for solution, rather than requiring the solution of differential equations. These numerical methods can then yield approximate values of unknowns at discrete points in the continuum.

Finite element analysis has a number of advantages. These advantages include the abilities to model:

1. Irregularly shaped or complex model geometry configurations.
2. Various types of loading.
3. Various types of materials.
4. Unlimited numbers and kinds of boundary conditions and other special features, like multi-point constraints.

5. Individual analyze dynamic, thermal, acoustic and other special effects or any of their combinations.
6. Nonlinear behavior with large deformations and/or nonlinear materials properties.

From later 60's, numerical simulation has been introduced in flexible pavement analysis and design (Waterhouse, 1967, Duncan, et al., 1968, Feeme and Marais, 1972).

Since the AASHO road test during the early 1960s, researchers in US has been trying to develop and calibrating a design procedure that would employ the mechanistic approach to precisely predict the pavement performance (Duncan et al., 1968, Dehlen and Monismith, 1968, Kent, et al., 1978, Gomez and Thompson, 1984, Uzan et al., 1985, Yandell, 1987, Zaghloul, 1994, Seibi, 1993, Hua, 2000, Huang et al., 2001, Long, 2001, Bahuguna, 2003). In order to achieve this objective, it is essential to know the stresses and strains within the pavement system under various traffic loads and environmental conditions. Layered elastic solutions led a great step forward for this endeavor (Burmister, 1943, Acum and Fox, 1951). However, many simplifications limited the applications of layered elastic closed form solutions to pavement engineering.

Numerical solutions, on the other hand, have greatly simplified the procedures in calculating stresses and strains within the pavement system. Among the different numerical procedures, finite element method (FEM) has been the most commonly used in pavement engineering.

Development of FEM for Flexible Pavement

Earlier Stage FEM for Asphalt Pavement Analyses

Earlier applications of FEM in asphalt pavements were almost exclusively completed through dedicated programs specifically design to solve the problems. Waterhouse (1967) was among the first to write a dedicated linear elastic based FEM program for stress and strain analysis of asphalt pavement under static wheel loads. Duncan et al. (1968) analyzed the asphalt pavement deflections for an in-service pavement near Gonzales, California with both FEM and closed form layered elastic solutions. The FEM program in their study employed two dimensional axisymmetric elements with non-linear elastic material properties for granular base and cohesive subgrade soil. They concluded that both FEM and closed form solutions gave comparable deflections under the wheel loads (Duncan et al., 1968).

An approximate nonlinear elastic finite element model was also used by Dehlen and Monismith (1971) developed an approximate nonlinear elastic FE procedure to analyze a full-depth asphalt pavement over a sandy clay subgrade. The FE analysis result indicated that although nonlinearity was included in the FE modeling, the relationship between the load and deflection is very similar to that of linear elastic analysis. Thus linear elastic analysis seems to be sufficiently accurate for the primary response of asphalt pavements under truck loads (Dehlen and Monismith, 1971).

Even during the early stages of FEM application, researchers tried to calibrate the FEA results with pavement in-situ measurement. Freeme (1971) examined the critical strains in asphalt pavements with linear elastic and nonlinear elastic finite element methods and compared the results with field measurements. He concluded that for thin asphalt pavement, tire pressure is the dominant factor to the critical tensile strain; whereas the gross wheel load is the secondary factor (Freeme, 1971). In another study, Freeme and Marais (1972) applied both linear-elastic and non-linear

elastic finite element methods to analysis asphalt pavement at various depths. Comparison between the measured and predicted behavior was examined. They found that stress dependent behavior of granular materials significantly influences the elastic deflection of asphalt pavement (Freeme and Marais, 1972).

Han et al. (1972) used an axisymmetrical FE procedure to evaluate the moduli of asphalt pavement layers through field tests in a part of an investigation into the applicability of the ASSHO Road Test Design Equations to Pennsylvania conditions. Burmister's two-layer elastic theory was also employed. Both FEA and elastic solutions produced similar results (Han et al., 1972).

Although most early researchers chose two-dimensional axisymmetrical geometrical model for their FEA, there were a few elected plane stress or plane strain element (Salam, 1973). It should be noted that both plane stress or plane strain elements would produce greater deflections than the two-dimensional axisymmetrical elements if all other conditions are the same.

As the FEM became a commonly procedure to analyze stresses and strains within the pavement structure, researchers started considering using the calculated stresses and strains to predict the development of various pavement distress. Notably for asphalt pavement, permanent deformation (rutting), fatigue cracking, and low temperature cracking has been identified as the three major types of distress. In addition, moisture damage has also been recognized as one of the key problems in the areas with abundance of water.

Majidzadech et al. (1972) used FEM to determine the stress intensity factor for different hot mix asphalt mixtures with various crack sizes and applied in asphalt pavement crack growth simulation. Non-linear material characteristics were applied in their FEA to predict the fatigue life of asphalt pavement (Majidzadech et al., 1972).

Uzan et al. (1972), through FE analyses, proposed a new cracking mechanism for flexible pavement. They found that some cracks appearing in the hot mix asphalt layers reflect the cracks in the underlying layers. They employed FEM to analyze part of this cracking mechanism and compared with field test results (Uzan et al., 1972). In another study, Uzan (1978) demonstrated, through FEA, that the interfacial adhesion, especially at upper layers, significantly influence the stress distributions in asphalt pavement system and ultimately influence the pavement performance (Uzan, 1978).

During the mid 1970s, researchers successfully applied FEM to analyze the environmental effects to the performance of asphalt pavements. Carpenter et al. (1975) used FEM to analyze asphalt pavement's thermal strains under different temperature conditions and predicted the development of low temperature cracking. During the same period, improved algorithms were also investigated to reduced the computer time and make the FEM more efficient (Nemesdy et al., 1977).

FEM for Asphalt Pavements during late 1970s and 1980s

After over a decade's development, FEM became more and more a common tool in flexible pavement analysis. Numerous standardized programs were developed as pavement design and analysis tools. These programs range from simple closed form layered elastic solutions (Ahlborn, 1972, Jong et al., 1973) to more sophisticated software incorporating pavement performance and pavement life predictions (Asphalt Institute, 1981, Walker et al., 1977, Kenis et al., 1978, Chen et al, 1990). Among these programs, the Federal Highway Administration (FHWA) developed program, VESYS (Kenis et al., 1978, 1982) has been widely used in the United State. Other programs such as Flexpass, ILLI-PAVE (1980) and KENLAYERS (Huang, 1991) were also been used frequently by researchers.

The level of applications of material modeling was greatly improved during this period. Viscoelastic modeling had been commonly incorporated into FE program to simulate the hot mix asphalt response under the wheel loads and predict pavement performance (Uzan, 1985, Huang, 1984). Stress dependent resilient modulus models had been commonly accepted and incorporated into a number of general pavement FEM programs (Hoffman, 1982, Uzan, 1985).

ILLI-PAVE, for example, incorporated nonlinear stress-dependent material properties for granular and cohesive subgrade soils in addition to its capabilities to predict other hot mix asphalt distress such as rutting and fatigue cracking. Among many researchers using ILLI-PAVE, Gomez (1984) proposed a mechanistic design procedure for full-depth asphalt pavement based on the ILLI-PAVE algorithms and data from the AASHO Road Test bituminous wedge sections.

Coetzee (1979) used FEM analyzed discontinuities between the cracked asphalt pavement and rubber asphalt stress absorbing membrane system, and successfully simulated the performance of reflective cracking in asphalt pavements.

Viscoelasticity and nonlinear elasticity improve the layered elastic solution, but they still fail to capture an important characteristic of paving materials, the plastic behavior under traffic loads. Smith and Yandell (1987) used elasto-plastic models of the pavement system and introduced a numerical procedure of Mechano-Lattice Analysis (Yandell, 1971, 1987). They applied the procedure for a number of flexible pavement analyses in the U.S., South Africa and Australia. Chan and other researchers applied elasto-plastic theory for a finite element analysis of a flexible pavement base course rutting study in Nottingham, UK (Chen et al., 1990).

FEM for Asphalt Pavements since 1990s

By the late 1980s, two-dimensional FEM with complicated material models had been frequently used by researchers in pavement engineering. Researchers felt the need to advance the pavement design method from the empirical (regression) based AASHTO Design Guide into a fully mechanistic based design procedure. The FHWA launched an ambitious research program, Strategic Highway Research Program (SHRP), during 1987 and 1992. Accompanying SHRP, the twenty-year Long Term Pavement Performance (LTPP) was started in 1987. The purpose of the SHRP was to standardize the mechanistic design tool for both asphalt and concrete pavements. Whereas the LTPP was design to overcome the many limitations of the earlier AASHO Road Test and become a standardized tool to calibrate the mechanistic design equations. Thus the pavement design in the US would be brought into a new level of Mechanistic-Empirical (M-E) design method.

The development of FEM in asphalt pavement analysis entered into a new stage, which was characterized by the ever increasing computer power and more sophistication of the mathematical modeling (Zaghloul, 1993, Seibi, 1993, Huang, 1995, White, 1998, Hua, 2000, Huang, 2000, 2001).

One unique feature characterizes many FE analyses in asphalt pavement is the application of three-dimensional FEM. Zaghloul (1993) developed a 3-D FEM procedure with the commercial FEM software, ABAQUS, to analyze the pavement responses under the moving wheels. 3-D FEM has a lot of advantages over the 2-D axisymmtric approximation. First, different pavement geometries, such as multiple lanes and shoulder configurations can be fully addressed with 3-D FEM. Vehicle axle configurations and traffic speed can also be correctly reflected with 3-D finite element models. In his dissertation work, Zaghloul (1993) employed viscoelastic material models to characterize hot mix asphalt mixtures, Drucker-Prager plastic model for granular aggregate base materials, and Cam-Clay plastic model to

characterize the subgrade soils. His study demonstrated practicality of 3-D FEM for various types of pavement analyses (Zaghloul, 1993).

White (1998) and his co-workers (Zaghloul, 1993, Huang, 1995, Pan, 1997, Hua, 2000) from Purdue University applied the 3-D FEM procedure they have developed in a number of projects to study the response of both asphalt and concrete pavements.

Uddin (1998) applied 3-D finite element dynamic analysis for the pavements under the impact load of the falling weight deflectometer (FWD) and back-calculates the elastic modulus of the pavement layers.

Seibi (1993) developed an elastic visco-plastic constitutive relation for the asphalt concrete under high rates of loading. The model adds the rate dependent characteristics to the traditional Drucker-Prager plastic model. He conducted some parametric studies for the pavement samples from the Federal Highway Administration's (FHWA) existing ALF (Accelerated Loading Facilities) sections. By incorporating the model into ABAQUS, he compared the analysis against the FHWA ALF test results.

Since late 1990s, there have been three international symposia/conferences exclusively with the theme of application of 3-D FEM in pavement engineering. The first two were held in Charleston, WV, and the third one was held at the Delft University of Technology in the Netherland.

Another trend should be mentioned for the FEM in asphalt pavement analysis is the combination of FEM and accelerated pavement testing (APT). APT, ranges from lab scaled system to full-scale test tracks, has been more and more frequently used as a calibration tool for FE procedures. Huang et al. (2001) compared their 3-D FEA with the Louisiana Accelerated Loading Facility (ALF). Long (2001) studied rutting behavior of hot mix asphalt mixtures with nonlinear viscoelastic FEM. Her model

was first validated by the Superpave repetitive simple shear test at constant height (RSST-CH) and further compared with the Heavy Vehicle Simulator (HVS), a South African designed full-scale APT (Long, 2001).

Garza (2003) used dynamic 3-D FEM to evaluate the seed modulus values in back-calculating pavement modulus from Falling Weight Deflectometer (FWD) test. Comparing conventional static analysis methods, the dynamic 3-D FEM back-calculation predicts pavement modulus more accurately.

Mun (2003) employed VECD-FEP++ to study failure mechanism of fatigue cracking. Viscoelastic continuum damage model was considered for asphalt layer. Unbound layers were simulated by nonlinear elastic Uzan-Witczak resilient modulus model. Under a variety of loading condition, the crack initiations were analyzed by monitoring a damage contour. The results indicated different failure mechanisms in different pavement structures (Mun, 2003).

Bahuguna (2003) proposed a four-component viscoplastic model to study the permanent deformation characteristics of asphalt pavements. The components in the model include a third order hyperelastic unit, a viscoelastic unit (Modified Kuhn model), a viscoplastic unit (based on Perzyna's theory of viscoplasticity), and a plastic unit (based on generalized plasticity). Repetitive Simple Shear Test at Constant Height (RSST-CH) was used to calibrate the model. A comparison between the finite element simulation and field observation agreed fairly well (Bahuguna, 2003).

Implementation of FEM on Asphalt Pavement

The three major distresses of flexible pavement are rutting (permanent deformation), fatigue and thermal cracking. The serviceability is influenced strongly by these distresses. FEM was employed to analyses the potential of these distresses. With the

approximated flexible pavement properties and FEM, the future asphalt pavement behavior is able to be predicted. The related implementations associated with each of the three major distresses are discussed in the following review.

Conversely, in some cases, we need to know the properties of asphalt pavement from nondestructive evaluation (NDE). The advent of FEM also provided the opportunity to backcalculate the asphalt pavement characteristics from in situ NDE test data. These techniques are utilized in wider range than destructive methods due to low cost, slight interruption of the traffic, small damage of the flexible pavement. One of most popular implementation is the backcalculation of moduli of different pavement layers on the basis of Falling Weight Deflectometer (FWD). In this review, the FEM development of backcalculation methodologies is also involved.

Within the last decade, the engineers and researches star to apply new materials to improve the bearing capacity of flexible pavement. One observable implementation is the geosynthetic material was utilized for reinforcement of asphalt pavement, after it's success in tensile reinforcement on earth structures and unpaved roads (Giroud and Noiray 1981; Holtz and Sivakugan 1987; Love et al. 1987). Because FEM is versatile, it was often emplyed on the reinforced flexible pavement to analyses the impact of geosynthetic materials. The application associated with methodologies was discussed in this review too.

FEM for Permanent Deformation of Flexible Pavement

Asphalt mixture is a very complex multi-phase material. Its behavior contains elasticity, plasticity, viscoelasticity, viscoplasticity, damping and creeping. Additionally, asphalt pavement's mechanical behaviors varied with loading time, temperature and other environmental factors. In order to produce proper asphalt pavement design procedure, tremendous tests were conducted. Many of them were expensive and time consumed. Successful simulation for those tests and asphalt

pavement behavior can save the cost and time. And sophisticated simulation techniques can predict most mechanical factors when the loading and environmental condition changed instead of expensive tests.

As one of popular numerical simulation tool, the implementation of finite element method on asphalt pavement leads to many successes on asphalt paving engineering. Finite element method can easily involve different constitutive models if proper algorithms available. Thus, after finite element method was introduced into asphalt pavement analysis, deriving proper numerical material model became the core issue.

From late 1960's, finite element methods were introduced to analysis asphalt pavement structure characteristics. The principal research scope was the stress and strain relationship in asphalt pavement (Waterhouse 1967, Duncan et al. 1968). The finite element approach was used to determine the stress in asphalt pavement under different load condition. At beginning, asphalt layer are treated as linear elastic material. As one of typical validation way, the finite element analysis results were compared with Boussinesq solution (Waterhouse 1967). The agreement between two different solutions was received (Waterhouse 1967 and Duncan et al. 1968).

Although the linear analysis results are acceptable in engineering approximation, the pavement with unbound granular materials appears to significant nonlinear characteristics (Dehlen and Monismith 1970). Freeme (1971) used non-linear elastic finite element computer program to predict the critical strains in the bituminous layers of an asphalt pavement construction. The comparison between computed result and field measurement indicated that the non-linear elastic finite-element computer techniques could provide more realistic prediction of deflections (Freeme 1971, 1972). Stress-dependent finite element software such as ILLI-PAVE was widely used to calculate the resilient response parameters of conventional flexible pavements subjected to traffic loads (Figueroa and Thompson 1980, Hoffman and Thompson 1981). With ILLI-PAVE, ILLI-CALC, a method to backcalculate nonlinear resilient

moduli based on the interpretation of measured deflection basins, was presented (Hoffman and Thompson 1982). Nonlinear stress-dependant material characterizations are directly incorporated into the ILLI-CALC procedure. Among tremendous researches had been done for mechanistic design procedures, Gomez (1984) proposed and validated a mechanistic design procedure which is based on ILLI-PAVE.

As linear and non-linear models could present asphalt mixture in engineering approximation, they failed to capture important characteristics of asphalt pavement such as permanent deformation and fatigue life assessment. Plastic models were proposed for analysis of rutting, one of criterias of asphaltic pavement structural design. Uzan (1985) proposed viscoelasticplastic model for predicting performance of asphaltic mixtures. The model is based on stress evaluation by the finite element method and on a comprehensive viscoelasticplastic material law. A critical octahedral shear strain is assumed to be the failure criterion(Uzan 1985). The viscoelasticplastic model made it possible to estimate rutting parameters, fatigue life curves, and crack propagation rate versus stress intensity factor for the sand-asphalt mixture. Based on a finite-element numerical method, the viscoplasticity was taken into account by force equivalent to the antecedent viscoplastic deformation. In equations systems, the rigidity matrix is constant and solved by an iterative method (Goacolou 1987).

In many cases of real world, the pavement was loaded with nonuniform pressure. 2 dimensional models have deficiency to model the true 3-dimensional asphalt pavement behavior. From middle of 1980's, 3-D finite element programs were introduced in asphalt pavement analysis. Still with elastic assumption, Chen et al. (1986) investigated the effect of high inflation pressure and heavy axle load on asphalt-concrete pavement performance by using a three-dimensional finite element model.

As an effective tool to backcalculate asphalt pavement moduli, Falling Weight Deflectometer (FWD) has mostly been analyzed by using the static layered elastic analysiss method. Static analysis ignore the dynamic effects on those tests, such as inertia, damping and resonance. After finite element technology greatly developed in 80's, dynamics analysis was introduced in asphalt pavement FEM. Ong et al. (1991) adopt dynamic finite element method to simulate FWD tests. During the simulation, dashpots were installed at the boundary nodes (bottom and lateral).

FEA in Fatigue Cracking Simulation

Trace back to 1970's, finite element method became an effective tool to determine stress and strain in elastic material. Some pioneers used finite element analysis to determine the stress intensity factors for various crack sizes. Then with the fracture mechanics application, the method of determination of crack growth parameters for asphaltic beams resting on elastic foundation is proposed (Majidzadech et. al. 1972).

Viscoelastic composites with growing damage can be simulated by replacing the physical displacements by quantities called pseudodisplacements (Schapery 1990).

Jenq et al. (1993) proposed a cohesive crack model, which is similar to the Dugdale-Barenblatt type of models used for ductile yielding of metals. The model was used to simulate the progressive crack formation and propagation in asphalt concrete.

Kim et al. (1997) developed a uniaxial viscoelastic continuum damage model by applying the elastic-viscoealstic correspondence principle to separate out the effects of viscoelasticity and then employing internal state variables based on the work potential theory to account for the damage evolution under cyclic loading and the microdamage healing during rest periods. Daniel and Kim(2002) discovered a unique damage characteristic curve was discovered regardless of the applied loading conditions (cyclic versus monotonic, amplitude/rate, and frequency). This characteristic curve describes the reduction in material integrity as damage grows in the asphalt concrete specimen. In addition, Chehab et al. (2002) demonstrated that the time-temperature superposition is valid not only in the linear viscoealstic state, but

also with growing damge. This finding allows the prediction of mixture responses at various temperatures from laboratory testing at a single temperature.

Myers et al. (2001) used the linear elastic finite element analysis to conclude that the major cause of the top-down cracking is due to tensile stresses resulting from the interaction between truck tires and pavement surface.

FEA for Thermal Cracking of Asphalt Pavement

At early stage of finite element method, environmental factors were difficult to be considered in computational program. So that, alternative simulation ways were conducted. Duncan (1968) used low stiffness modulus in the range 120,000 to 280,000 psi to represent asphalt concrete at comparative high temperature, and high stiffness modulus about 1,500,000 psi to simulate asphalt concrete at low temperature. And the analysis involved nonlinear elastic material properties. The predicted results were founded in the same range as those measured with the California traveling deflectometer.

Thermal environmental conditions greatly influence the assessment of pavement deflection, estimation of frost action and frost penetration, and predicting the cooling rate of freshly laid asphalt layers. How to calculate the asphalt layer temperature distribution not only related to a more sophisticated specification but also has correlations with construction costs. From 1987 to 1992, the Strategy Highway Research Program(SHRP) was conducted in the USA and Canada. A new grading system named performance grading (PG) was proposed. The proper asphalt binder is required to resist pavement rutting in hot temperatures and to resist cracking in cold temperatures. Since PG system may lead to modify and further constrain the available crude oil sources, the cost of asphalt increased significantly. For this reason, the prediction of asphalt layer temperature became strongly correlated with construction cost.

Statistical and probabilistic methods are widely used to predict temperature gradients in asphalt pavements. However, it is not easy to avoid underestimate high temperature or overestimate low pavement temperature. Statistical probabilistic methods often raise questions about the accuracy and reliability. Numerical approaches with employment of energy balance equation are adopted to accurately and reliably estimate asphalt pavement temperature at variety of pavement depths and horizontal locations under known ambient environmental condition.

FEM for Falling Weight Deflectometer(FWD) Backcalculation of Flexible Pavement

The FWD (Falling Weight Deflectometer) is a non-destructive testing device that is used to complete structural testing for pavement rehabilitation projects, research, and pavement structure failure detection. It is used for conventional and deep strength flexible, composite and rigid pavement structures. The FWD is a device capable of applying dynamic loads to the pavement surface, similar in magnitude and duration to that of a single heavy moving wheel load. The response of the pavement system is measured in terms of vertical deformation, or deflection, over a given area using seismometers.

The backcalculation procedure involves theroretical calculations of the deflections produced under a known applied load using an assumed set of layers' moduli. The predicted deflections are compared with in situ test data. The assumed pavement layers moduli are adjusted and the process is repeated until the agreement between the theoretical and measured values is received or the errors are in acceptable engineering approximation.

In 1980's and earlier stage, the essential dynamic load factors f FWD were ignored on the basis of contemporaneous computer ability and FEM development. Most of backcalculation programs utilized multilayer elastic theory (SHRP 1991; Stubstad and Connor 1983; Irwin 1977; McCullough and Taute 1982). Because it's elastostatic

assumption, important characteristics of FWD were not considered, such as inertia and damping. Due to those limitations Chou et al. (1994) pointed out the ability lack to predict accurate moduli. Different estimations were received from same backcalculation software which were employed by different agencies simultaneously (Chou et al. 1994)

In summary, FEM has been used in asphalt pavement analyses for about forty years. It has been evolved from a numerical simplification of closed form layered system solution into today's dynamic simulation tool for pavement response, laboratory test, and prediction tool in mechanistic based pavement design procedure. The level sophistication of FEM in asphalt pavement analysis depends on several factors: (i) speed and capacity of computer, (ii) material modeling theory and testing method; and (iii) field calibration and validation tools.

Chapter 2 Introduction of FE Analysis for ALF

Background

Asphalt mixture is a very complicated multi-phase material. Its behavior includes elasticity, plasticity, viscoelasticity, viscoplasticity, damping and creeping. Asphalt pavement's mechanical behaviors varied with loading time, temperature and other environmental factors. In order to produce proper asphalt pavement design procedure, many tests are required. Many of these tests are expensive and time consumed. Successful simulation for these tests and asphalt pavement behavior can save cost and time. Well calibrated simulations can predict most engineering performance when the loading and environmental condition changed instead of expensive tests.

As one of popular numerical simulation tool, the implementation of finite element method on asphalt pavement leads to many successes on asphalt paving engineering. Finite element method can easily involve different constitutive models if proper algorithms available. Thus, after finite element method was introduced into asphalt pavement analysis, deriving proper numerical material model became the core issue.

Objective and Scope

This study is for numerical simulation techniques of ALF (Accelerated Loading Facility). The commercial finite element code ABAQUS was implemented with user defined subroutines. The focus was to accommodate moving load condition and material viscoelasticity and nonlinearity elasticity which includes anisotropy characters. Variety of speed is applied to investigate pavement nonlinear elastic behavior.

FE (Finite Element) models were constructed with exact same actual geometry size in order to simulation ALF (Accelerated Loading Facility) tests. The interaction between pavement layers are modeled as fully bonded and frictional contacted. The

moving load regenerated by contact pressure between tires and pavement were simulated by sinusoidal continuous loading pattern. The cement soil, compacted soil and subgrade were predicted with linear elasticity or stress rate dependant constitutive model (Uzan-Witczak 1988). The asphalt pavement layer and base course are treated as viscoelastic and anisotropic elastic materials respectively.

Model validation is performed through mesh converge and comparison with elasticity analytical solution. Sensitivity analysis is conducted for variety of speed and constitutive model.

The complexities of the simulation of ALF (Accelerated Loading Facitity) are involved in many factors. The major factors are the following:

1) The non-uniformity of stress and deflection relationship in ALF tests
2) The appearance of three-dimensionality
3) The computation is expensive in terms of time and required disk space
4) The complex interaction problems

Chapter 3 3-D ALF Model

Model Geometry

The test lane was simplified as layered cuboids. Figure 44 shows the geometry of a test lane. Total test lane is 60 m long. The length of loading portion is 40 feet (12.192m), the width is 13 feet (3.9624m), and the height is 150 inch (3.81m). On the basis of the order from top layer to the bottom, the model information including thickness of each layer, material properties were listed in Table 7. 3-D model was built according to geometry information in Figure 44. All layers are assumed fully bonded. The model was divided into 320 equal portions along longitudinal direction. The biased seeds were assigned in transverse direction. A mesh converge analysis was conducted. 8 nodes linear brick element type (C3D8) was selected. The whole model contains 69120 C3D8 elements (Figure 45).

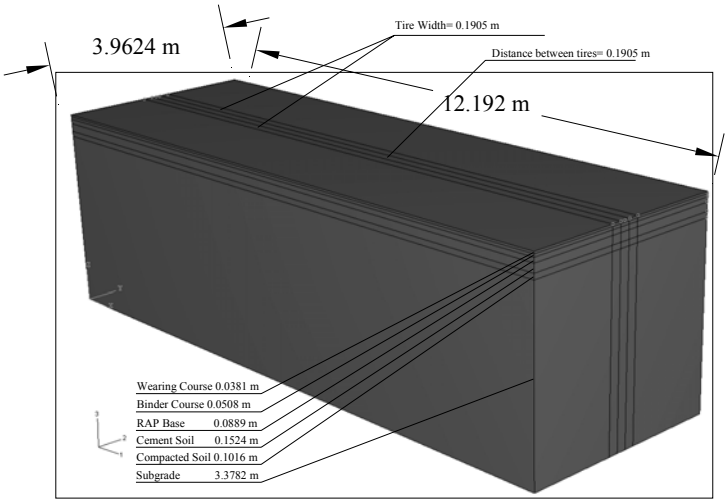

Figure 44 ALF Finite Element Model Geometry Schematic

Table 7 ALF Layer Thicknesses

Layer Sequence	Name	Thickness	
		Unit: cm	Unit: inch
1st	Wearing Course	3.81	1.5
2nd	Binder Course	5.08	2.0
3rd	RAP	8.89	3.5
4th	Cement Soil	15.24	6.0
5th	Compacted Soil	10.16	4.0
6th	Subgrade	337.82	133

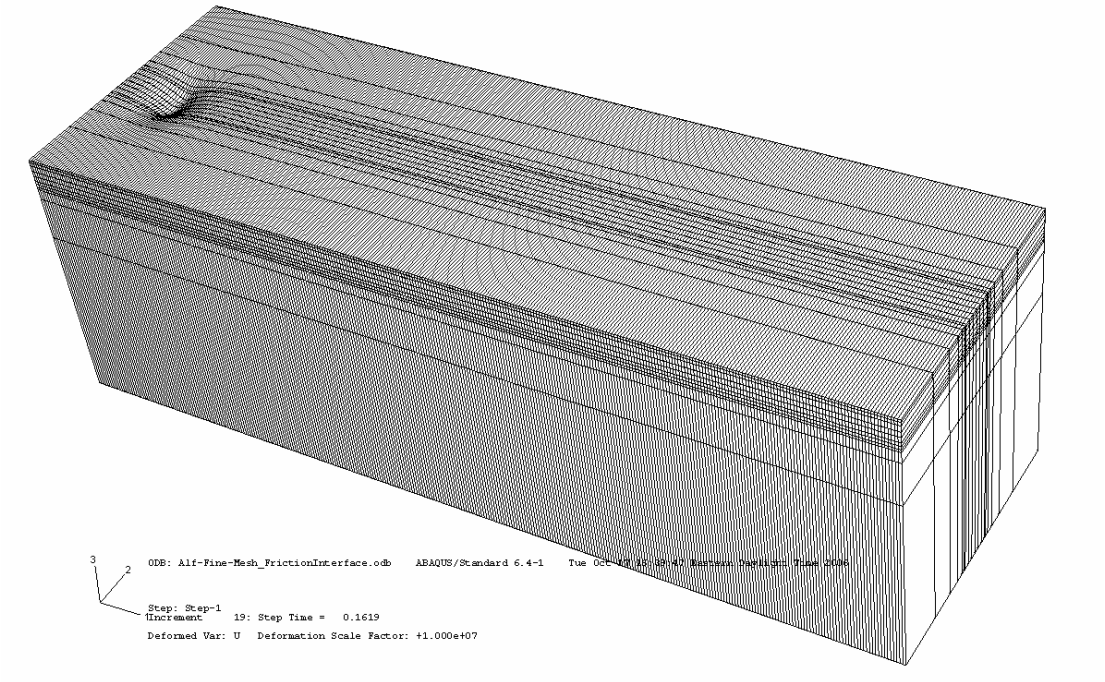

Figure 45 Deformed 3-D Meshed Finite Element Model

Figure 45 presented the meshed model with scaled deformation. Exclusively hexahedral elements were meshed in mesh control tools of ABAQUS 6.4. Dense mesh was observed in tire-pavement contact area. Course mesh was assigned to the area where less stress occurred.

Moving Load Condition

As of Figure 46, the tire print area is simplified as rectangle. The applied load varied with different loading cycle range (Huang 2000). During the ALF experiment, from beginning to 400,000 cycles, the load is 44.5 kN. Then the load increased to 54.7 kN from 400,000 cycles to 500,000 cycles. From 500,000 to 650,000 cycles, the load is 65.0 kN. After 650,000 cycles, the load is 75 kN. In this research, the objective was analyzed stress-strain relationship other than rutting estimation. Thus, the calculated load was 44.5kN which is for first 400,000 cycles.

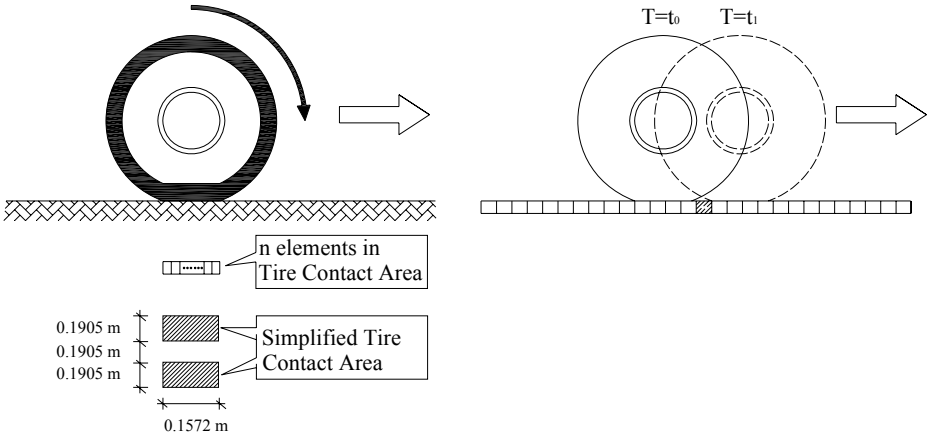

Figure 46 Moving Wheel Load Schematic

In order to simulate the moving load in 3-D finite element analysis, proper assumption is needed for tire approaching and leaving processing. Conventionally a trapezoid shaped load amplitude-time function was widely applied to simulate wheel approaching and leaving mechanism. As presented in Figure 47, the segment AB presented the approaching of the wheel, the segment BC represented the full wheel load, and the segment CD represented the departure of the wheel. In the 3D finite element analysis, the segment AB and CD occupied ¼ of the total wheel loading time.

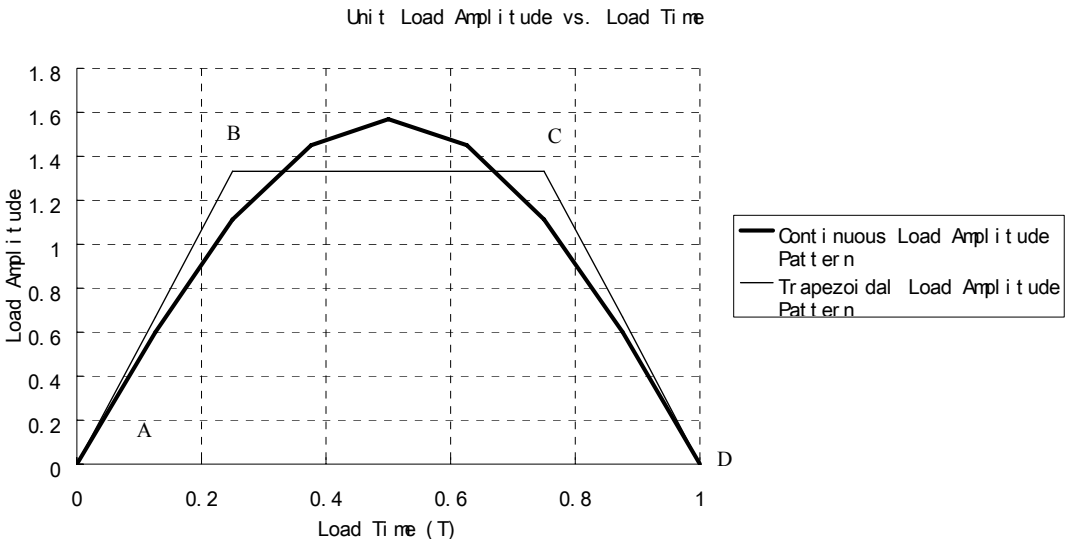

Figure 47 Trapezoidal Load vs. Continuous Load in Time Coordinate

Although the conventional trapezoid load-time relationship was palpable, recent research results indicated the load-time relationship could be more complicated. The load amplitude keeps constant between point B and point C (Figure 47). However, the Yoo et. al. (2006) indicated the trapezoidal impulsive loading amplitude is closely resembled as a hammer. Depending on the loading type, each element is implemented equal loading time and amplitude during phase B and C in Figure 47. Yoo et. al. (2006) proposed a continuous loading method which is non-uniform normalized longitudinal vertical pressure distribution. The amplitude of the leaving element changes linearly from unity to zero. Yoo et. al. (2006) applied different loading amplitudes on variety of elements with continuous loading pattern, while same load amplitude is assumed on all elements in same thread under trapezoidal load pattern. Furthermore, the tire induces greater stresses at its entrance than exit (Yoo et. al. 2006). In this study, due to the lack of field measurement, we assumed the equivalent loading rate and amplitude in approaching and leaving process. However, the amplitude of approaching and leaving changes nonlinearly. As just for an example, a sinusoidal loading curve was obtained for this study. In future, field contact stress should be measured in order to verify the loading pattern assumption.

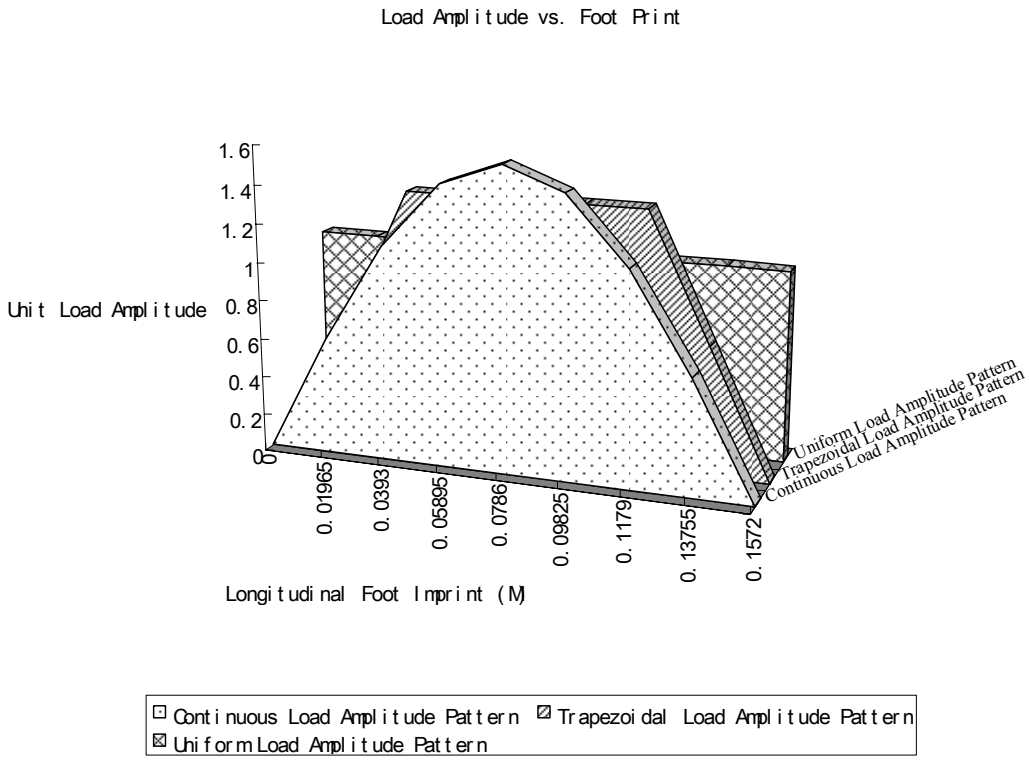

Figure 48 Trapezoidal Load vs. Continuous Load in Longitudinal Coordinate

With same load, different loading pattern will produce different load amplitude. The sum of total load must be equal. Based on this conclusion, load amplitude is calculated as the indication in Figure 48. If the uniform pressure under equal load is 1, the amplitude of trapezoidal pattern is 1.3333; the amplitude of continuous sinusoidal pattern is 1.5708. In other words, if 44.5 kN load rests on 2 rectangles with 0.1905X0.1572M (Figure 46), uniform pressure is 742989Pa; the amplitude of trapezoidal pattern is 990627Pa; the amplitude of continuous sinusoidal pattern is 1167087Pa.

In order to simulate the moving wheel loading at desired speed, quasi-static approach was adopted with amplitude and ramp loading concept. Moving load was simulated gradually entering the loading area and leaving with 320 increments to achieve one entire pass over the whole tire driveway. In each increment, the load moved 38.1 mm

over 1 element. Simultaneously, the loading time was adjusted with correspondence to pre-defined wheel load.

Model Validation

The objective of model validation is to assure the output of 3-D finite element model is reliable. The mesh converge analysis is conducted firstly. Then, the vertical, horizontal and shear stress are compared with linear elasticity analytical results. The acceptable error between finite element results and analytical solution lead to the confidence of correct mesh density and proper boundary condition.

Single concentrated load in center of model was selected for both mesh converge and linear elastic comparison. The boundary conditions were kept identical: pinned on model bottom and restricted horizontal displacement on four outside surface.

The mesh converge analysis is indicated in Figure 49. The vertical stress under wearing course was selected as the converge criterion. From the chart, early converge is observed in less elements. With the increase of element number, the vertical stress under wearing course converges to a certain level. After the inflexion, the tremendous element number contributes little to the vertical stress value. Based on the converge characterization, appropriate mesh refinement around inflexion is selected for following validation and sensitivity analysis.

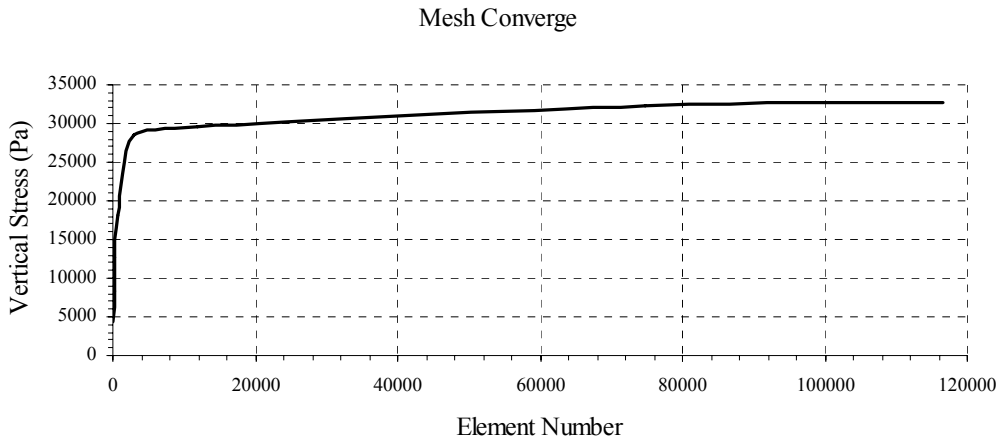

Figure 49 Mesh Converge Study

If a concentrated load is applied on an elastic half-infinite plane, the analytical solution of stress is calculated with the following equations.

$$\begin{cases} \sigma_x = -\dfrac{2F}{\pi}\dfrac{x^3}{\left(x^2+y^2\right)^2} \\ \sigma_y = -\dfrac{2F}{\pi}\dfrac{xy^2}{\left(x^2+y^2\right)^2} \\ \tau_{xy} = \tau_{yx} = -\dfrac{2F}{\pi}\dfrac{x^2y}{\left(x^2+y^2\right)^2} \end{cases}$$

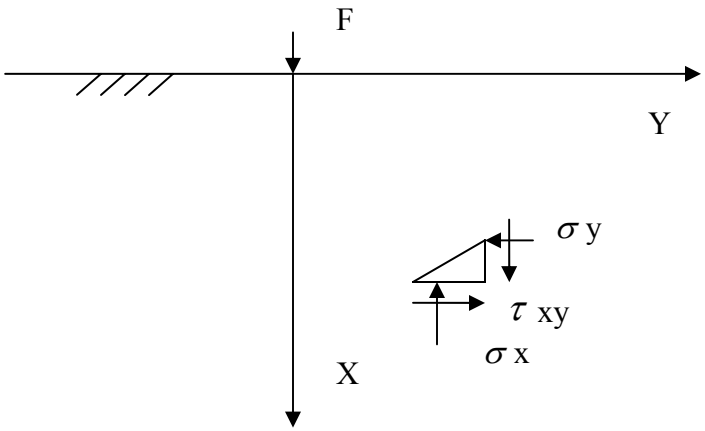

Although the horizontal geometry of 3-D model is limited, the model could be approximately considered as a half-infinite elastic body. Therefore, the comparison of finite element results and analytical elastic solution would be able to indicate the validity of model. In Figure 50 ~ 52, the finite element analysis produces similar vertical, horizontal and shear stresses compared with elastic solutions. In addition, it is indicated that extreme fine mesh does not lead to dramatic accuracy improvement. In order to save computation cost and time, moderate mesh density is selected for following sensitivity analysis.

Firstly, 8-node linear brick elements were assigned on all elements because of economical reason in terms of computation time. Then, 20-node quadratic brick elements with reduced integration and hourglass control are introduced.

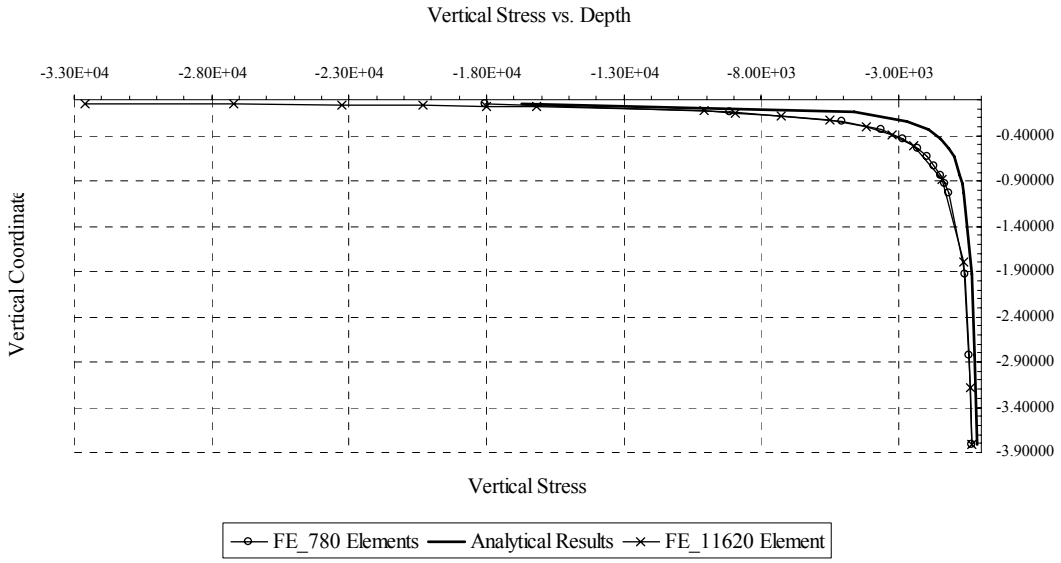

Figure 50 Finite Element and Analytical Solution of Vertical Stress

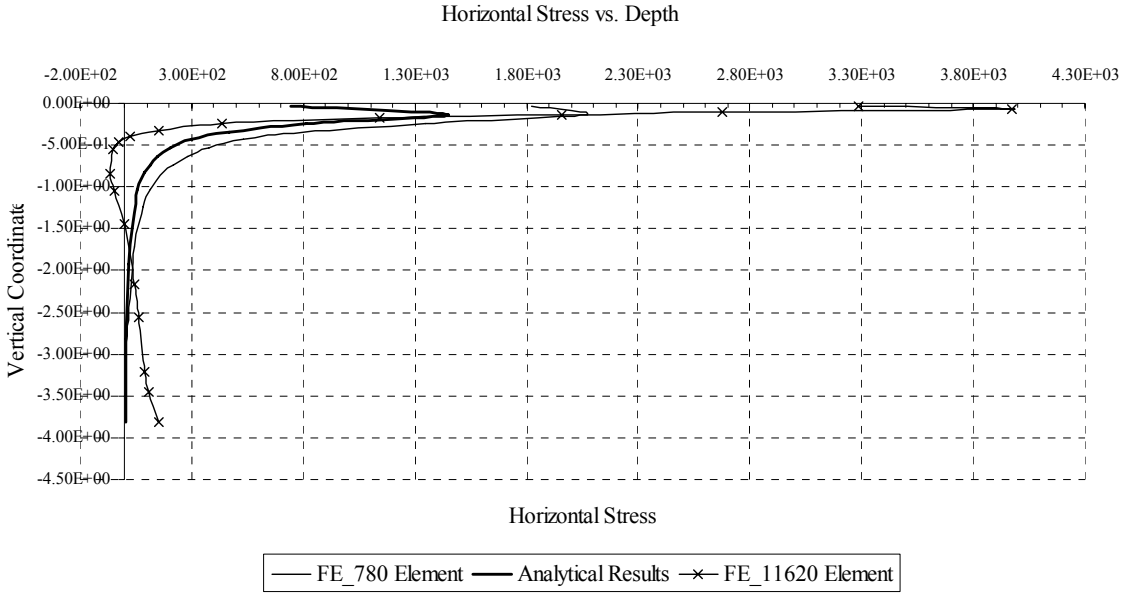

Figure 51 Finite Element and Analytical Solution of Horizontal Stress

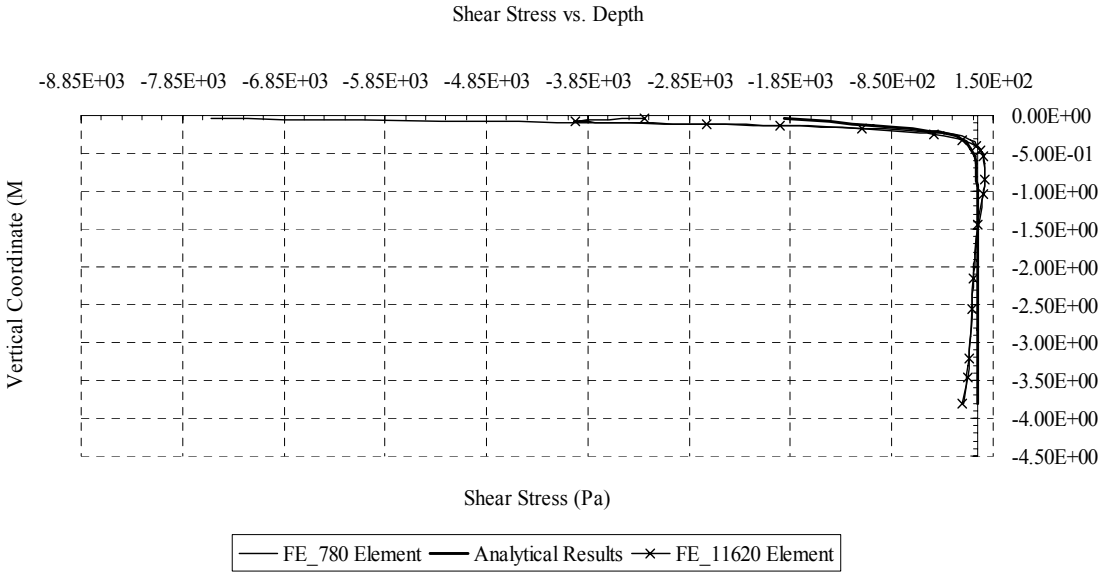

Figure 52 Finite Element and Analytical Solution of Shear Stress

Chapter 4 Pavement and Base Material Properties

Material Properties of Asphalt Mixture

Viscoelastic Model

The viscous behavior of asphalt mixture is simplified with two modulus: a time-dependent shear modulus-$G_R(t)$, and a time-dependent bulk modulus, $K_R(t)$. Both of moduli are represented in a Prony Series in terms of corresponding instantaneous modulus (ABAQUS 2004),

$$\frac{G_R(t)}{G_0} = 1 - \sum_{i=1}^{2} \bar{g}_i^P \left(1 - \exp\left(-\frac{t}{\tau_i}\right)\right)$$

$$\frac{K_R(t)}{K_0} = 1 - \sum_{i=1}^{2} \bar{k}_i^P \left(1 - \exp\left(-\frac{t}{\tau_i}\right)\right)$$

In the current study, the Prony Series was assumed with 2 terms due to a demonstration purpose. In first term, relative shear modulus $\bar{g}_i^P$ is assumed as 0.2; relative bulk modulus $\bar{k}_i^P$ is assumed as 0.5; time constant τ_i is assumed as 0.05. Furthermore, the wearing course and bearing course relaxes pressures faster than shear stresses. Relative moduli $\bar{g}_i^P$, $\bar{k}_i^P$ and time constant τ_i in the second term of Prony Series are selected as 0.1, 0.2, 1. This model results in instantaneous behavior which is assumed as linear elasticity with Young's modulus of 5.43 MPa and Poisson's Ratio of 0.35. The linearelastic parameters were obtained from the reference of Louisiana Transportation Research Center (Huang 2000). This viscoelastic material model was not defined from any particular asphalt mixture. In future, the real viscous parameters of asphalt mixture will be obtained from proper tests. Indirect creep compliance test has been used for characterization of the viscoelastic properties (Mostafa 2006). To determine the material constants, multistep

nonlinear regression is necessary for obtaining extra terms of Prony Series expansion until acceptable fit is achieved. Generally, 6-10 Prony Series terms are required to ensure accurate fit. Current study has been focusing on the different effects of the pavement with assumption of viscoelasticity or linear elasticity. Laboratory viscoelasticity characterization could be considered as future work. ABAQUS version 6.4 was employed to fulfill the viscoelastic constitutive model with quasi-static analysis approach.

Material Properties of Unbound RAP (Reclaimed Asphalt Pavement) Base

Nonlinear Anisotropic Elastic Model

Upon recent researches, it is shown that significant directional dependency (anisotropic behavior) of the resilient properties (Tutumluer and Seyhan 1999; Adu-Oser et al. 2000). Empirical equations with parameters of functions with confining pressure and octahedral stress were often employed to present the horizontal and vertical resilient moduli (Tutumluer and Seyhan 1999; Adu-Oser et al. 2000). In this report, the nonlinear anisotropic elastic properties of unbound granular bases was simulated by the micromechanics-based anisotropic elasticity model developed by Zysset and Curnier (1995) and validated by Masad et al (2004) through series of tests.

Generally, there are two approaches to derive micromechanics-based constitutive models. One is to implement a microstructure tensor to evaluate average stress within representative volume element (RVE) (Christoffersen et al 1981). The alternative way is to represent the relationship of microstructure tensor, stress tensor, and strain tensor to satisfy the principle of material objectivity or frame indifference (Truesdell and Noll 1965; Cowin 1985; Tobita 1989). With the lateral approach, Zysset and Curner (1995) proposed one anisotropic elasticity model where the polynomial dependency of the elastic constants with the power law relationship of the microstructure tensor invariants. The constitutive relationship matrix was shown below:

$$C_{ijkl} = \begin{bmatrix} (\lambda_c + 2G_c)m_1^{2k} & \lambda_c m_1^k m_2^k & \lambda_c m_1^k m_3^k & 0 & 0 & 0 \\ & (\lambda_c + 2G_c)m_2^{2k} & \lambda_c m_2^k m_3^k & 0 & 0 & 0 \\ & & (\lambda_c + 2G_c)m_3^{2k} & 0 & 0 & 0 \\ & & & 2G_c m_2^k m_3^k & 0 & 0 \\ & SYM & & & 2G_c m_1^k m_3^k & 0 \\ & & & & & 2G_c m_1^k m_2^k \end{bmatrix}$$

Where $\lambda_c = \frac{E_c \mu_c}{(1+\mu_c)(1-2\mu_c)}; G_c = \frac{E_c}{2(1+\mu_c)}$

m_1, m_2, and m_3 are major, intermediate, and minor principal components of the microstructure tensor, respectively. They are derived from microstructure tensor as the following (Oda and Nakayama 1989)

$$M_{ij} = \begin{bmatrix} (2+A/(6+A) & 0 & 0 \\ 0 & (2+A/(6+A) & 0 \\ 0 & 0 & (2-A/(6+A) \end{bmatrix}$$

$$A = \frac{2\sum_{k=1}^{N} \cos(2\theta_k)}{N}$$

N=number of aggregate projections on a vertical section

θ_k =orientation of an individual aggregate projection on a vertical section from -90 to +90.

The principal components of the microstructure were derived on the basis of M_{ij}.

$$m_1 = m_2 = \frac{2+A}{6+A}; m_3 = \frac{2-A}{6+A}$$

Mathematical manipulation was conducted to obtain the ratio of the vertical elastic modulus to the horizontal elastic modulus (Masad 2004)

$$\frac{E_y}{E_x} = \left(\frac{2+A}{2-A}\right)^{2k}$$

The anisotropic ratio is derived from aggregate orientation. Masad et al. (2004) combined this relationship with anisotropy ratio which is based on the orientation of contacts to find the relationship of k and r (ratio of the average shear contact stiffness to the average normal contact stiffness). Du and Dusseaut (1994) presented the following anisotropic stress-strain relationship.

$$\begin{pmatrix}\sigma_{11}\\ \sigma_{22}\\ \tau_{12}\end{pmatrix} = D\begin{bmatrix} 3+r-2Ac-\frac{1}{2}rA^2s^2 & 1-r+\frac{1}{2}rA^2s^2 & As-\frac{1}{2}rA^2sc \\ & 3+r+2Ac-\frac{1}{2}rA^2s^2 & As-\frac{1}{2}rA^2sc \\ SYM & & 1+r-\frac{1}{2}rA^2c^2 \end{bmatrix}\begin{bmatrix}\varepsilon_{11}\\ \varepsilon_{22}\\ \gamma_{12}\end{bmatrix}$$

Where D is material constant, θ_0 =inclination of the major principal direction of aggregate contact from the horizontal axis. C=cos $2\theta_0$;s=sin $2\theta_0$. For transverse anisotropy, the major axis of the material anisotropy is in the horizontal direction, s=0, c is constant. Then simplified relationship was presented (Masad 2004)

$$\begin{pmatrix}\sigma_{11}\\ \sigma_{22}\\ \tau_{12}\end{pmatrix} = c\begin{bmatrix} 3+r-2A & 1-r & 0 \\ & 3+r+2A & 0 \\ SYM & & 1+r-\frac{1}{2}rA^2 \end{bmatrix}\begin{bmatrix}\varepsilon_{11}\\ \varepsilon_{22}\\ \gamma_{12}\end{bmatrix}$$

Masad (2004) solved the stiffness matrix for axial loading conditions in the vertical and horizontal directions gives stiffness anisotropy.

$$\frac{E_y}{E_x} = \left(\frac{3+r+2A}{3+r-2A}\right)$$

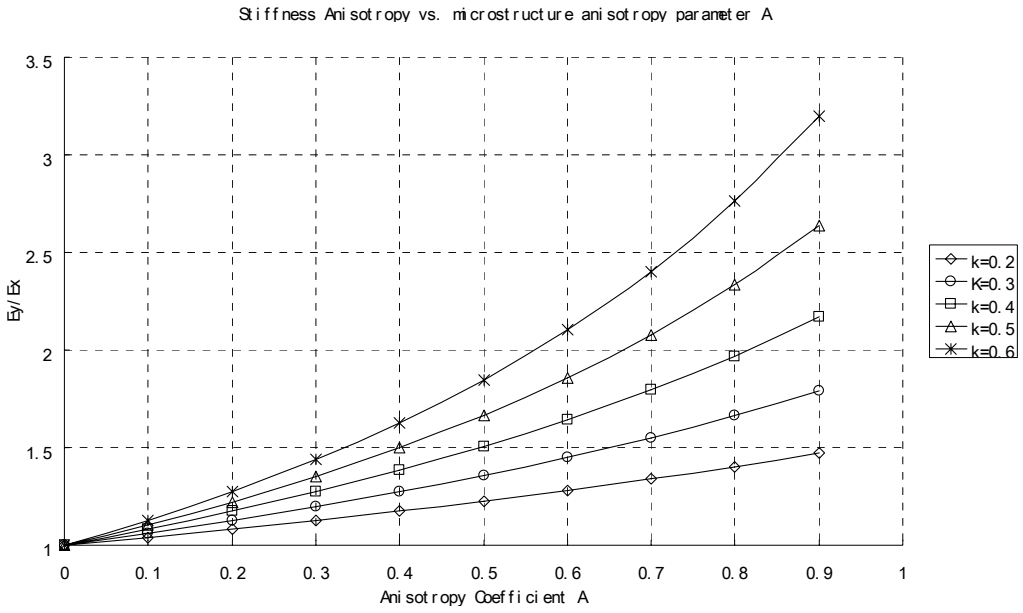

Figure 53 Stiffness Anisotropy vs. Microstructure Anisotropy Parameter K (Masad et. al. 2004)

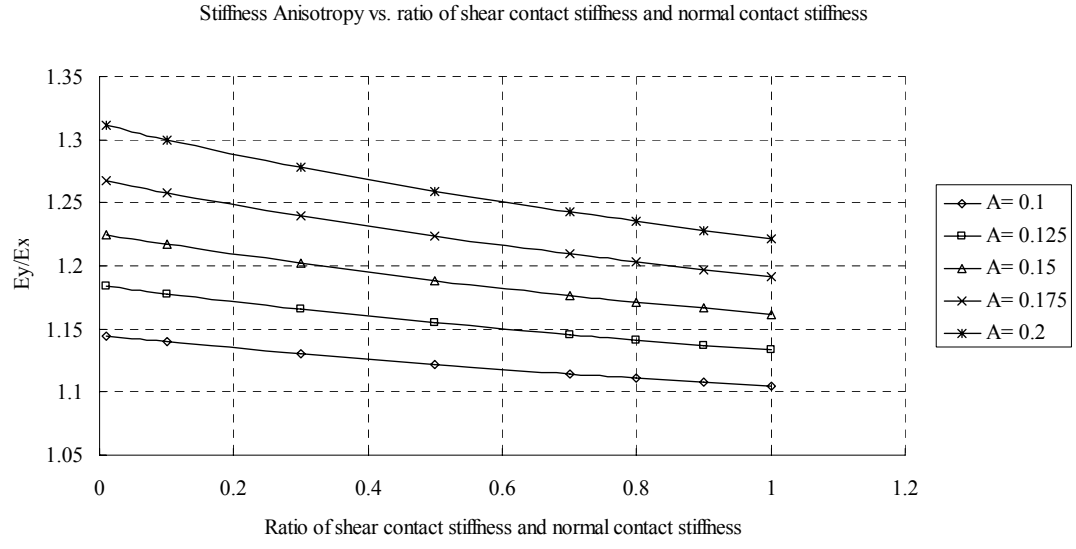

Figure 54 Stiffness Anisotropy vs. Ratio of Shear Contact Stiffness and Normal Contact Stiffness

Notice that the A in above equation is evaluated based on the directional distribution of the contact normal vectors $E(I) = \frac{1}{4\pi}(1 + M_{ij} l_i l_j)$ (Kanatani 1984). E(I) is probability density function.

According to homogeneity assumption, the two A derived by different ways qualify equal level of inherent anisotropy. Then the following k-r relationship was yielded (Masad 2004).

$$k = \frac{\log\left(\frac{3+r-2A}{3+r+2A}\right)}{\log\left(\frac{2+A}{2-A}\right)^2}$$

For the reason of simplicity, average A value was assumed to be 0.5. So in this study, the average k-r relationship was assumed as the following equation.

$$k = 2.25\log\left(\frac{4+r}{2+r}\right)$$

A nonlinear anisotropic elastic material property was introduced by user defined ABAQUS subroutine on the basis of the above-mentioned derivation. The file can be referred in Appendix B.

Stress-dependent Model

The unbound base and subgrade are simulated with Uzan-Witczak resilient model. Uzan (1985) proposed a three-parameter resilient model.

$M_r = K\theta^n \sigma_d^m$

where $\sigma_d = \sigma_1 - \sigma_2$, $\theta = (\sigma_1 + 2\sigma_2)/3$, k,n and m are material constants.

After observing that σ_d coincides with octahedral shear stress when the stress rate is restricted to the triaxial test configuration, Witczak and Uzan(1988) generalized Uzan's resilient model as the following

$$M_r = K\theta^n \tau_{oct}^m$$

where $\tau_{oct}^m = \frac{1}{3}\sqrt{(\sigma_1 - \sigma_2)^2 + (\sigma_2 - \sigma_3)^2 + (\sigma_3 - \sigma_1)^2}$

A fixed point iteration algorithm has been commonly used to implement Uzan's model into various computer programs. However, the fixed-point iteration is eventually bound to diverage if the load level is too high. Even if the fixed-point iteration converges, the performance of the algorithm is bound to degrade with increased load level (Hjelmstad and Taciroglu, 2000). Hijelmstad and Taciroglu(2000) proposed an algorithm to implement Uzan's model, in which the resilient modulus is updated based on the strains of the last iteration rather than the previous stresses as in the fixed point iteration algorithm.

$$M_r = (1+\nu)\left[\frac{K}{1+\nu}\left(\frac{\nu}{1-2\nu} + \frac{1}{3}\right)^n\right]^\mu \rho^{um}\gamma^{um}$$

where $\rho = |\varepsilon_1 + \varepsilon_2 + \varepsilon_3|$, γ is Octahedral shear strain, the other material constants are the same as the previous.

Zuo(2003) made some minor changes to the model. The power of the octahedral shear strain, m, is negative for fine materials. An overflow error would occur if the octahedral shear strain is very small. Uzan (1985)'s resilient modulus model can be incorporated into the analysis using user materail vas user subroutine UMAT. The UMAT file can be referred in Appendix A.

Chapter 5 Sensitivity Analysis

The sensitivity analysis involved two aspects: speeds and constitutive models. The influence due to variety of speeds and constitutive models is investigated through above-mentioned 3-dimensional finite element simulation.

Speed factor related to Linear elasticity and Viscoelasticity

According to the viscous nature of asphalt pavements, the viscoelasticity is more appropriated for wearing and bearing courses than linear elasticity assumption. Thus, the speed became one of the important factors to affect performance of asphalt pavement. In order to verify the essence of asphalt pavement, viscoelastic model was compared with linearelastic model.

In this study, the asphalt pavement structure was assumed as fully bonded linearelastic body. Then basic stress-strain data is obtained under both high wheel speed (60 mile/hour) and low wheel speed (10 mile/hour). Then, wearing course, bearing course and RAP base were assigned viscoelastic material property as listed in Table 8. Again, low speed (10 mile/hour) and high speed (60 mile/hour) were applied to partial viscoelastic models. The difference of linearelastic model and viscoelastic model was obtained to investigate the speed factor related to viscoelasticity.

The comparison in strains on bottom of wearing course, bearing course and RAP is presented in the following Figure 55-68.

Table 8 Linearelastic and Viscoelastic Properties in ALF Layers

	Linear elasticity		Viscoelasticity		
	E (Pa)	υ	$\bar{g}_i^P$	$\bar{k}_i^P$	τ_i
Wearing Course	5.43E09	0.35	0.2	0.5	0.05
			0.1	0.2	1
Binder Course	4.41E09	0.35	0.2	0.5	0.05
			0.1	0.2	1
RAP	5.93E09	0.35	0.2	0.5	0.05
			0.1	0.2	1
Cemented Soil	5.00E08	0.35	-	-	-
Compacted Soil	2.60E08	0.30	-	-	-
Subgrade	1.50E08	0.45	-	-	-

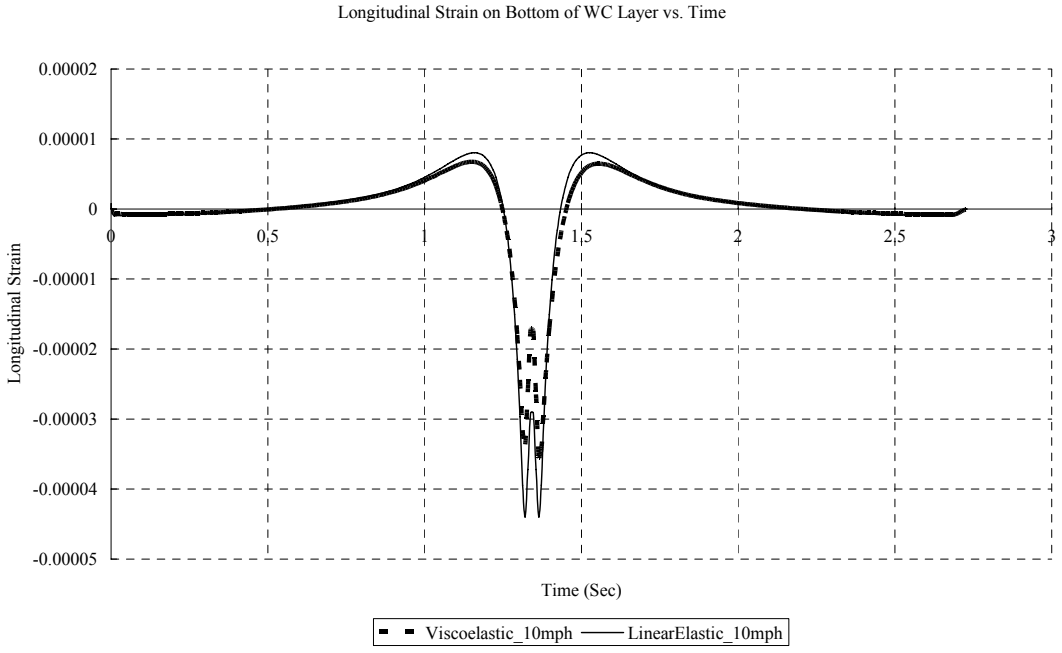

Figure 55 Longitudinal Strain under WC at 10mph

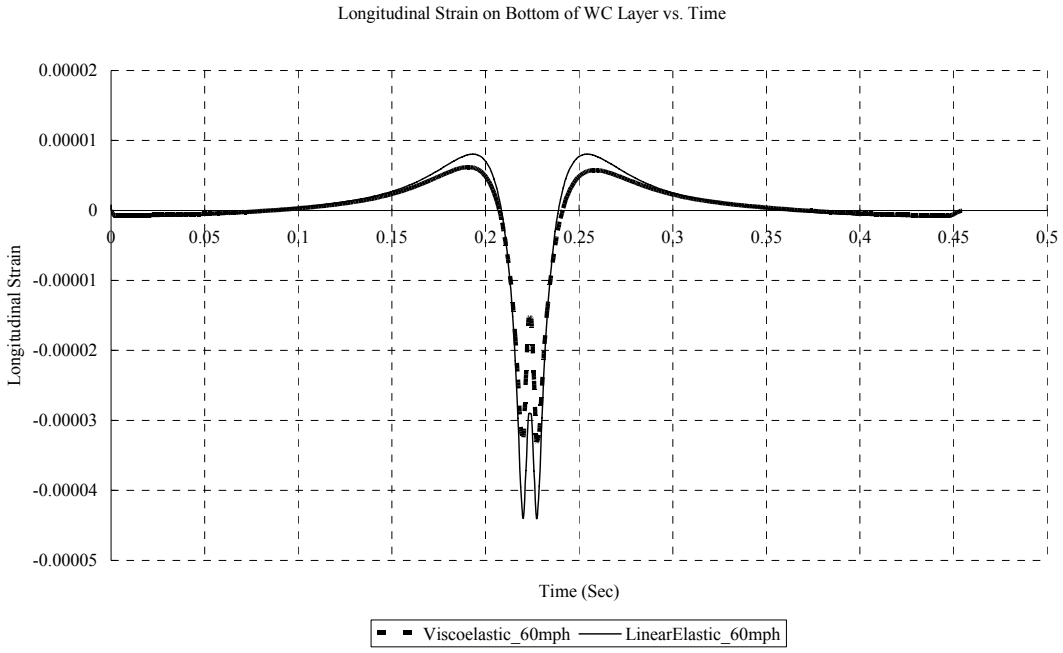

Figure 56 Longitudinal Strain under WC at 60mph

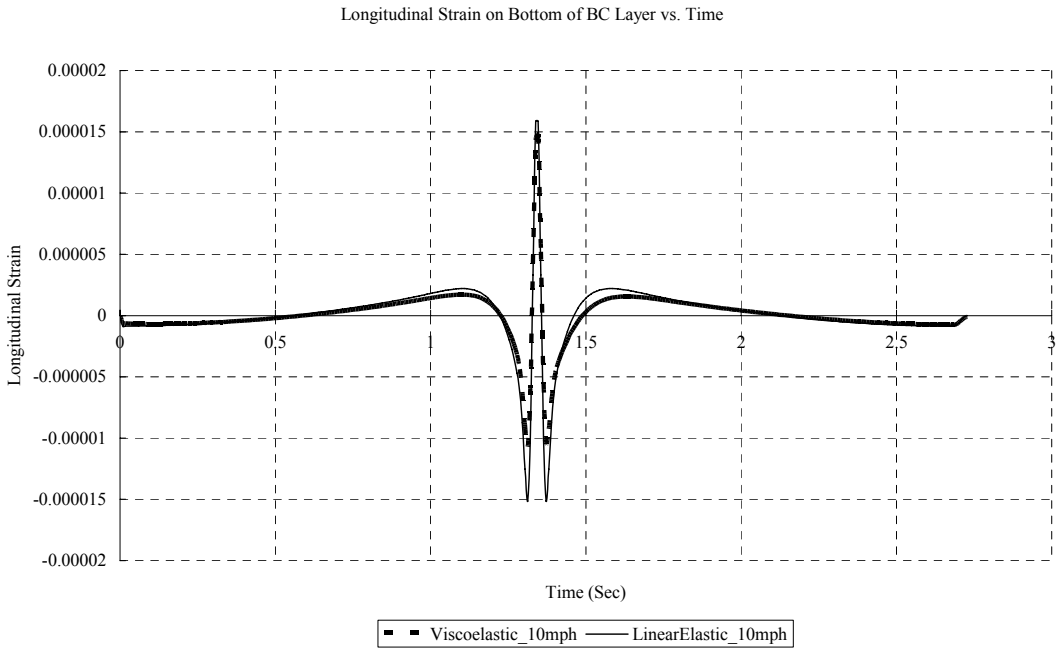

Figure 57 Longitudinal Strain under BC at 10mph

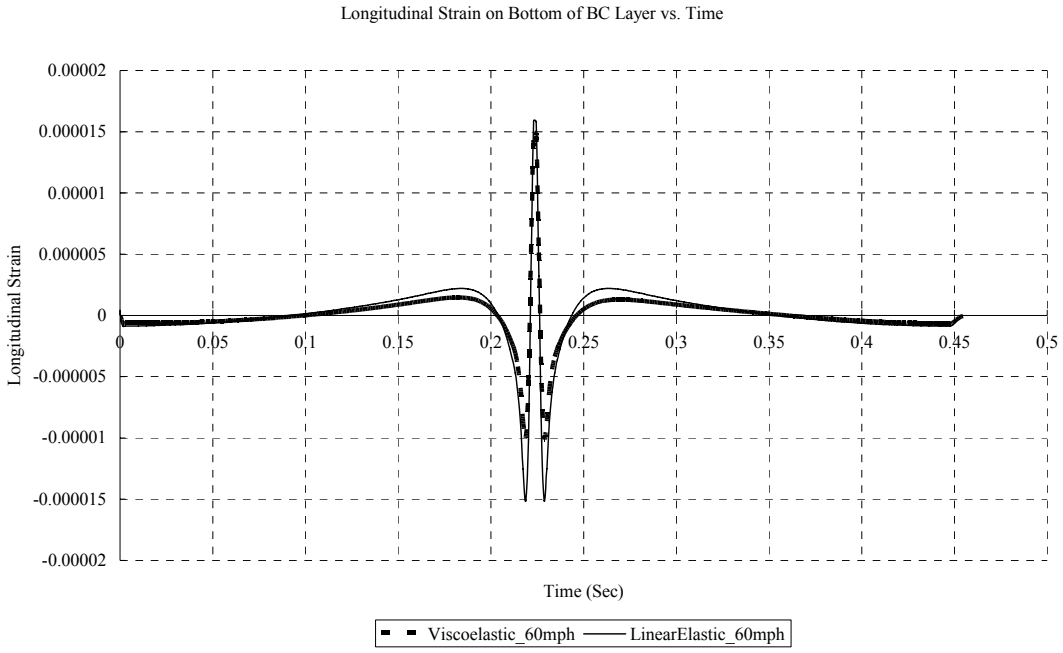

Figure 58 Longitudinal Strain under BC at 60mph

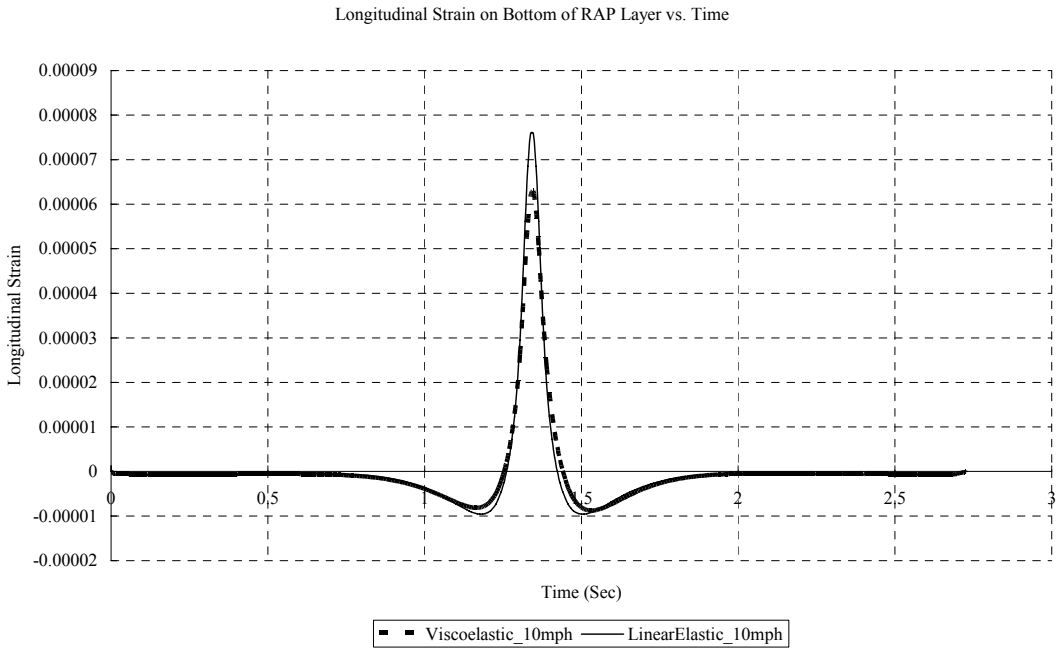

Figure 59 Longitudinal Strain under RAP at 10 mph

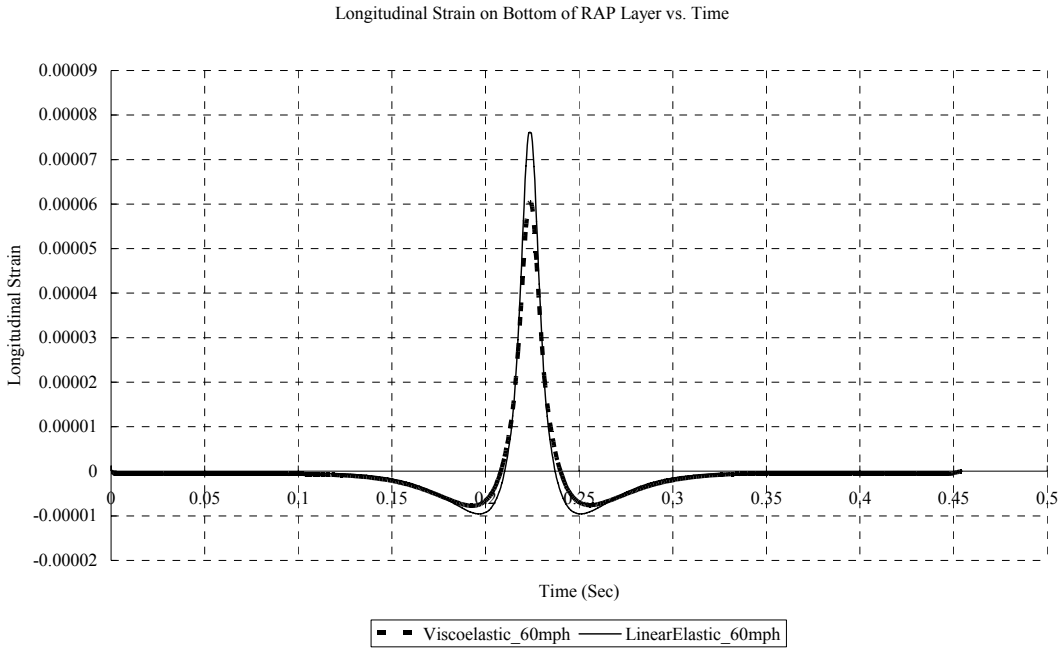

Figure 60 Longitudinal Strain under RAP at 60mph

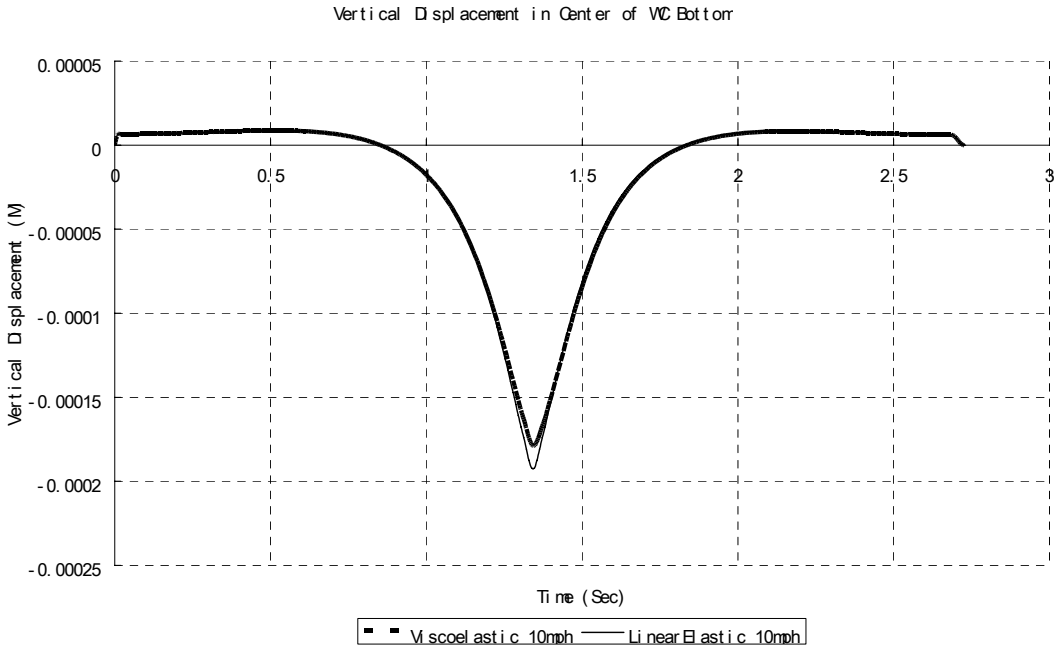

Figure 61 Vertical Displacement under WC at 10mph

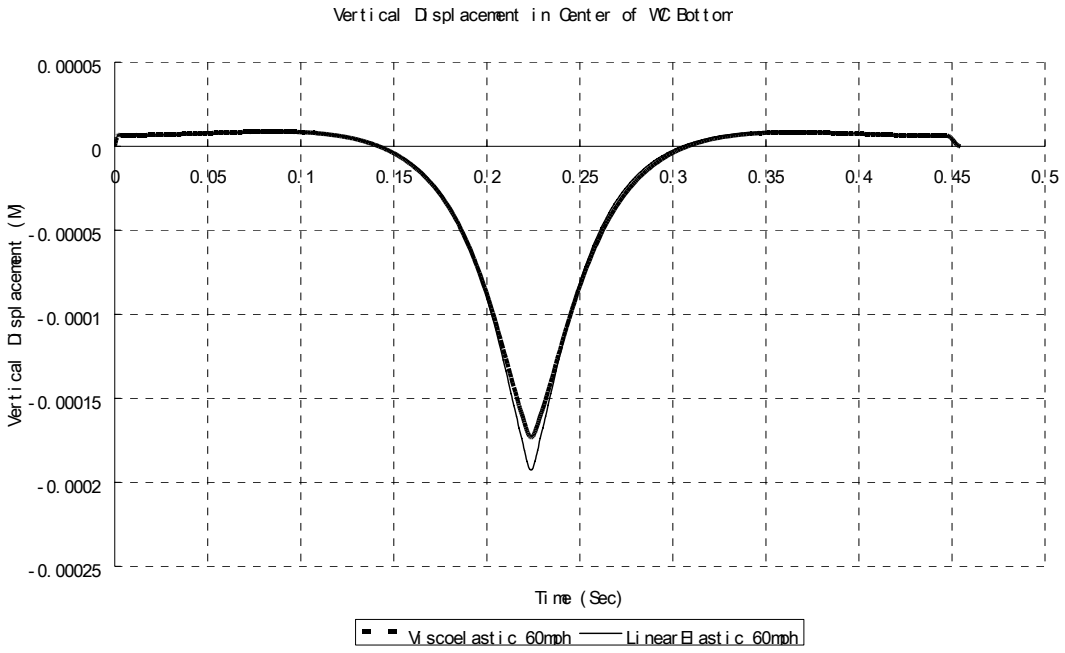

Figure 62 Vertical Displacement under WC at 60mph

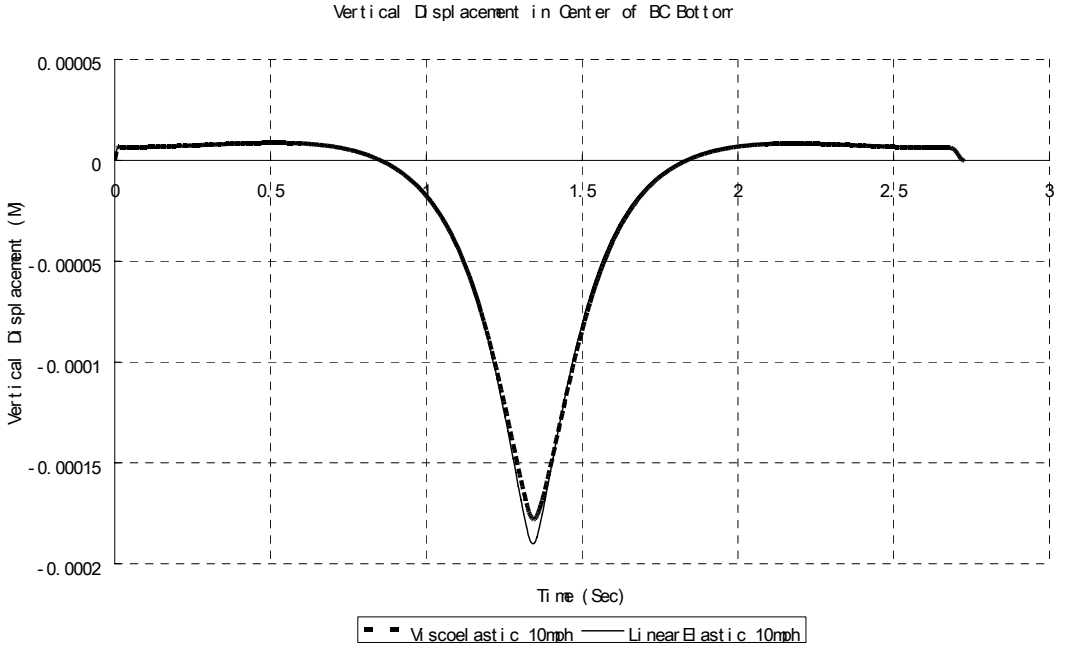

Figure 63 Vertical Displacement under BC at 10mph

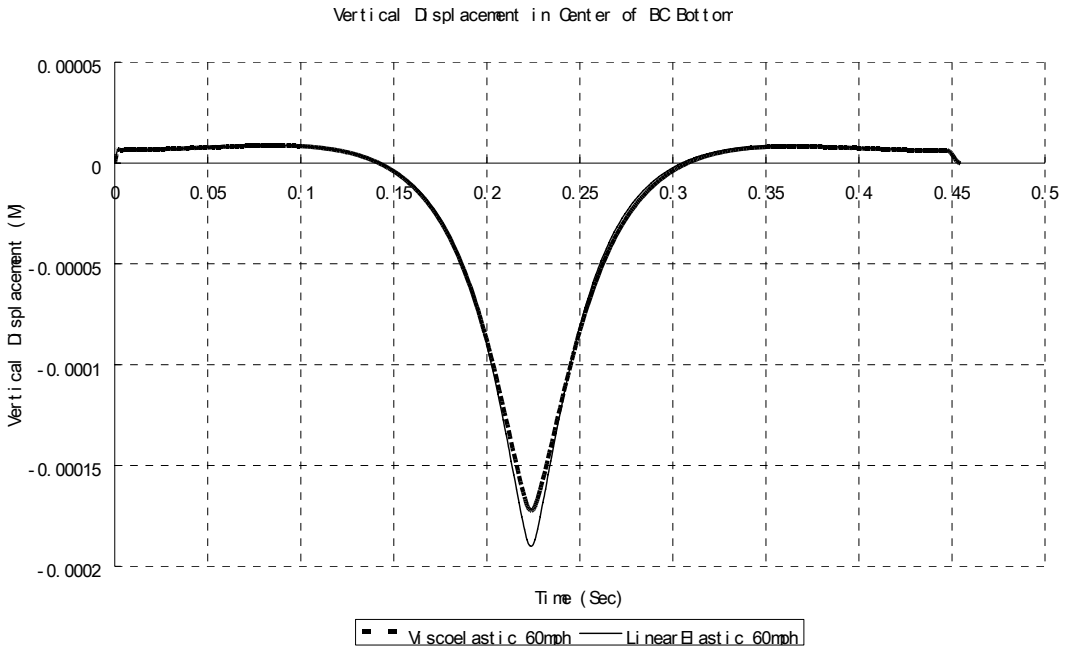

Figure 64 Vertical Displacement under BC at 60mph

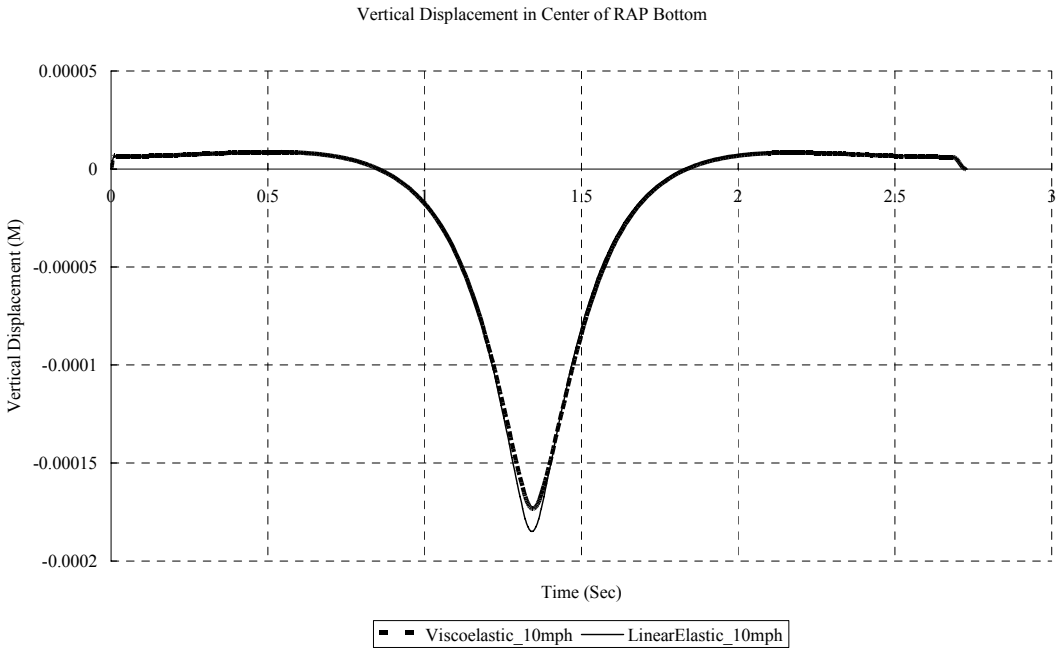

Figure 65 Vertical Displacement under RAP at 10mph

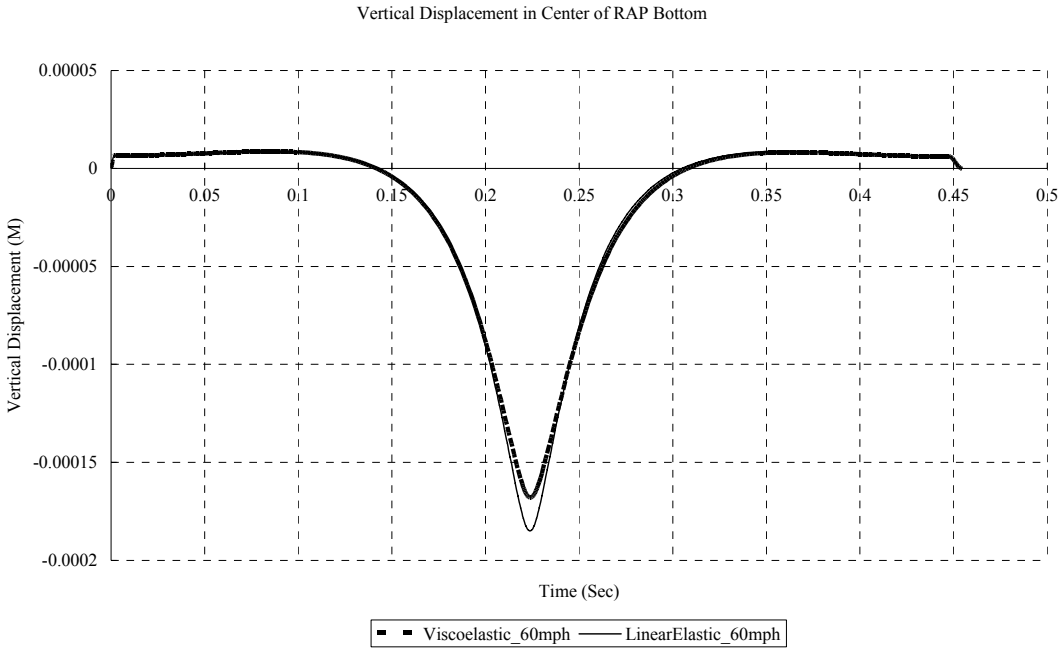

Figure 66 Vertical Displacement under RAP at 60mph

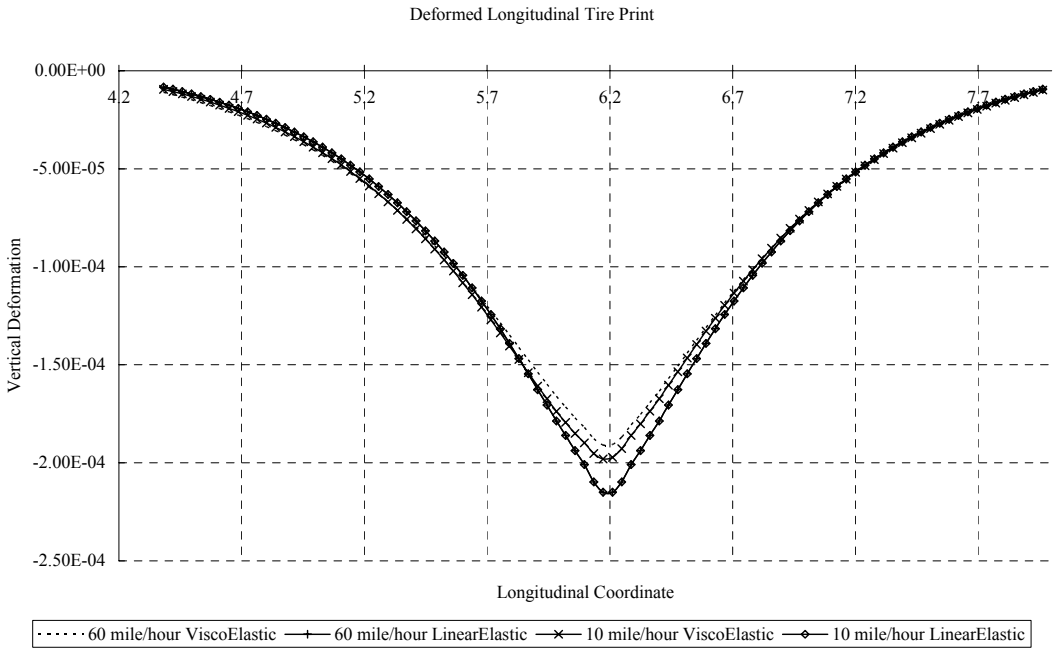

Figure 67 Deformed Longitudinal Tire Print

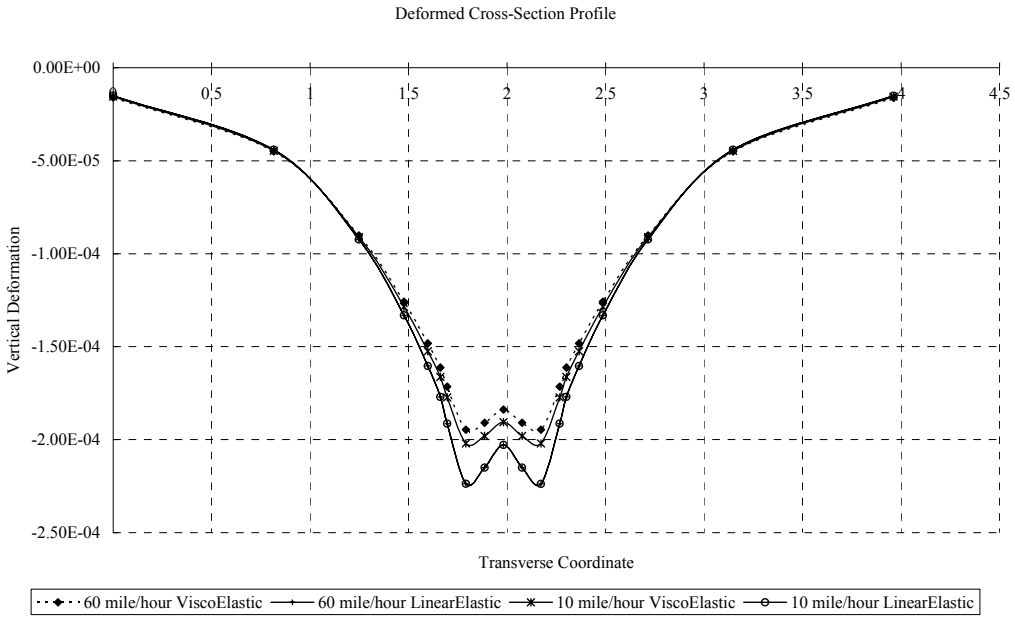

Figure 68 Deformed Cross-Section Profile

Although elastic model was employed to simulate asphalt pavement for decades, and the results of elastic model were accepted by comparison with field measurements since 1960's (Waterhouse, 1967, Duncan, et al., 1968, Feeme and Marais, 1972), shortcomings were presented through the comparison with viscoelastic models. As shown in Figure 55-57, the elastic FE model failed to simulate delayed recovery of asphalt pavement under transient loading condition. In contrast, the assumed viscoelastic models successfully simulated the time retardation of the response as well as the asymmetry of the signal, as shown in Figure 55-57. In addition, the fast recovery of the material in the longitudinal direction was manifested in the calculated pavement response.

Additional observations were drawn from Figure 67-68. The deformed longitudinal and transverse footprint cross-sections under speeds of 10 mile/hour and 60 mile/hour are identical. It is proven that the vertical deformation predicted by elastic FE models was independent of speed. However, viscoelastic model is capable to catch the speed related performance of asphalt pavement. It was found that the predicted strains are

related to wheel load speeds. The vertical deformation trends to increase along with moving wheel speed decreasing. Similar observation was achieved in longitudinal strains. Comparing Figure 55 and 56, the peak amplitudes of retarding longitudinal strain under viscosity vary in different wheel speeds. In Figure 57 and 58, as well as Figure 59 and 60, obvious differences in peak amplitudes of retarding longitudinal strain are observed as well on bottom of bearing course and RAP layer.

On the basis of above-mentioned comparisons, one can conclude that viscoelasticity is better to model asphalt concrete pavement under the moving wheel load.

Although the essential differences exist between viscoelasticity and linear elasticity, the difference is not uniform along the depth. From Figure 55-61, the difference between linearelastic and viscoelastic models under equivalent load tends to diverse at different depths. In Figure 55, 57 and 59, the smallest difference between viscosity and elasticity were achieved on RAP layer bottom. It was found that the implementation of linearelastic model in RAP layer will affect the prediction of the pavement behavior in defects less than the linearelastic assumption in wearing course and bearing course. Thus, the one of important characteristics of unbound granular material, transverse anisotropy, could be considered in elastic assumption.

Anisotropic Model Compared with Isotropic Model

The discussion in the last session indicates the elastic assumption for RAP layer will induce much smaller inaccuracy than viscoelastic assumption. In addition, milled RAP is unbounded material. No asphalt bond between aggregate like asphalt mixture. Mostly, the behavior of viscoelasticity is less significant than wearing and bearing course. Therefore, transverse anisotropy, another important material properte of unbound granular material, could be considered in RAP layer under elastic assumption.

The nonlinear transverse anisotropic constitutive model was implemented in RAP layer. Wearing course and bearing course kept identical viscoelastic model in Table 8. The micromechanics-based anisotropic elasticity model discussed in Chapter 4 was obtained. To invest how this model cause pavement response change upon equivalent load, parameters r=-0.7 and A=0.5 were selected. Those parameters are not measured by any physical test of real materials. They may not represent any unbound material. However, the micromechanics-based anisotropic elasticity model was verified with triaxial tests (Masad et al. 2004). Masad et al. (2004) draw a conclusion that the model produces reasonable results within the range Ey/Ex less than 3. With parameters r=-0.7 and A=0.5, the ration of vertical elastic modulus over horizontal elastic modulus is 2.538 which is in the predictable range. The comparison between isotropic viscoelastic RAP layer and micromechanics-base transverse anisotropic elastic RAP layer presents in Figure 69-76.

.

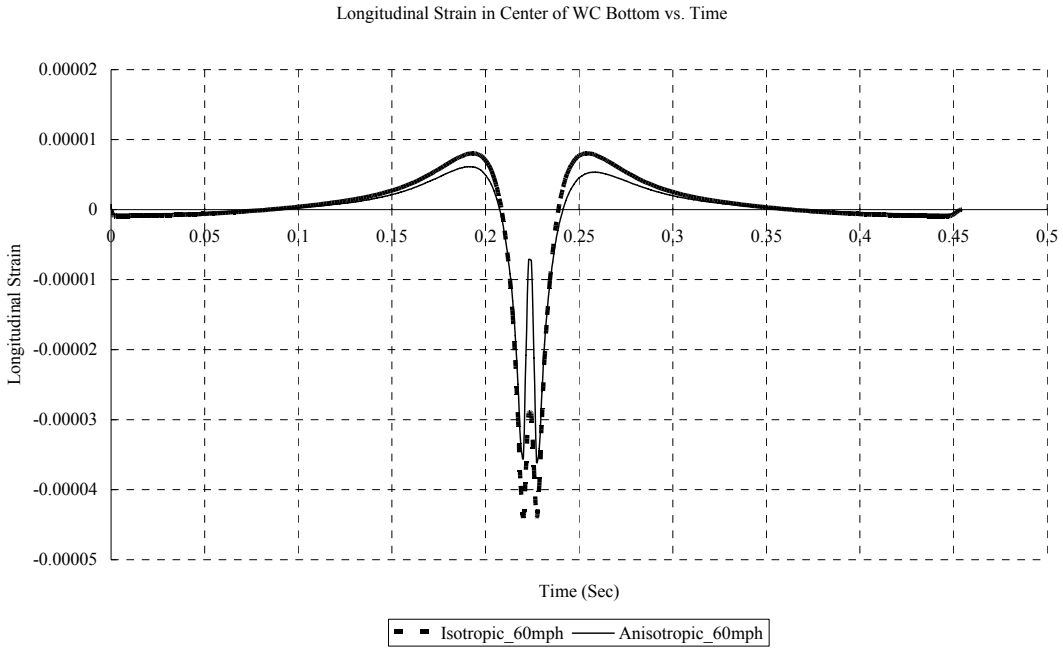

Figure 69 Longitudinal Strain under WC at 60mph

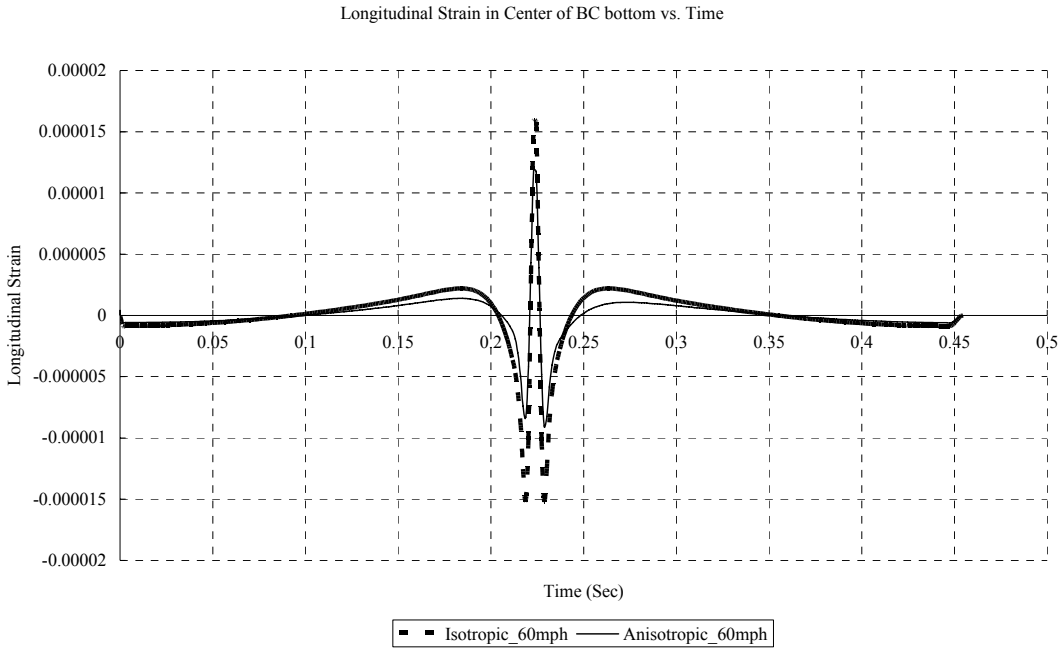

Figure 70 Longitudinal Strain under BC at 60mph

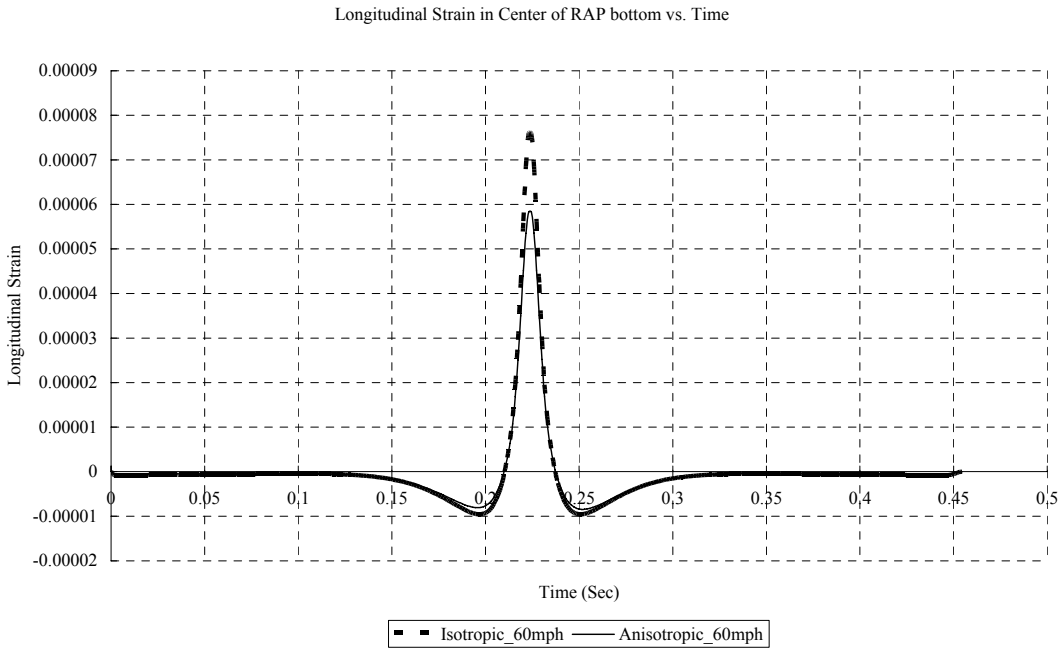

Figure 71 Longitudinal Strain under RAP at 60mph

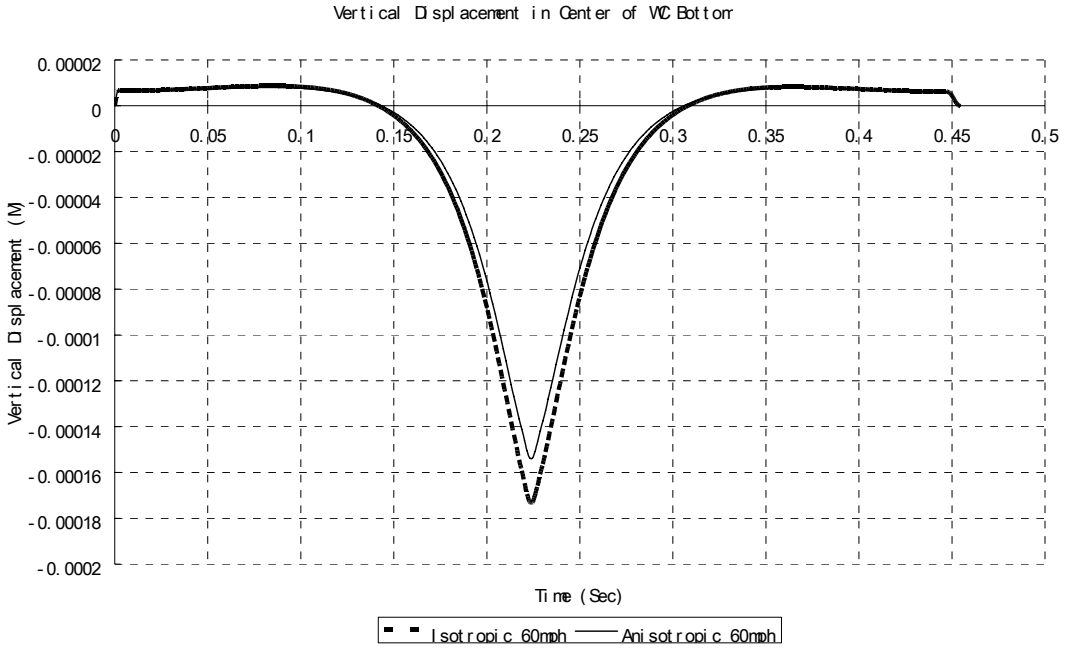

Figure 72 Vertical Displacement under WC at 60mph

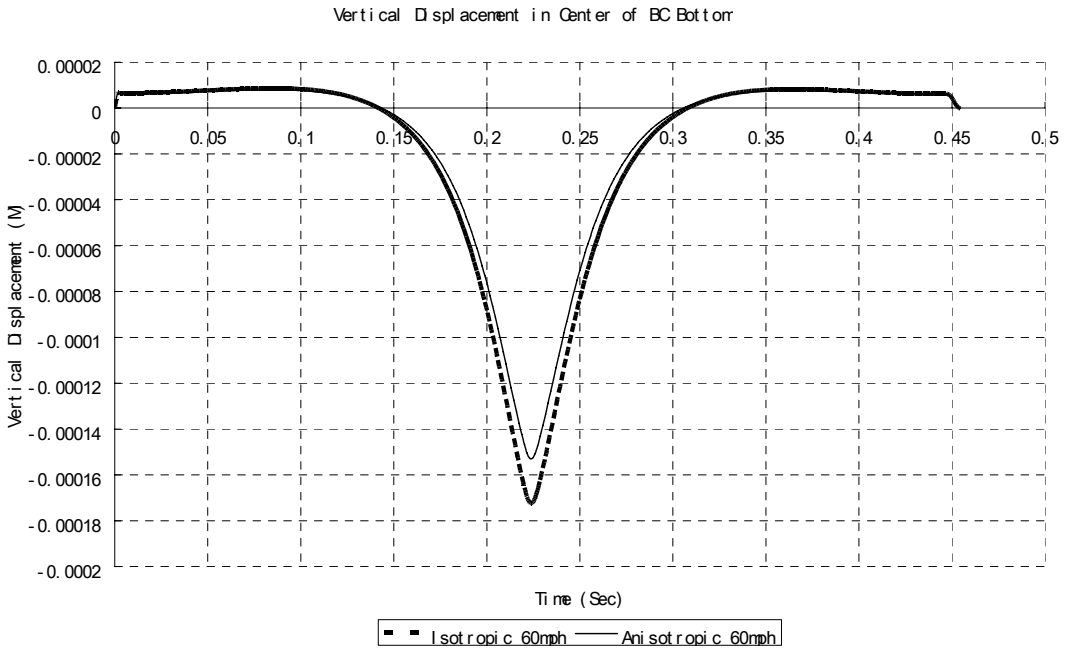

Figure 73 Vertical Displacement under BC at 60mph

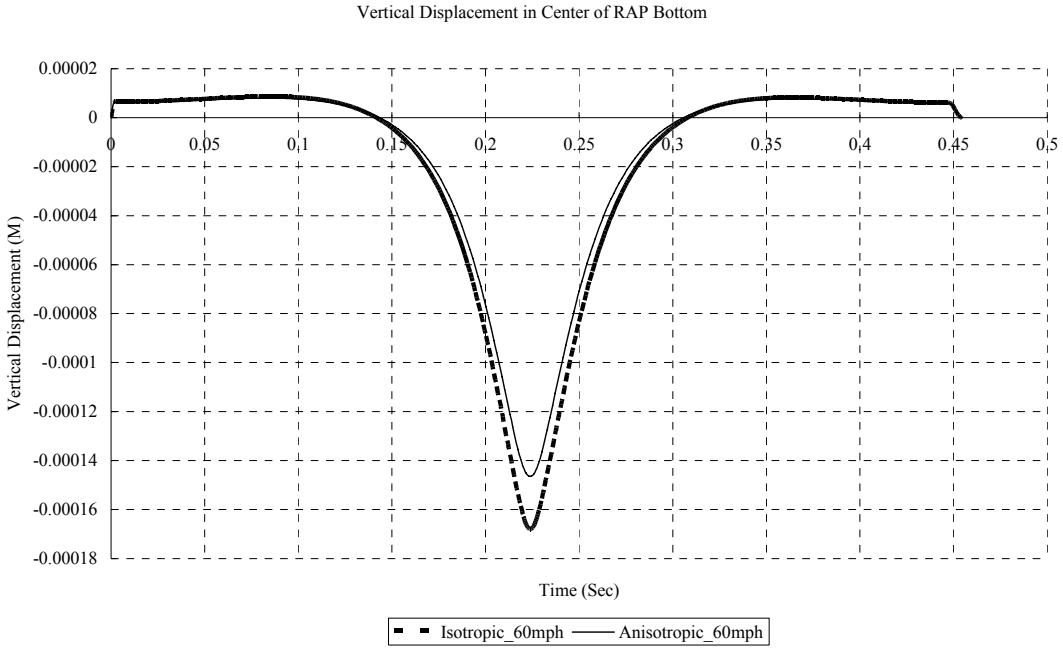

Figure 74 Vertical Displacement under RAP at 60 mph

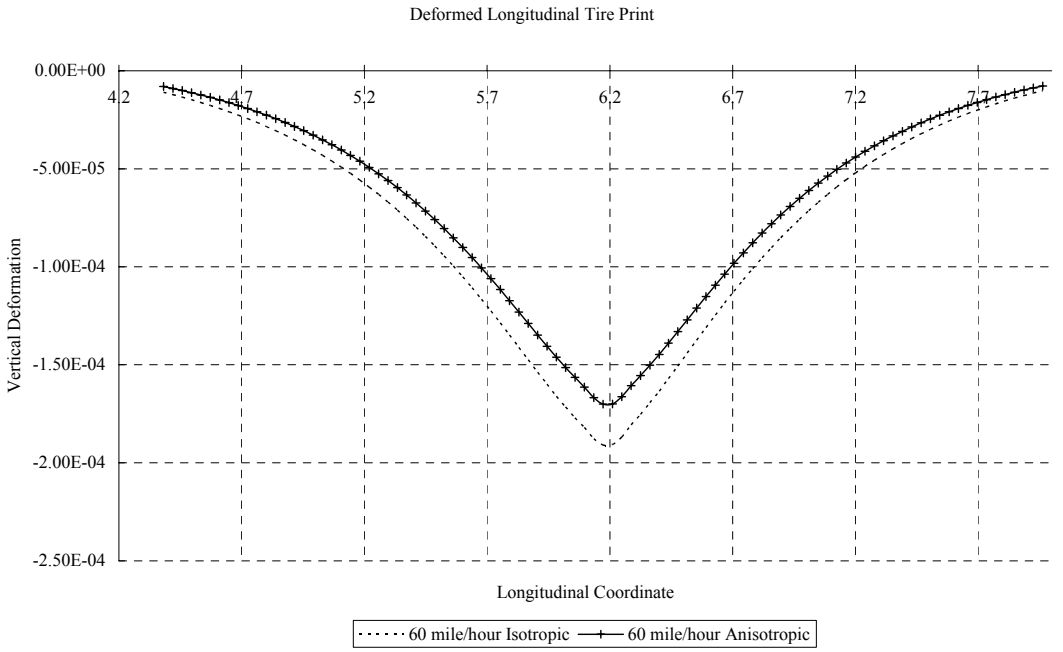

Figure 75 Deformed Longitudinal Tire Print

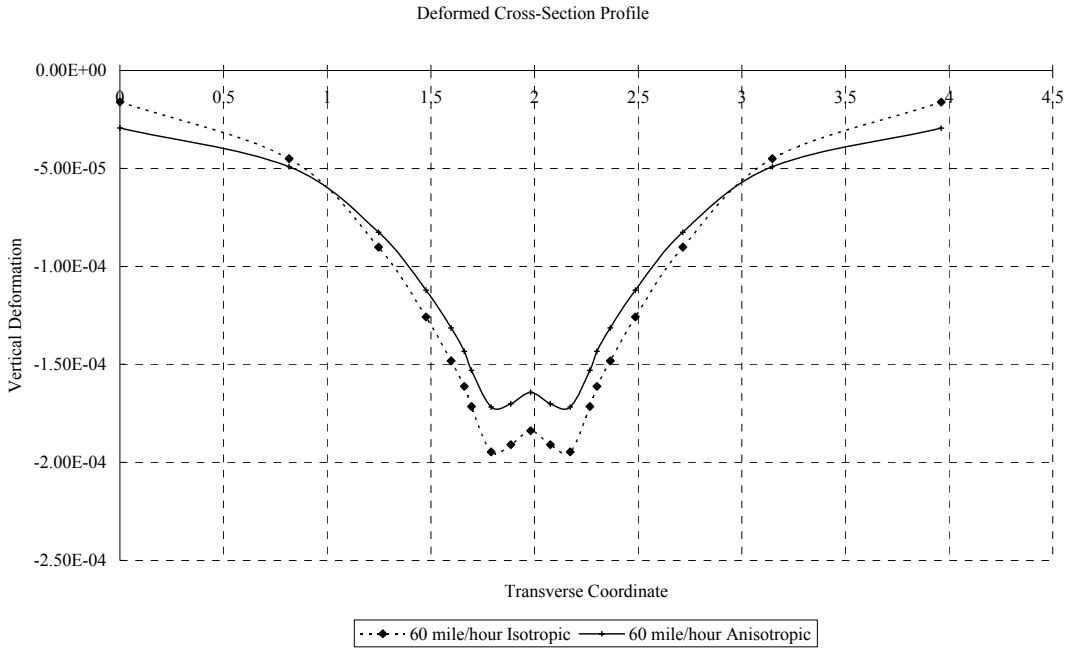

Figure 76 Deformed Cross-Section Profile

Nonlinear transverse anisotropic constitutive model leads to different horizontal and vertical moduli and Poisson's ratios. The longitudinal and transverse displacement is different from those with linear elasticity (Figure 74-76) due to non-uniform moduli and Poisson's ratios.

From Figure 74-76, we observed that the vertical deformation with anisotropic elastic model is less than that with isotropic elastic model. That indicated the transverse anisotropic model is able to simulate the phenomenon that is the vertical modulus is stiffer than horizontal modulus. This phenomenon of unbound granular material is approved by many triaxial tests (Tutumluer and Seyhan 1999).

From Figure 69-71, it was found the transverse anisotropy not only causes the vertical displacement smaller, but also leads to unsymmetrical longitudinal strain. The amplitude of differences in strain trends to diverse with direct proportion to load approaching and leaving (Figure 69-70). When the load is far from the probe point,

the difference in strain is small. Otherwise, the peak of difference in strain happened at the load application on the right top of probe point. Transparently, transverse anisotropic material will perform variously depending on variety anisotropy parameters. In addition, the transverse deformed profiles is dissimilar each other due to the anisotropy (Figure 76). The comparison results revealed that anisotropy is severely critical factor to analysis a pavement system accurately.

Stress-dependent Model Compared with Stress-independent Model

Viscoelasticity and anisotropy are both stress-independent. However, granular subgrade is stress-dependent materials. Stress-independent assumption may lead to a large inaccuracy of finite element analysis. In order to investigate how the stress-dependent model, especially Uzan-Witczak, will affect the analysis results, the subgrade is assigned as Uzan-Witczak model and the rest of layers keep linear elasticity as listed in Table 8.

Because the resilient modulus of subgrade is derived from certain stress state which is defined by power law of mean stress and octahedral stress, the initial geostress could not equal to zero. In order to avoid converge problem due to incorrect low geostress, a geostatic step is added to achieve equivalent geostress due to gravity. In this case, a uniform density is assumed as 2000 kg/m^3 for each layer. The deformation values in geostatic step are neglected from the moving wheel loading step. In other words, the deformation values in geostatic step are considered equal to zero which is what the stress-independent model begins with. The comparison of Uzan-Witczak subgrade and stress-independent linearelastic model is presented from Figure 77 to 82. In this finite element model, the Young's modulus is 1.95 E8 Pa and Poisson's ration is 0.35; n, as the power of mean stress, is 0.26; m, as the power of octahedral stress, is -0.31 due to fine granular material property (Zuo 2003).

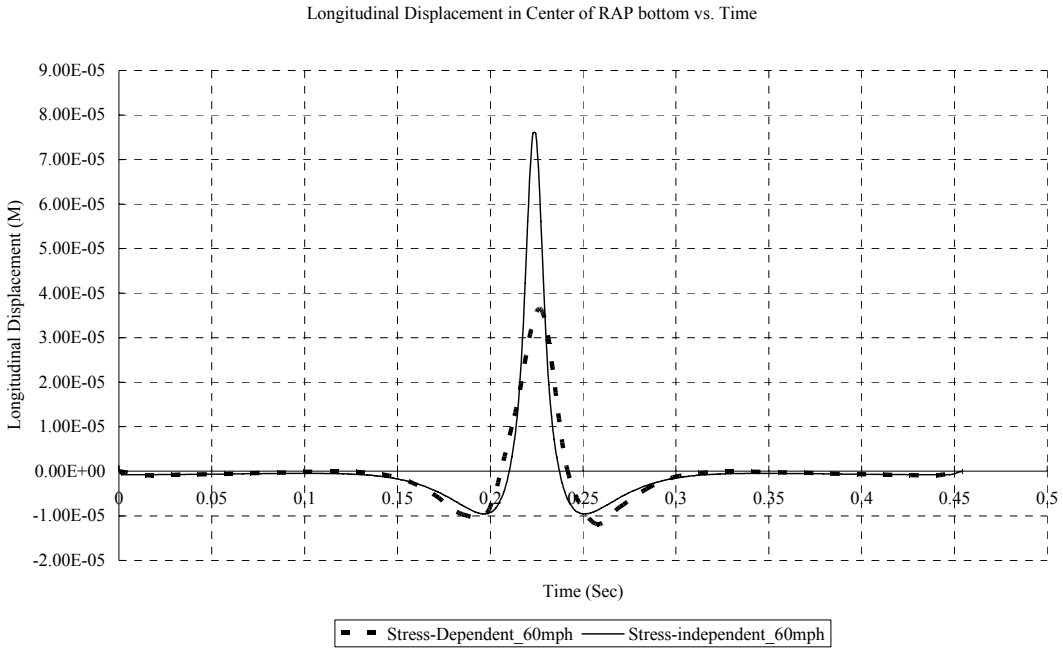

Figure 77 Longitudinal Strain under RAP at 60 mph

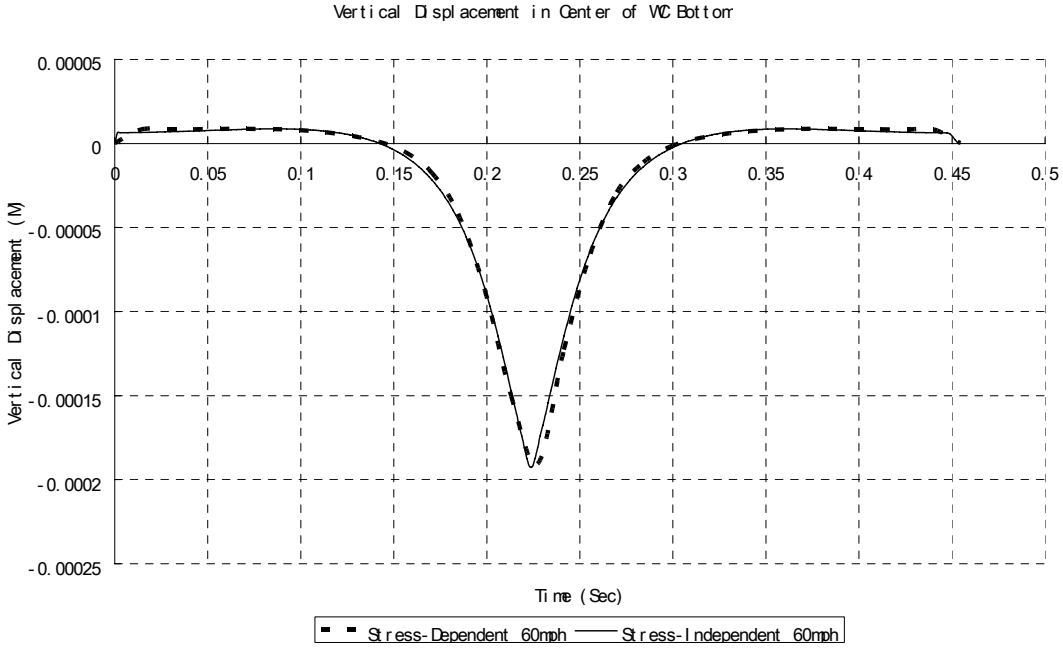

Figure 78 Vertical Displacement under WC at 60 mph

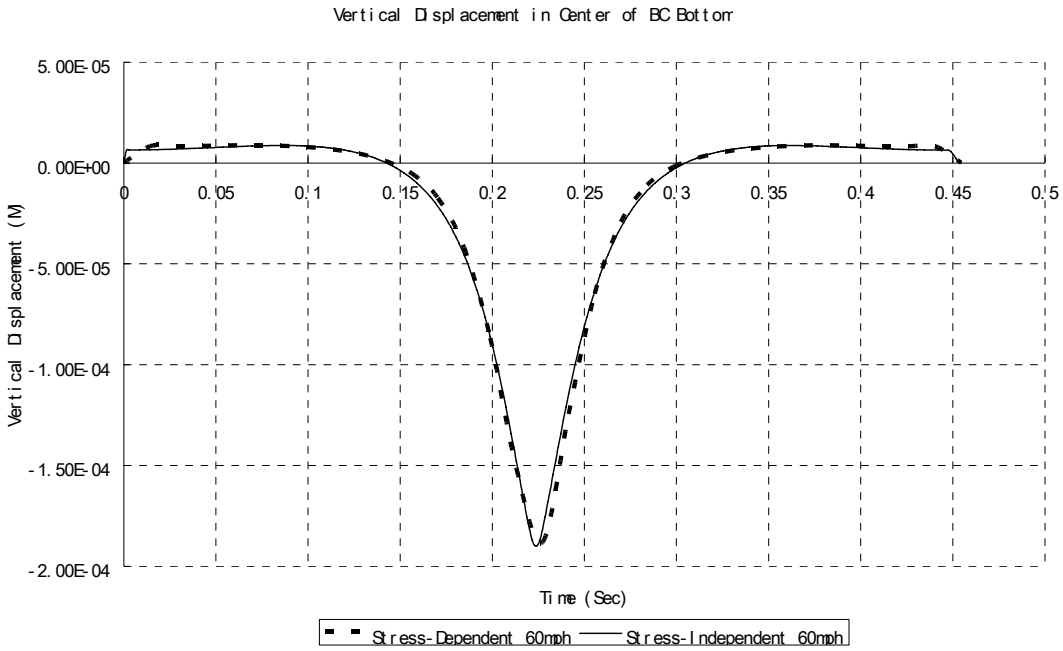

Figure 79 Vertical Displacement under BC at 60 mph

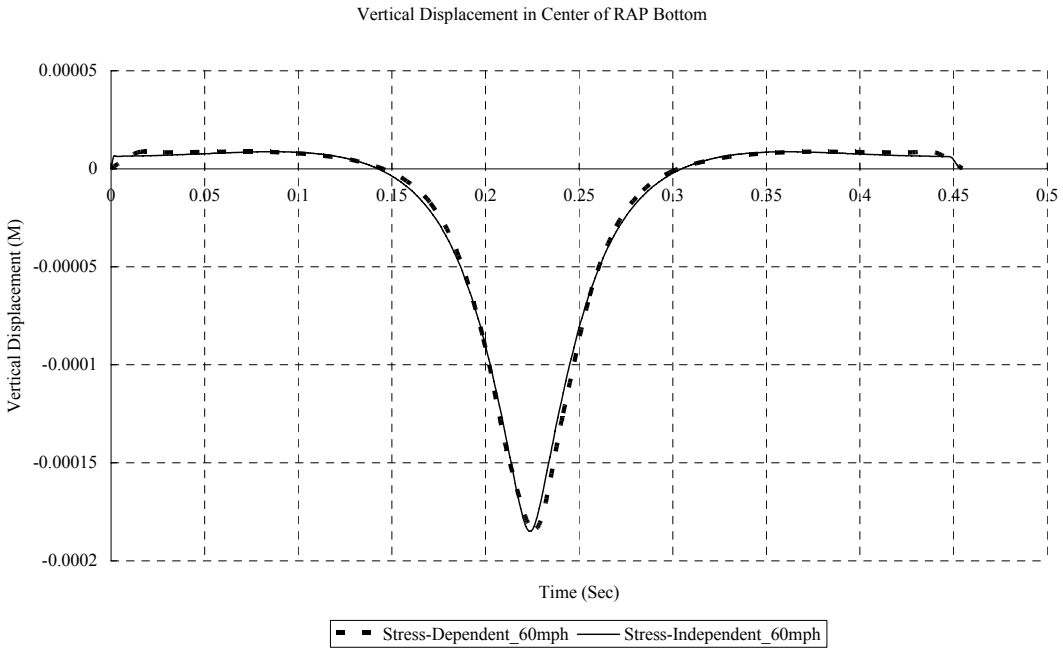

Figure 80 Vertical Displacement under RAP at 60 mph

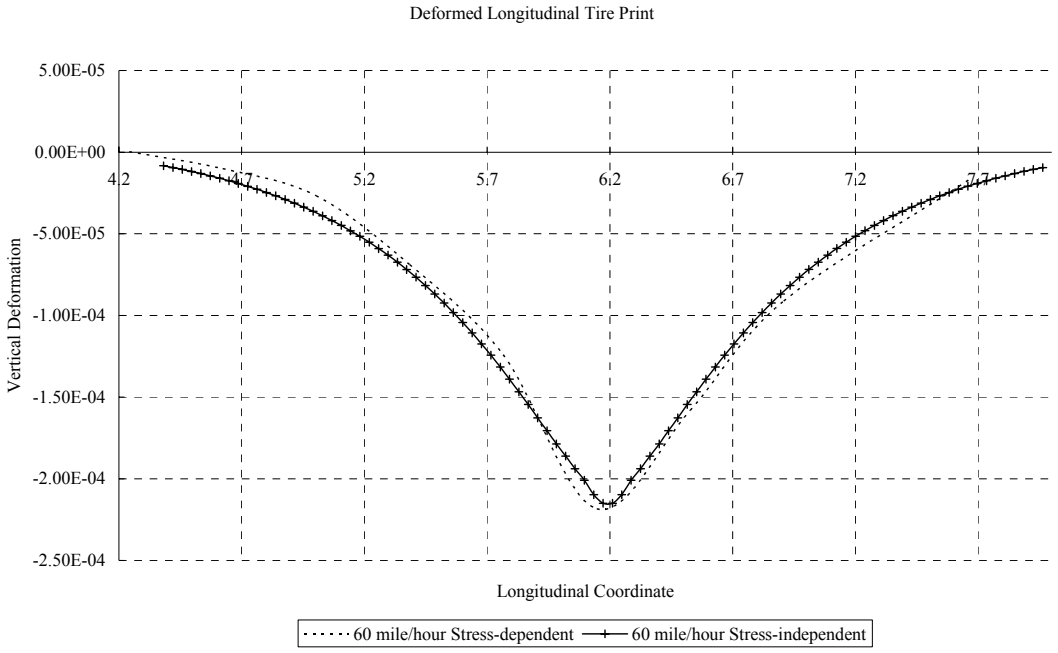

Figure 81 Deformed Longitudinal Tire Print

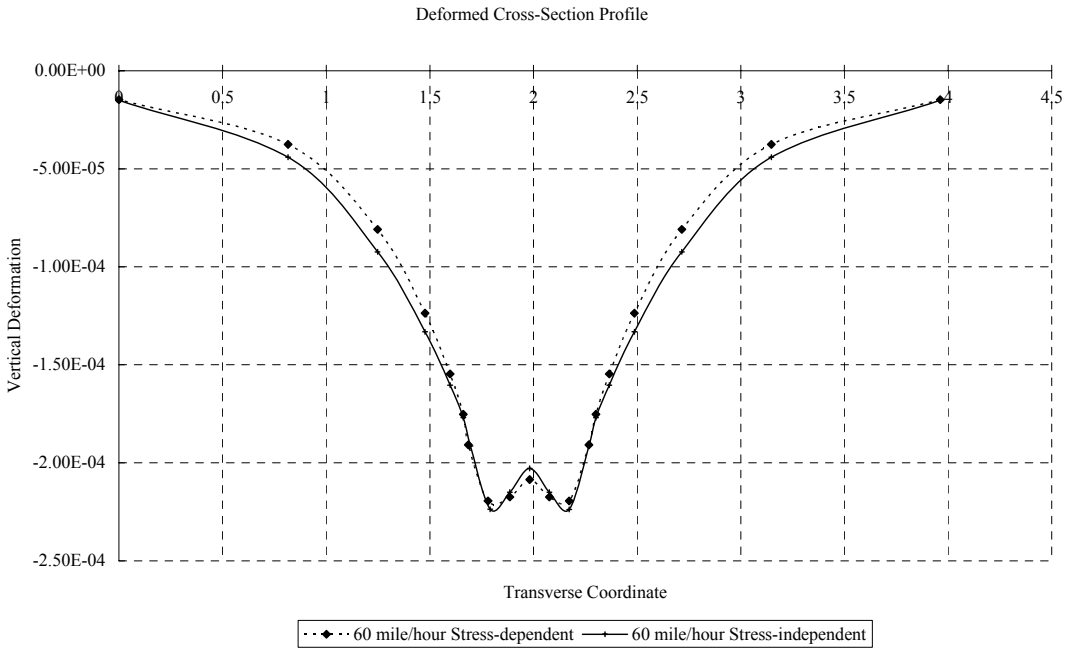

Figure 82 Deformed Cross-Section Profile

Generally, the implementation of Uzan-Witczak will not affect the vertical deformation significantly as Figure 79-82 shows. However, the horizontal deformation, especially the longitudinal strain, is strongly influenced with the application of Uzan-Witczak model. This is indicated in Figure 77. It was additionally observed that the longitudinal strain is changed from symmetric to unsymmetrical due to stress-dependent model. As the layer closest to stress-dependent subgrade, longitudinal strain on bottom of RAP layer achieved approximate equal position peak. However, stress-dependent subgrade model leads to a significant larger negative longitudinal horizontal.

Summary

Through the function analysis of viscoelasticity, nonlinear cross-anisotropy and stress-dependent characteristics, we can find all three of them play important roles to simulate the pavement system. Elasticity which is the most popular method to characterize the pavement constitutive behavior simplifies the pavement response to pavement materials. To improve the accuracy of pavement analysis procedure, viscoelastic model represented with Prony series is necessary to involve the time factor. Additionally, the cross-anisotropy is critical to correctly predict horizontal and vertical stain. Function analysis cross-anisotropy will produce significant different deformation shape in longitudinal and transverse direction. Correspondingly, strains in bottom of each layer will be incorrect estimated if using isotropy assumption. The stress-dependent property is widely accepted for characteristics of the granular material. In this function analysis, the stress-dependent Uzan-Witczak model not only affects the response of subgrade, but also influences the horizontal deformation as well.

To sum up, the viscoelasticity should be employed to simulate the response of pavement system relating with time. And the cross-anisotropy and stress-dependent characteristics should be considered in order to obtain correct horizontal and vertical

deformation. The combination of the above-mentioned material properties will contribute the improvement of accuracy of asphalt pavement simulation.

Sensitivity Analysis

From the constitutive modeling analysis, viscoelasticity, stress dependency and anisotropy were believed to influence the simulation. Series of sensitivity analysis were conduction on the basis of orthogonal test design method. There were 2 levels in each model. In viscoelasticity model, 4 factors were selected. In Uzan's model, 3 parameters were selected. 2 parameters were selected for transverse anisotropic model. Totally, 16 tests ran to conduct sensitivity analysis. The deflection on asphalt pavement surface, the longitudinal strain at bottom of RAP layer and vertical stress on the base layer were selected as comparison criterion. In Table 9, 10 parameters in 3 models were listed into two levels. In table 10, the assignment on each of 12 tests was presented in sequence.

The sensitivity analysis composed of 3 group tests. Test 1 to 8 are designed to analysis the parameters in viscoelasticity. Group which contains test 1 to 8 was defined as group-viscoelasticity. Test 9 to 10 are designed to analysis the parameters in Uzan's model. Group which contains test 9 to 10 was defined as group-Uzan. Test 13 to 16 are designed to analysis the parameters in transverse anisotropy. Group which contains test 13 to 16 was defined as group-anisotropy.

Table 9 Factors and Levels in Sensitivity Analysis

	viscoelasticity				Uzan			Anisotropy	
	g1	g2	τ1	τ2	k	n	m	A	r
	0.2	0.1	0.05	1	195000000	0.26	-0.31	0.5	-0.7
Level 1	0.02	0.01	0.005	0.1	19500000	0.026	-0.031	0.05	-0.07
Level 2	0.5	0.4	0.5	10	1950000000	2.6	-3.1	5	-7

Table 10 Test Sequences in Sensitivity Analysis

viscoelasticity — Remarks: 2 levels and 4 factors

Factors	g1	g2	τ1	τ2
Test 1	0.02	0.01	0.005	0.1
Test 2	0.02	0.01	0.005	10
Test 3	0.02	0.4	0.5	0.1
Test 4	0.02	0.4	0.5	10
Test 5	0.5	0.01	0.5	0.1
Test 6	0.5	0.01	0.5	10
Test 7	0.5	0.4	0.005	0.1
Test 8	0.5	0.4	0.005	10

Uzan — 2 levels and 3 factors

Factor	k	n	m
Test 9	19500000	0.026	-0.031
Test 10	19500000	2.6	-3.1
Test 11	1950000000	0.026	-3.1
Test 12	1950000000	2.6	-0.031

Anisotropy — 2 levels and 2 factors

Factor	A	r
Test 13	0.05	-0.07
Test 14	0.05	-7
Test 15	5	-0.07
Test 16	5	-7

Figure 83-85 presents the sensitivity analysis results in viscoelasticity group. Figure 86-88 presents the sensitivity analysis results in Uzan's model group. Figure 89-91 presents the sensitivity analysis results in transverse anisotropy group.

From sensitivity analysis in viscoelasticity group, the various levels in parameter values lead to the changes in three of comparison criterion, deflection on asphalt pavement surface, tensile strain on base and vertical stress on base. The various value in Uzan's model only changed the vertical deflection on asphalt pavement surface significantly. The transverse anisotropy parameters have significant influence only on the vertical stress on base course.

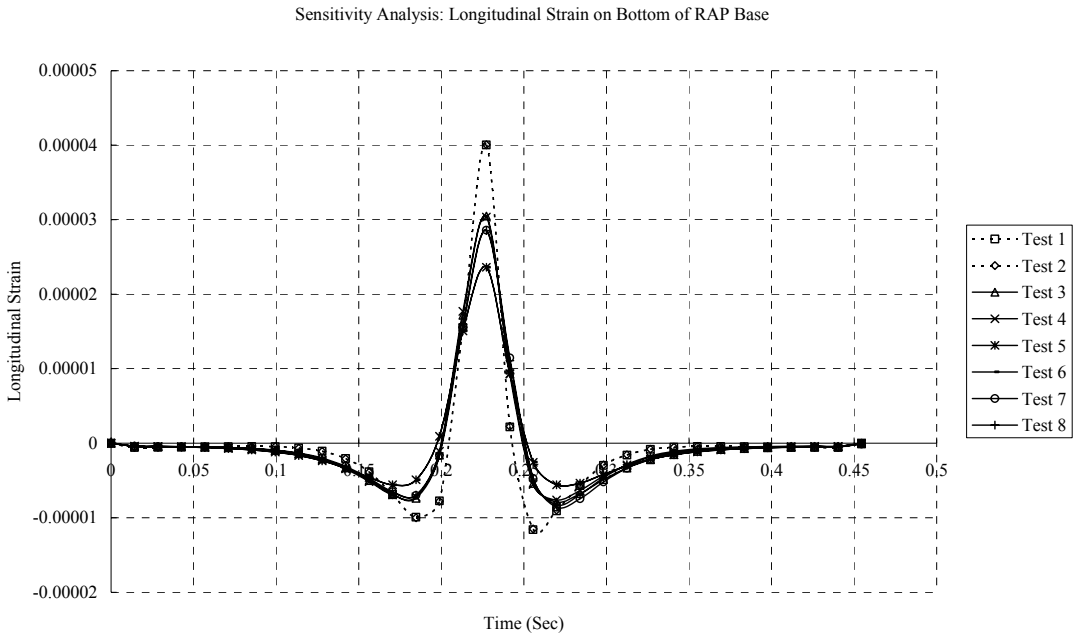

Figure 83 Longitudinal Strain on Bottom of RAP Base (Group-Viscoelasticity)

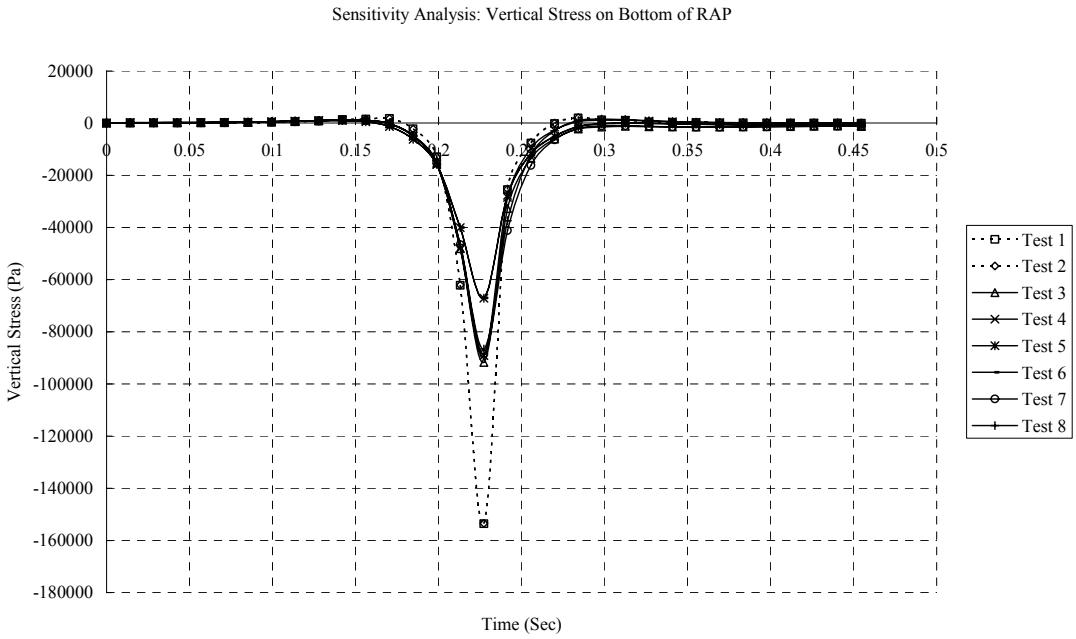

Figure 84 Vertical Stress on Bottom of RAP Base (Group-Viscoelasticity)

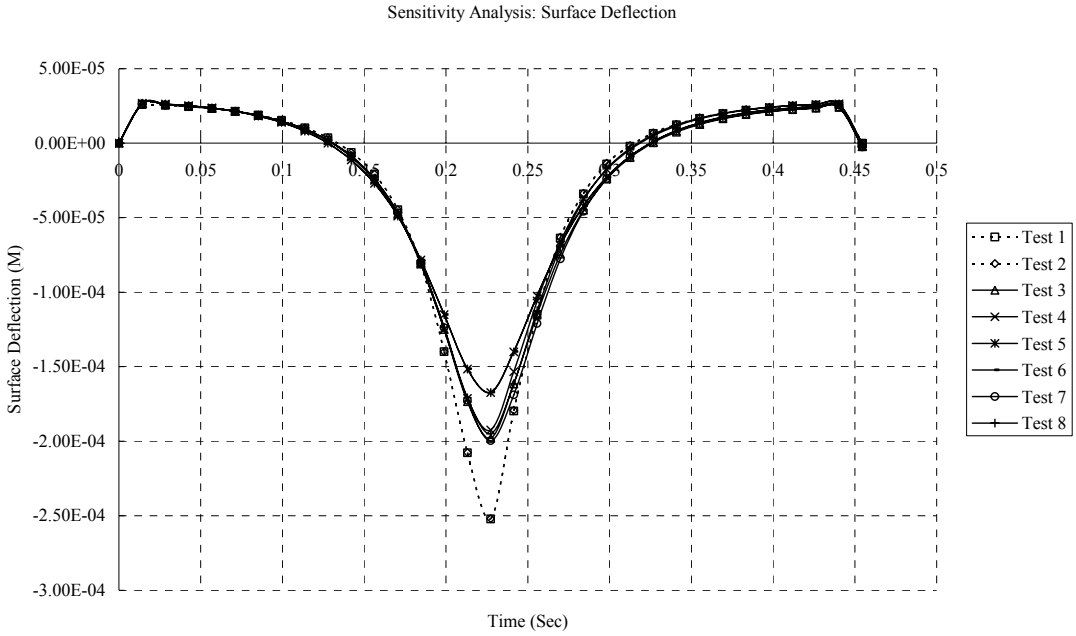

Figure 85 Vertical Deflection on Asphalt Pavement Surface (Group-Viscoelasticity)

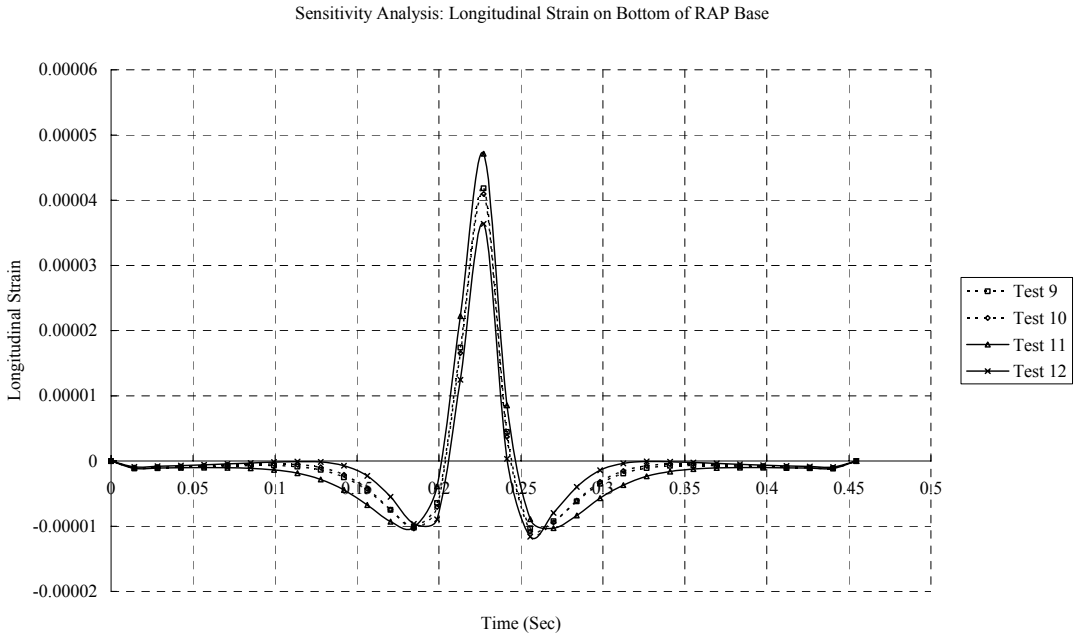

Figure 86 Longitudinal Strain on Bottom of RAP Base (Group-Uzan)

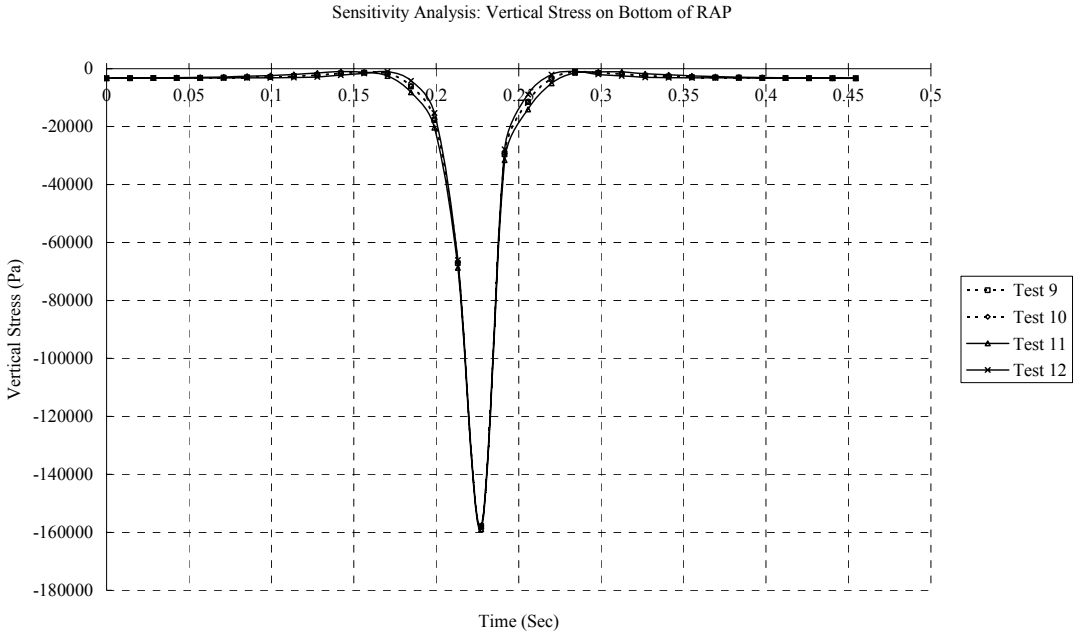

Figure 87 Vertical Stress on Bottom of RAP Base (Group-Uzan)

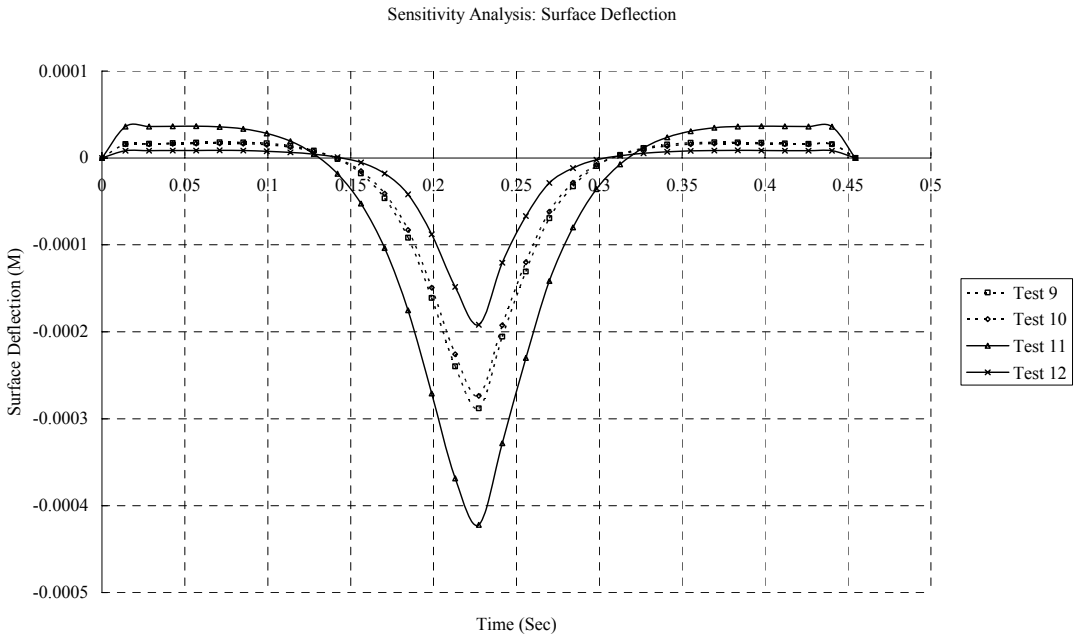

Figure 88 Vertical Deflection on Asphalt Pavement Surface (Group-Uzan)

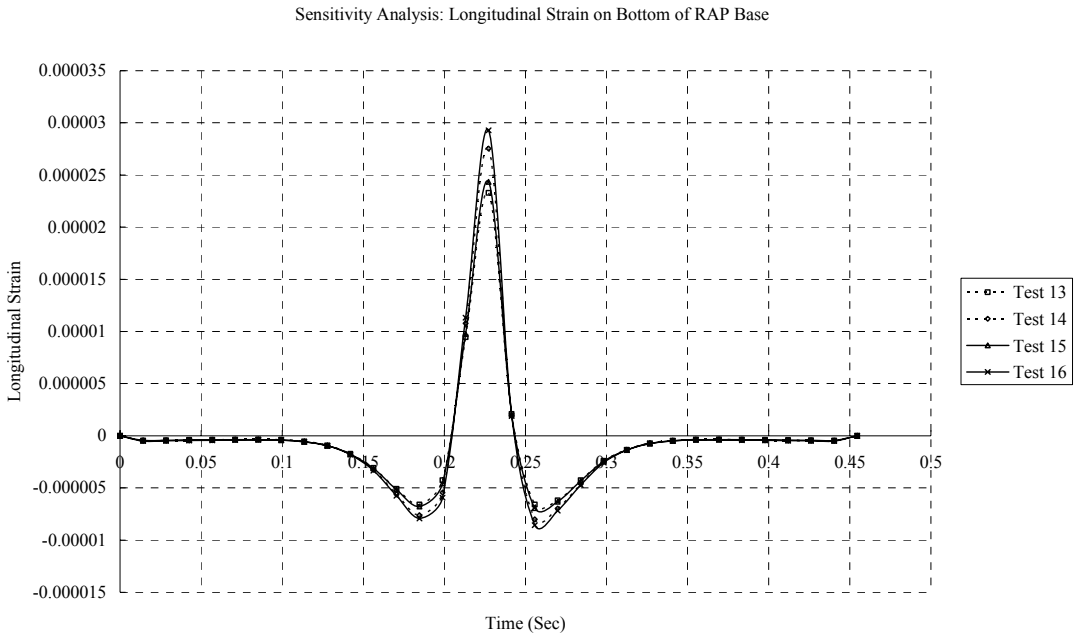

Figure 89 Longitudinal Strain on Bottom of RAP Base (Group-Anisotropy)

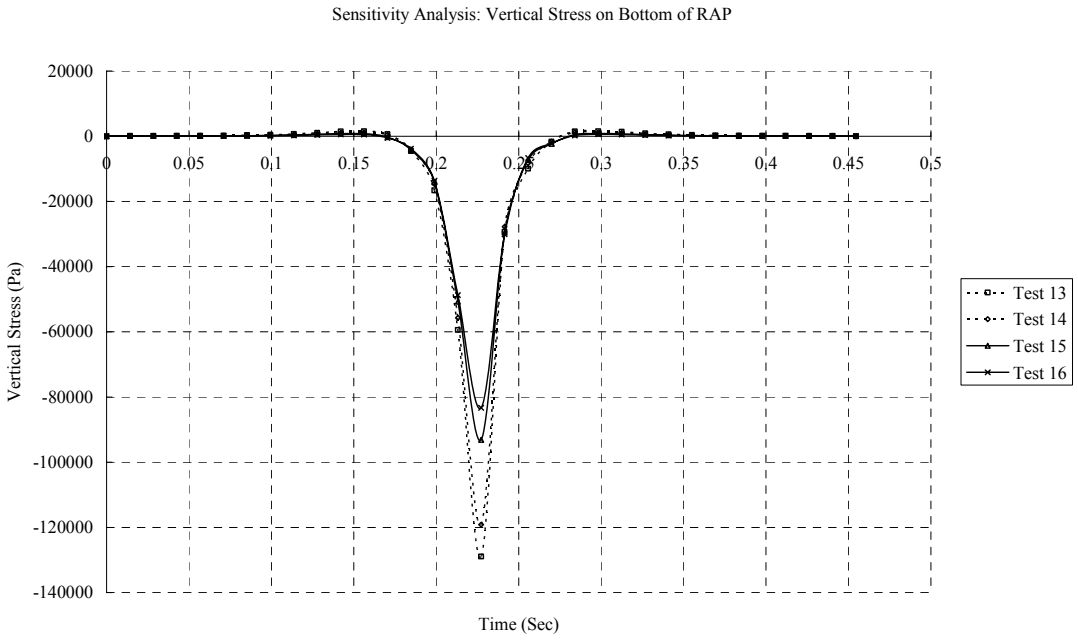

Figure 90 Vertical Stress on Bottom of RAP Base (Group-Anisotropy)

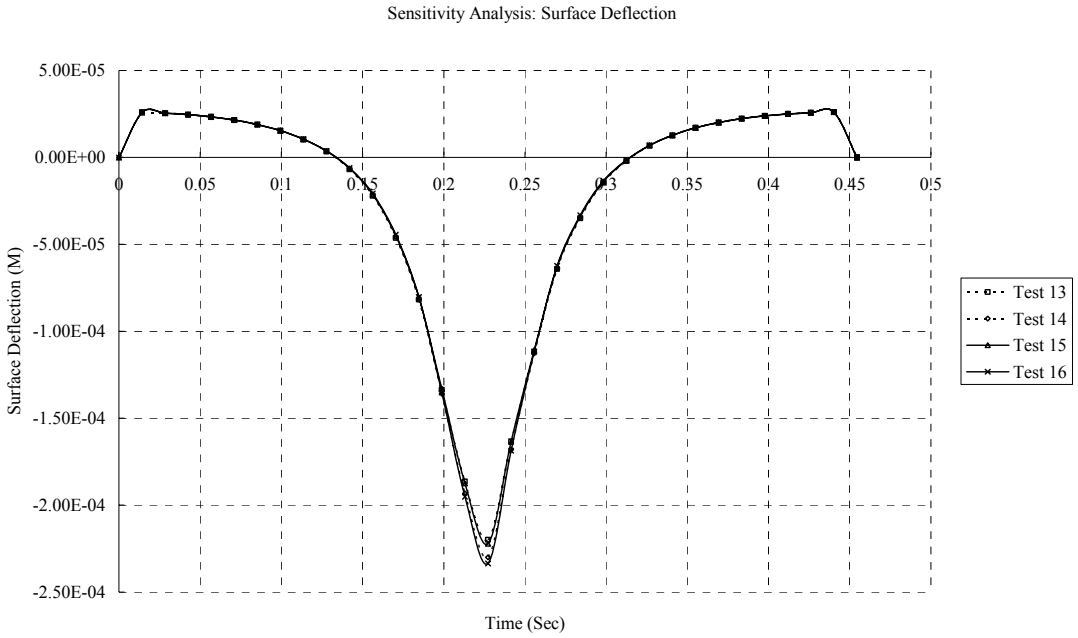

Figure 91 Vertical Deflection on Asphalt Pavement Surface (Group-Anisotropy)

C: UMAT for Transverse Anisotropy Nonlinear Model

```
SUBROUTINE UMAT(STRESS,STATEV,DDSDDE,SSE,SPD,SCD,
     1RPL,DDSDDT,DRPLDE,DRPLDT,
     2STRAN,DSTRAN,TIME,DTIME,TEMP,DTEMP,PREDEF,DPRED,CMN
AME,
     3NDI,NSHR,NTENS,NSTATV,PROPS,NPROPS,COORDS,DROT,PNEW
DT,
     4CELENT,DFGRD0,DFGRD1,NOEL,NPT,LAYER,KSPT,KSTEP,KINC)
C
      INCLUDE 'ABA_PARAM.INC'
C
C     IMPLICIT INTEGER (I-N),

      CHARACTER*8 CMNAME
      DIMENSION STRESS(NTENS),STATEV(NSTATV),
   1DDSDDE(NTENS,NTENS),DDSDDT(NTENS),DRPLDE(NTENS),
     2STRAN(NTENS),DSTRAN(NTENS),TIME(2),PREDEF(1),DPRED(1),
     3PROPS(NPROPS),COORD(3),DROT(3,3),DFGRD0(3,3),DFGRD1(3,3),
   4ANIP(3)

      IF(NDI.NE.3) THEN
      WRITE(7,*) 'THIS UMAT MAY ONLY BE USED FOR ELEMENTS
     1WITH THREE DIRECT STRESS COMPONENTS'
      CALL XIT
      ENDIF
      EMOD=PROPS(1)
      ENU=PROPS(2)
      ANIR=PROPS(3)
      ANIA=PROPS(4)
      ANIRATIO=(3.+ANIR-2.*ANIA)/(3.+ANIR+2.*ANIA)
      ANIK=(log10(ANIRATIO))/(log10(((2.-ANIA)/(2.+ANIA))**2))
      ANIP(1)=((2.+PROPS(4))/(6.+PROPS(4)))**ANIK
    ANIP(2)=((2.+PROPS(4))/(6.+PROPS(4)))**ANIK
      ANIP(3)=((2.-PROPS(4))/(6.+PROPS(4)))**ANIK
      PS=2*ANIP(1)*ANIP(2)*ANIP(3)
      EBULK3=EMOD/(1.-2.*ENU)
      EG2=EMOD/(1.+ENU)
      EG=EG2/2.
      ELAM=(EBULK3-EG2)/3.
C     D Components for Principal Stress
      DO K1=1,NDI
      DO K2=1,NDI
      DDSDDE(K2,K1)=ELAM
      END DO
      DDSDDE(K1,K1)=EG2+ELAM
      END DO
```

```
c     Anisotropic Parametric Components for Principal Stress
      DO K1=1,NDI
            DO K2=1,NDI
            DDSDDE(K1,K2)=DDSDDE(K1,K2)*ANIP(k2)
      DDSDDE(K1,K2)=DDSDDE(K1,K2)*ANIP(k1)
            END DO
            END DO
c     D Components for Shear Stress
            DO K1=NDI+1,NTENS
            DDSDDE(K1,K1)=EG
            END DO
c     Anisotropic Parametric Components for Shear Stress
      DO K1=NDI+1,NTENS
            DDSDDE(K1,K1)=DDSDDE(K1,K1)*PS/ANIP(K1-NDI)
            END DO
c     Stress Calculation
            DO K1=1,NTENS
            DO K2=1,NTENS
            STRESS(K2)=STRESS(K2)+DDSDDE(K2,K1)*DSTRAN(K1)
            END DO
            END DO
            IF(NOEL.EQ.1) WRITE(7,*) DSTRAN
            RETURN
            END
```

VITA

Wenbin He was born in 1975. He received his Bachelor's degree majored in civil engineering from Hefei University of Technology in 1996. After that, he worked for Guizhou Provincial Bridge Engineering Corp. and Guizhou Provincial Highway Engineering Corp. from 1996 to 2003 as an assistant engineer and certificated civil engineer. He earned his Master of Science degree majored in Structure Engineering from Guizhou University of Technology in 2001. He pursued his Master of Science degree in Guizhou University of Technology through part time study. From 2004 to 2006, he pursued for Master of Science degree majored in geotechnical engineering in University of Tennessee. His Master of Science degree majored in Geotechnical Engineering will be awarded by University of Tennessee in December, 2006.